Titre: Title:	Controlled Drug Delivery for Cancer Treatment Using Electrospun Structure
Auteur: Author:	Ginevra Stile
Date:	2020
Type:	Mémoire ou thèse / Dissertation or Thesis
Référence: Citation:	Stile, G. (2020). Controlled Drug Delivery for Cancer Treatment Using Electrospun Structure [Mémoire de maîtrise, Polytechnique Montréal]. PolyPublie. https://publications.polymtl.ca/5555/

POLYTECHNIQUE MONTRÉAL
affiliée à l'Université de Montréal

Controlled drug delivery for cancer treatment using electrospun structure

GINEVRA STILE
Institut de génie biomédical

Mémoire présenté en vue de l'obtention du diplôme de *Maîtrise ès sciences appliquées*
Génie biomédical
Décembre 2020

POLYTECHNIQUE MONTRÉAL
affiliée à l'Université de Montréal

Ce mémoire intitulé :

Controlled drug delivery for cancer treatment using electrospun structure

présenté par **Ginevra STILE**
en vue de l'obtention du diplôme de *Maîtrise ès sciences appliquées*
a été dûment accepté par le jury d'examen constitué de :

Marc LAVERTU, président
Abdellah AJJI, membre et directeur de recherche
Géraldine MERLE, membre

DEDICATION

To my grandparents,
that never doubt me...

Ai miei nonni,
che hanno sempre fede in me...

ACKNOWLEDGEMENTS

First and foremost, I would like to thank my supervisor at Polytechnique Montréal, professor Abdellah Ajji, for giving me the opportunity to embark on this journey in a foreign country, and for giving me the freedom to explore the research world in a supporting and understanding environment.

I thank my supervisor at Politecnico di Milano, professor Silvia Farè, for taking a chance on trusting me to carry out my project in the best way at such a far distance from our home institution.

To Claire Cerclé and Matthieu Gauthier goes a special *remerciement*, for helping me on a daily basis with the most practical aspects of my project throughout its whole length, from training me, to coating my samples, to transporting them from one zone to another in the most recent times.

To Richard Silverwood, that helped putting in place the protocol for the last phase of my project, as well as literally moving heavy instrumentation from one building to another.

To everyone in the research group that I have not mentioned, thank you for providing me with advice and company during the long hours in the laboratories.

I could have never gotten to this point without my friends.

The newer ones, that lead me through discovering all that Montréal and Canada have to offer, its quiet beauties and peculiarities. The friends that experienced with me astonishing marvels that I would have never been able to observe, had I not landed in this country. To Canadians in general, that have taught me that venturing out in the sun, whichever the temperature may be, is always worth it, provided you have the right jacket on.

To the friends I have made at Polimi, words could never describe the gratitude I feel everyday for having found you. You witnessed the many steps of my journey in discovering myself and you never hesitated to accept me or backed away from helping me through my doubts and moments of sadness. I can only hope to be able to provide even just an ounce of the same unconditional love to you. Thank you.

To my oldest friends. You have seen it all. You have continuously been at my back and call ever since we met. You have always provided me with the feeling that no matter how far we may go in life, we will always care deeply for one another and we will find each other and not a second will have gone by from when we last left it off.

Finally, I want to thank my family. I love you all so deeply.

Thanks to my grandparents for always being our beacon of light, to my aunts and uncles for being my parents when they couldn't, to my cousins for sticking together and supporting each other from afar.

To my sisters, that are, knowingly or not, my guide through life. You were and will always be an example for me, and not a day goes by where I don't look up to you.

To my parents, you give me the courage to be brave, the knowledge that were I to fall you would be ready to catch me and nurse me back to my feet. You made me the person I am today and I know that you'll continue to push me and support me in whichever endeavour I put my mind to.

To myself, and learning to live life with no regrets.

Montréal, October 2020

RÉSUMÉ

Le cancer étant l'une des premières causes de décès dans les pays développés, les chercheurs doivent continuer à mettre au point de nouvelles stratégies efficaces pour traiter les patients. De nombreux traitements couramment utilisés agissent souvent sur des processus cellulaires de base, entraînant des effets secondaires et nuisant à la qualité de vie du patient. En outre, ces médicaments ont souvent des fenêtres thérapeutiques très étroites et, en raison de leur mode d'administration, leur concentration initiale dépassera le seuil de toxicité. Les stratégies récemment développées pour répondre à ces problèmes sont la combinaison d'une administration contrôlée et ciblée des médicaments, visant un traitement localisé avec un dosage plus faible libéré sur une plus longue période.

D'autre part, l'électrofilage et l'électronébulisation sont des méthodes qui suscitent un intérêt croissant pour la fabrication de composés pharmaceutiques. Ces techniques partagent une configuration simple qui permet une grande polyvalence, permettant même l'électrofilage de plusieurs solutions à la fois, en électrofilage coaxial. Cette caractéristique permet d'obtenir des particules noyau-enveloppe en une seule étape, différemment de la plupart des méthodes actuellement employées pour ce faire.

Ce projet vise à utiliser la technique d'électronébulisation pour concevoir et tester un vecteur d'administration de médicaments. La littérature a été examinée afin de trouver un agent pharmaceutique présentant un profil de toxicité qui nécessiterait le plus une libération progressive, *in situ*. En fait, le médicament choisi, doxorubicin (DOX), est connu pour augmenter les risques de cardiomyopathies à long terme, même à très faible dose. Le délai et les conditions les plus appropriés pour l'administration ont ensuite été recherchés, afin de comprendre les exigences que le matériau de piégeage devrait avoir. Cela a abouti au choix d'un copolymère 50/50 poly(lactic-co-glycolic acid) (PLGA), qui serait capable de perdre lentement de la masse et de libérer le médicament sur une période de trois à quatre semaines. Afin de réduire les coûts et les risques, l'ibuprofène a été choisi comme médicament test lors des étapes préliminaires des travaux.

L'optimisation du processus d'électronébulisation, par un mélange d'analyse de la littérature et d'essais et erreurs, a permis d'obtenir des particules de 598 $\pm$286 nm. Malheureusement, les expériences se sont arrêtées lorsque les mesures contre le Covid-19 ont été mises en place et une fois l'accès aux laboratoires rétabli, les conditions environnementales ont changé et les paramètres optimisés n'ont pas donné les mêmes résultats. Après une phase de tests visant à rétablir les conditions idéales pour les paramètres optimisés, la production a été transférée

dans une installation différente, équipée d'un système capable de surmonter les problèmes. Grâce aux connaissances acquises lors de la précédente optimisation, des particules de 685,9 ±286 nm ont été rapidement produites, permettant au projet de passer à la phase suivante.

La dégradation du polymère et l'administration du médicament ont été caractérisées par une série de tests qui ont consisté à immerger deux groupes d'échantillons de particules pendant 28 jours, un groupe dans une solution de PBS avec un pH de 7.4, l'autre dans une solution similaire avec un pH de 6.6, afin d'imiter l'environnement acide que l'on trouve dans les tissus cancéreux. Le pH des échantillons, ainsi que leur perte de poids, ont été suivis au fil des semaines, tandis que des spectres FTIR étaient acquis pour caractériser la libération du médicament et que les échantillons étaient mis de côté pour être lyophilisés et observés plus tard avec MEB. La baisse du pH a permis de confirmer la dégradation du PLGA. L'observation avec le MEB a montré que les particules avaient formé des agglomérats en PBS. En ce qui concerne l'administration du médicament, la présence d'agglomérats plus gros a certainement retardé le délai prévu. Si ces tests ont permis d'avoir une première idée du comportement des particules, plusieurs problèmes rencontrés ont mis en évidence la nécessité de les répéter afin de fournir un aperçu beaucoup plus précieux des structures produites.

Enfin, les travaux présentés ici ont permis de tester la faisabilité de l'utilisation de la technique d'électro-pulvérisation coaxiale comme autre moyen de produire des particules nanométriques cœur-enveloppe. Deux questions principales ont permis de conclure que cette technique pourrait être mieux appliquée à l'échelle micrométrique. En effet, si les particules peuvent être obtenues à plus petite échelle, le processus d'optimisation peut être long et il peut y avoir des concessions à faire en ce qui concerne leur morphologie. En outre, le rendement a tendance à être très faible et devrait certainement être amélioré pour être compétitif dans un cadre industriel.

ABSTRACT

With cancer being one of the first causes of death in developed countries, researchers need to keep coming up with new, efficient strategies to treat patients. Many of the treatments commonly employed often act on basic cellular processes, causing side effects and hindering the patient's quality of life. Moreover, these drugs often have very narrow therapeutic windows and, due to their administration methods, their initial concentration will overshoot the toxicity threshold. The recent strategies developed to address these issues are the combination of controlled and targeted drug delivery, aiming for a localized treatment with a lower dosage released over a longer time.

On the other hand, the electrospinning and electrospraying are methods gaining increased interest for the fabrication of pharmaceutical compounds. These techniques share a simple set-up that allows for great versatility, even allowing for the electrospinning of multiple solution at once, in coaxial electrospinning. This feature can obtain core-shell particles in a single step, differently than most methods currently employed to do so.

This project set out to employ the coaxial electrospraying technique to design and test a drug delivery carrier. The literature was looked into to find a pharmaceutical agent with a toxicity profile that would most need a gradual, *in situ* release. In fact, the chosen drug, doxorubicin (DOX), is known to increase risks of long-term cardiomyopathies even with very low dosages. The most appropriate time frame and conditions for the delivery were then researched, to understand the requirements that the entrapping material would need have. This resulted in the choice of a 50/50 poly(lactic-co-glycolic acid) (PLGA) copolymer, which would be able to slowly lose mass and release the drug over the course of three to four weeks. To reduce costs and risks, ibuprofen was selected as a test drug during the preliminary steps of the work.

The optimization of the electrospraying process, through a mix of literature review and trial and error, allowed to obtain particles of 598 $\pm$286 nm. Unfortunately, the experiments came to a halt as measures against Covid-19 were put in place and once access to the laboratories was reestablished the environmental conditions had changed and the optimized parameters were not achieving the same results. After a phase of tests geared towards restoring the ideal conditions for the optimized parameters, the production moved to a different set-up, equipped with a system able to overcome the issues. Thanks to the knowledge acquired with the previous optimization, particles of 685.9 $\pm$286 nm were quickly produced, allowing the project to proceed to its next phase.

The degradation of the polymer and the delivery of the drug were characterized in a series of tests which involved submerging two sample groups of particles over the course of 28 days, one group in a PBS solution with a 7.4 pH, the other in a similar solution with a 6.6 pH, in order to mimic the acidic environment found in cancer tissues. The pH of the samples, as well as their weight loss was monitored through the weeks, while FTIR spectra were being taken to characterize the drug release and samples were put aside to be freeze dried and later observed with SEM. The pH decrease was able to confirm the degradation of PLGA. The SEM observation showed that the particles had formed agglomerates in PBS. For what concerns the drug delivery, the presence of bigger clusters has certainly delayed the expected time frame. While these tests allowed for an initial outlook over the particles' behaviour, several issues encountered highlighted the need to repeat them in order to provide a much more valuable insight regarding the structures produced.

Finally, the work here presented was able to test the feasibility of employing the coaxial electrospraying technique as an alternative way to produce nanometric core-shell particles. Two main issues brought to the conclusion that this technique might be better applied to the micrometric scale. In fact, while particles can be obtained in the smaller scale, the optimization process can be lengthy and there might be concessions to be made for what concerns their morphology. Moreover, the yield tends to be very poor and would need to be certainly improved to be competitive in an industrial setting.

TABLE OF CONTENTS

DEDICATION iii

ACKNOWLEDGEMENTS iv

RÉSUMÉ vi

ABSTRACT viii

TABLE OF CONTENTS x

LIST OF TABLES xii

LIST OF FIGURES xiv

LIST OF SYMBOLS AND ACRONYMS xxi

LIST OF APPENDICES xxii

CHAPTER 1 INTRODUCTION 1
1.1 Breast Cancer, treatment problematics, clinical motivation 1
1.2 Electrospinning & Electrospraying 2
1.3 Research Objectives 4
1.4 Outline 4

CHAPTER 2 LITERATURE REVIEW 6
2.1 Cancer drug delivery 6
2.2 Electrospinning & Electrospraying 9
2.2.1 Theoretical mechanism and parameters 9
2.2.2 Comparison to other methods, advantages and challenges 13
2.2.3 Applications in drug delivery 16

CHAPTER 3 MATERIALS AND METHODS 20
3.1 Choice of materials 20
3.2 Electrospraying optimization 21
3.2.1 Adjustments and Big box set-up 22
3.3 Particle characterization 25

3.3.1 Scanning Electron Microscopy (SEM) . . . 25
3.4 Degradation tests . . . 25
3.5 Image analysis . . . 26

CHAPTER 4 RESULTS AND DISCUSSION . . . 28
4.1 Choice of materials . . . 28
4.2 Electrospraying optimization . . . 28
4.2.1 Initial optimization . . . 28
4.2.2 Size optimization . . . 34
4.2.3 Different solutions for core and shell . . . 37
4.2.4 Final Tong Li optimization . . . 45
4.2.5 Particle collection . . . 46
4.2.6 Adjustments and Big box set-up . . . 48
4.3 Degradation tests . . . 55
4.3.1 Fourier-transform infrared spectroscopy (FTIR) . . . 55
4.3.2 pH . . . 64
4.3.3 Mass remaining . . . 64
4.3.4 Scanning Electron Microscopy (SEM) . . . 65
4.4 Image analysis . . . 71

CHAPTER 5 CONCLUSION AND RECOMMENDATIONS . . . 72

REFERENCES . . . 75

APPENDICES . . . 81

LIST OF TABLES

Table 4.1 Final optimized parameters for the Tong Li set-up. 46
Table 4.2 Final optimized parameters for the Big box set-up. 55
Table 4.3 Breakdown of the main peaks from the PLGA spectrum [1]. . 57
Table 4.4 Breakdown of the main peaks from the ibuprofen spectrum. . 57
Table 4.5 Breakdown of the main peaks from the PLGA-ibuprofen particles spectrum. 58
Table A.1 Same solvent combination of 50/50 THF/MeCN; drum collector. 81
Table A.2 Same solvent combination of 50/50 THF/MeCN; combination A for the solutes; drum collector. 82
Table A.3 Same solvent combination of 30/70 THF/MeCN; combination A for the solutes; drum collector. 82
Table A.4 Same solvent combination of 50/50 THF/MeCN; combination A for the solutes; drum collector. 83
Table A.5 Same solvent combination of 40/60 THF/MeCN; combination A for the solutes; drum collector. 84
Table A.6 Inner solvent was 40/60 THF/MeCN; Outer solvent was 10/30/60 DMF/THF/MeCN; combination A for the solutes; drum collector. . . 85
Table A.7 Inner solvent was 40/60 THF/MeCN; Outer solvent was 15/35/50 DMF/THF/MeCN; both with 2.5 wt% of drug and polymer; flat plate collector. 86
Table A.8 Inner solvent was 40/60 THF/MeCN; Outer solvent was 15/35/50 DMF/THF/MeCN; with 5 wt% of drug and 2.5 wt% of polymer; flat plate collector. 86
Table A.9 Combination A for the solutes; Core solvent 40/60 THF/MeCN; flat plate collector. 86
Table A.10 Inner solvent was 40/60 THF/MeCN; Outer solvent was 60/40 DMF/ MeCN; combination A for the solutes; ethanol bath collector. . 87
Table A.11 Inner solvent was 40/60 THF/MeCN; Outer solvent was 60/40 DMF/ MeCN; combination A for the solutes; flat plate collector; the substrate was covered with a silicone-based spray. 87
Table A.12 Inner solvent was 40/60 THF/MeCN; Outer solvent was 60/40 DMF/ MeCN; combination A for the solutes; flat plate collector. . . . 88

Table A.13 Big box set-up parameters. Inner solvent was 40/60 THF/MeCN; Outer solvent was 60/40 DMF/MeCN; flat plate collector. 88

LIST OF FIGURES

Figure 1.1 Evolution of interest into electrospinning and electrospraying techniques in the biomedical field: (a) Articles published in the considered years relating to the exposed techniques in the biomedical field; (b) Pie graph highlighting the specific research areas in which the exposed techniques have been used in the biomedical field in the considered years. [From Scopus, search parameters: (TITLE -ABS-KEY (electrospinning OR electrospraying) AND TITLE-ABS-KEY (biomed OR med OR drug)) in a time range from 1993 to 2021]. 2

Figure 1.2 The electrospinning set-up. A syringe is loaded with the polymeric solution while a high voltage potential is applied between the spinneret and the grounded collector. Fibers or droplets will then deposit on the collector. Adapted from: [2] 3

Figure 2.1 Schematic representation of active and passive delivery [3] . . 8

Figure 2.2 Close-up of cone-jet mode electrospraying process. From left to right it's possible to note the formation of the solution jet and its consequent break up into droplets [4]. 10

Figure 2.3 Coaxial set-up scheme. 13

Figure 2.4 Smart multifunctional TiO_2 capsules capable of: magnetic targeting, imaging through quantum dots and paclitaxel delivery. (a) through (c), SEM images of the particles ultrasound for: (a) 5 min; (b) 15 min; (c) 30 min. (d) and (e), size distribution and particles' status of sample ultrasound for: 5 min; 15 min. (f) representation of shell cracking mechanism until drug release from the particles with increasing ultrasound time [5]. 17

Figure 2.5 PLA particles loaded with gambogic acid. SEM images and particle size distribution of: (a) 70 nm particles; (b) 185.6 nm particles; (c) 358 nm particles; (d) 7.5 μm particles [6]. 18

Figure 2.6 Electrosprayed ELP-DOX particles: (a) SEM image and (b) particle size distribution [7]. 19

Figure 3.1 Chemical structures of the materials involved: a) DOX; (b) ibuprofen; c) PLGA [8]. 20

Figure 3.2 Tong Li Electrospinning Unit (Shenzhen Tong Li Tech Co. LTD). 22

Figure 3.3 Set-up close-ups of Tong Li Electrospinning Unit (Shenzhen Tong Li Tech Co. LTD): (a) internal Tong Li set-up; (b) coaxial system; (c) external pump. 23
Figure 3.4 (a) Wet set-up, Tong Li Electrospinning Unit (Shenzhen Tong Li Tech Co. LTD); (b) close up. 24
Figure 3.5 Big box set-up: (a) pumps and high voltage source; (b) coaxial spinneret and collector; 25
Figure 3.6 Code developed to improve the image processing and analysis time. 27
Figure 4.1 Examples of tests with the use of THF as lone solvent with 2 wt% for both the drug and the polymer: (a) Porous incomplete particles; (b) Inconsistencies caused by a too high flow rate of 1 mL/h; Scale bar: (a) 10 μm; (b) 100 μm. 29
Figure 4.2 Example of tests with the use of MeCN as lone solvent with 2 wt% for both the drug and the polymer. Scale bar: 10 μm. 30
Figure 4.3 The first results from the 50/50 combination of THF and MeCN (test 10C, see Table A.1, Appendix A). Scale bar: 30 μm. 31
Figure 4.4 THF and MeCN with 3 wt% polymer and drug (test 11A, see Table A.1, Appendix A). (a), (b): particles with a reduced porosity in comparison to ones obtained from THF alone but not fully complete. Scale bar: (a) 30 μm; (b) 20 μm. 31
Figure 4.5 THF and MeCN with 5 wt% polymer and drug (test 12B, see Table A.2, Appendix A). The particles show no evident porosity. Scale bar: (a) 20 μm; (b) 10 μm. 32
Figure 4.6 Distribution size of the particles obtained in test 12B (For parameters, see Table A.1, Appendix A). 32
Figure 4.7 Comparison between the average values for the particles obtained with 0.7 mL/h as flow rate in trial 12 and 13. In order from left to right: 12H, 13C, 12B, 13H. (For parameters, see Table A.1, Appendix A). 33
Figure 4.8 Results from the reduction of TTC distance: (a) connected mat-like particles (Test 15E); (b) particles with several shapes and sizes, connected by thin filaments, some of these filaments are highlighted by the white arrows (Test 16H); Scale bar: (a), (b) 20 μm. (For parameters, see Table A.4, Appendix A). 34

Figure 4.9 Results from the reduction of TTC distance: (a) particles with several shapes and sizes, with 30/70 THF/MeCN as solvent (Test 14C, see Table A.3, Appendix A); (b) spherical particles, average diameter 700 nm, standard deviation ±240 nm, with 40/60 THF/MeCN as solvent (Test 19H, see Table A.5, Appendix A). The arrows highlight some of the particles with a diameter over 1000 nm; Scale bar: (a), (b) 20 μm. 35

Figure 4.10 Distribution size of the particles electrosprayed in test 19H (see Table A.5, Appendix A). 36

Figure 4.11 Results from inner solvent 40/60 THF/MeCN, outer solvent 10/30/60 DMF/THF/MeCN: (a) collapsed particles, paired flow rate of 0.5 mL/h (Test 21B); (b) particles, average diameter 570 nm, standard deviation ±166 nm, paired flow rate of 0.2 mL/h (Test 21H); Scale bar: (a), (b) 20 μm. (For parameters, see Table A.6, Appendix A). 37

Figure 4.12 Distribution size of particles obtained in test 21H (for parameters, see Table A.6, Appendix A). 38

Figure 4.13 Comparison between uncoupled and paired flow rates: (a) particles, average diameter 547 nm, standard deviation ±164 nm, inner flow rate of 0.2 mL/h, outer flow rate of 0.5 mL/h (Test 24F); (b) particles, average diameter 670 nm, standard deviation ±348 nm, paired flow rate of 0.5 mL/h (Test 25F); Scale bar: (a), (b) 20 μm. (For parameters, see Table A.6, Appendix A). 39

Figure 4.14 Distribution size comparison of particles obtained in two different trials: (a) 24F; (b) 25F. (For parameters, see Table A.6, Appendix A). 39

Figure 4.15 Comparison between same parameters except TTC distance: (a) collapsed misshapen particles, TTC distance 15 cm (Test 24D); (b) particles, it is possible to notice the effect of the Rayleigh disintegration thanks to the presence of larger and smaller particles, TTC distance 20 cm (Test 26C, for parameters see 25I); Scale bar: (a), (b) 20 μm. (For parameters, see Table A.6, Appendix A). 40

Figure 4.16 Distribution size of particles obtained in test 26C. (For parameters, see 25I, Table A.6, Appendix A) 40

Figure 4.17 Effect of multi-jet cone: (a) particles of several sizes (Test 29E); (b) distribution size of test 29E. The effect of a multi-jet cone can be noticed in the wide range of sizes; Scale bar: (a) 20 μm. (For parameters, see Table A.7, Appendix A). 41

Figure 4.18 Beaded filaments structure (Test 29D); Scale bar: (a) 20 μm. (For parameters, see Table A.7, Appendix A). 42

Figure 4.19 Effect of TTC distance on size: (a) spherical particles (Test 33C); (b) particles of several sizes (Test 33F); Scale bar: 20 μm. (For parameters, see Table A.12, Appendix A). 43

Figure 4.20 Effect of TTC distance on distribution size: (a) particles produced in test 33C; (b) particles produced in test 33F. (For parameters, see Table A.12, Appendix A). 43

Figure 4.21 Test 33 comparison between different voltages at different TTC distances. In order from left to right: 33A, 33F, 33B, 33G, 33C, 33H, 33D, 33I, 33E. For parameters, see Table A.12, Appendix A. 44

Figure 4.22 Effect of flow rate: (a) particles, average diameter 570 nm, standard deviation $\pm$292 nm, core flow rate of 0.2 mL/h, shell flow rate of 0.5 mL/h, total applied voltage 15 kV, TTC distance 21 cm (Test 38B); (b) particles, average diameter 598 nm, standard deviation $\pm$286 nm, core flow rate of 0.1 mL/h, shell flow rate of 0.3 mL/h, total applied voltage 15 kV, TTC distance 21 cm (Test 38C); Scale bar: 20 μm. (For parameters, see Table A.12, Appendix A). 45

Figure 4.23 Effect of flow rate on distribution size: (a) test 38B; (b) test 38C. For parameters, see Table A.12, Appendix A. 46

Figure 4.24 Wet set-up results: (a) merged particles (Test 36B); (b) aggregated particles (Test 37F); Scale bar: (a) 20 μm; (b) 30 μm. (For parameters, see Table A.10, Appendix A). 47

Figure 4.25 Relative humidity values in the electrospraying laboratory from December to July. The dashed line represents the closing period, from mid-March to mid-June. 48

Figure 4.26 Effect of increased relative humidity on the optimized parameters (Test 45E, see 38B for parameters, Table A.12, Appendix A): (a) test 45E; (b) Test 45E, close-up; Scale bar: (a) 20 μm; (b) 10 μm. . . 49

Figure 4.27 Effect of increased temperature on the optimized parameters (Test 46F, see 38C for parameters, Table A.12, Appendix A): (a) test 46F; (b) test 46F, close-up; Scale bar: (a) 20 μm; (b) 10 μm. 50

Figure 4.28 Effect of Indicating DRIERITE (Test 48D, see 38B for parameters, Table A.12, Appendix A): (a) test 48D; (b) Test 48D, lower magnification; Scale bar: (a) 20 μm; (b) 1 mm. 50
Figure 4.29 Effect of Indicating DRIERITE (Test 48F, see 38C for parameters, Table A.12, Appendix A): (a) test 48F; (b) Test 48F, close-up; Scale bar: (a) 20 μm; (b) 10 μm. 51
Figure 4.30 Tong Li optimized parameters tested in Big box set-up: (a) fragments and a few particles (Test 49E, see 44B for parameters, Table A.13, Appendix A); (b) elongated random fragments (Test 49F, see 44A for parameters, Table A.13, Appendix A); Scale bar: (a), (b) 20 μm. 52
Figure 4.31 Big box set-up with TTC distance of 34 cm: (a) crumpled incomplete particles (Test 50A); (b) crumpled incomplete particles (Test 50C); Scale bar: (a), (b) 20 μm. (For parameters, see Table A.12, Appendix A). 53
Figure 4.32 Final particles with Big box set-up (Test 53E, see 52C for parameters, Table A.12, Appendix A): (a) particles, average diameter 685.9 nm, standard deviation $\pm$286 nm, core flow rate of 0.1 mL/h, shell flow rate of 0.3 mL/h, total applied voltage 15 kV, TTC distance 15 cm; (b) distribution size of particles obtained in test 53E. Scale bar: (a) 20 μm. 54
Figure 4.33 FTIR spectrum of PLGA obtained in reflection mode. 56
Figure 4.34 FTIR spectrum of ibuprofen powder obtained in reflection mode. 57
Figure 4.35 FTIR spectrum of PLGA-Ibuprofen particles obtained in reflection mode. 58
Figure 4.36 Comparison of FTIR spectra of 1μL droplet of PBS and the same droplet dried on the crystal obtained in reflection mode. 59
Figure 4.37 Comparison of FTIR spectra of a 1μL droplet of PBS, a 1μL droplet of PBS with 0.05 M ibuprofen and the same droplet dried on the crystal obtained in reflection mode. It can be noticed that the spectra of the two droplets are equivalent, safe for a small difference in intensity. The dried PBS with ibuprofen however present some peaks in the 1000-1200 cm^{-1} region. 60

Figure 4.38 FTIR spectra of Group A obtained in reflection mode [Part 1]. No significant difference can be noticed between the spectra of the sample and PBS. The noise present for 0 and 1 Hour, noticeably the smaller peak in the midst of the 3000-3500 cm^{-1} peak was also there in the plain PBS spectra recorded on the same day and never reappeared over the course of the experiment. 61

Figure 4.39 FTIR spectra of Group A obtained in reflection mode [Part 2]. No significant difference can be noticed between the spectra of the sample and PBS. 61

Figure 4.40 FTIR spectra of Group A obtained in reflection mode after a 10μL droplet of the sample was dried on the FTIR crystal. In the dried state new peaks appear in the 1000-1300 cm^{-1} region. 62

Figure 4.41 FTIR spectra of Group B obtained in reflection mode [Part 1]. No significant difference can be noticed between the spectra of the sample and PBS. The noise present for 0 and 1 Hour, noticeably the smaller peak in the midst of the 3000-3500 cm^{-1} peak was also there in the plain PBS spectra recorded on the same day and never reappeared over the course of the experiment. 62

Figure 4.42 FTIR spectra of Group B obtained in reflection mode [Part 2]. No significant difference can be noticed between the spectra of the sample and PBS. 63

Figure 4.43 FTIR spectra of Group B obtained in reflection mode after a 10μL droplet of the sample was dried on the FTIR crystal. In the dried state new peaks appear in the 1000-1300 cm^{-1} region. 63

Figure 4.44 pH monitoring over the course of the experiment. Group A and Control A starting from a pH of 7.4; Group B and Control B starting from a pH of 6.6 64

Figure 4.45 Particle aggregation on SEM images from day 3 of testing: (a) aggregates wider view; (b) close up of aggregates; Scale bar: (a) 30 μm; (b) 20 μm. 66

Figure 4.46 SEM images from the degradation tests (Part 1). On the left, are samples from Group A (pH 7.4), on the right are samples from Group B (pH 6.6). The time-points represented are as follows: a) and b) are from day 3; c) and d) are from day 9; e) and f) are from day 16. 68

Figure 4.47 SEM images from the degradation tests (Part 2). On the left, are samples from Group A (pH 7.4), on the right are samples from Group B (pH 6.6). The time-points represented are as follows: g) and h) are from day 23; f) and j) are from day 28. 69

Figure 4.48 SEM image from the degradation tests. Group A (pH 7.4), from day 16. A smaller cluster seems to be further away in the degradation process than larger ones in the same sample (Figure 4.46e) 70

LIST OF SYMBOLS AND ACRONYMS

DLS	Dynamic Light Scattering
DMF	Dimethylformamide
DOX	Doxorubicin
EPR	Enhanced Permeability and Retention
FESEM	Field Emission Scanning Electron Microscopy
FTIR	Fourier-Transform Infrared Spectroscopy
GPC	Gel Permeation Chromatography
MeCN	Acetonitrile
PBS	Phosphate Buffer Saline
PCL	Polycaprolactone
PEG	Polyethylene glycol
PLA	Polylactic acid
PLGA	Poly(lactic-co-glycolic acid)
PVP	Polyvinylpyrrolidone
SEM	Scanning Electron Microscope
THF	Tetrahydrofuran
TTC	Tip to collector

LIST OF APPENDICES

Appendix A Electrospraying parameters 81

CHAPTER 1 INTRODUCTION

1.1 Breast Cancer, treatment problematics, clinical motivation

Breast cancer is the second most diagnosed cancer worldwide in both sexes, and the first leading cause of cancer death if only females are considered. The Global Cancer Observatory estimates that in 2018 there have been 2.1 million newly diagnosed cases of breast cancer in females, with higher incidence rates in developed areas such as Europe and North America [9].

Depending on the stage of development and the location of the cancer, the usual treatments are surgery, chemotherapy or radiotherapy. Pharmaceutical cancer treatments, such as chemotherapy, are often invasive and debilitating for the patients. This is explained by the fact that the active principles used in such therapies act on basic cellular mechanisms that are found in the majority of human cells. The consequence is that the classical therapies hinder the viability of not only the cancerous cells but also the healthy ones. Moreover, the treatment is often administrated with systemic methods that spread the medical agents in the whole body [10]. This lack of targeting not only means an exposure of healthy cells to the chemotherapeutic agents, but also results in an obligation to increase the dosage to ensure that an adequate quantity of agents reaches the cancerous area. For these reasons, research is now focusing on the design of a delivery system able to release the therapeutic agents *in situ*, in order to limit the exposure to only the targeted cells and reduce the dosage.

On the other hand, the current treatment method of having the chemotherapeutic agents injected in a singular occasion every month, raises the issue of fitting into the, usually narrow, therapeutic window, where there is the maximum benefit for the patient with relatively minimum side effects. In fact, what often happens is an overshoot of the toxicity levels in the immediate time after administration, when the drugs' concentrations are higher, and, once the concentrations are lower, a decrease under the therapeutic threshold. The answer to this further issue seems to be a controlled delivery, where the same dosage is administered over a longer period of time in an effort to keep the concentration of the pharmaceuticals in the patient's body in the therapeutic window. The combination of controlled and targeted drug delivery would result in a localized treatment with a lower dosage released over a longer time, reducing the systemic drug circulation and targeting only the cancerous cells without affecting the other cells of the body. This would also allow the patients to have a better quality of life during the treatment and side effects of a lower impact than the ones currently observed [11].

1.2 Electrospinning & Electrospraying

The use of the electrospinning and electrospraying techniques for biomedical purposes is a fairly recent development, with the first applications in the field dating to the turn of the 21st century and a continuously rising interest (Figure 1.1).

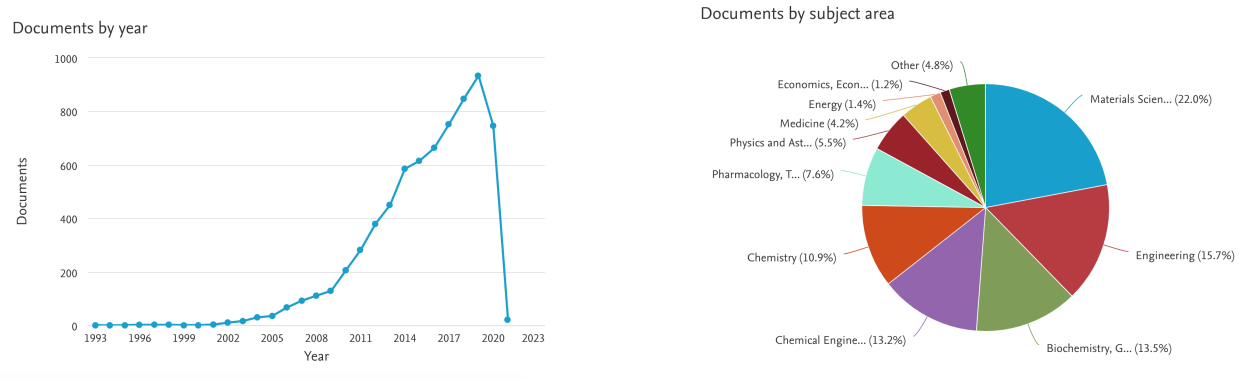

(a) (b)

Figure 1.1 Evolution of interest into electrospinning and electrospraying techniques in the biomedical field: (a) Articles published in the considered years relating to the exposed techniques in the biomedical field; (b) Pie graph highlighting the specific research areas in which the exposed techniques have been used in the biomedical field in the considered years. [From Scopus, search parameters: (TITLE -ABS-KEY (electrospinning OR electrospraying) AND TITLE-ABS-KEY (biomed OR med OR drug)) in a time range from 1993 to 2021].

The common set-up between the two is composed of four main parts: a syringe pump, a metallic needle (spinneret), a high voltage power supply and a collector (Figure 1.2).

The summarized and simplified process is the following:

1. the syringe is loaded with the material solution and inserted into a flow feeding pump;
2. at the tip of the needle, the surface tension will cause the formation of a spherical droplet;
3. a high-voltage field is applied between the needle and the collector;
4. when the voltage exceeds a certain value, the equilibrium between the electric forces and the surface tension will be destabilized and the droplet will assume a conical shape called "Taylor cone";
5. a solution jet will be emitted from the spinneret, forming fibers or particles of micro-/nano-metric dimensions;

6. solvent evaporation will take place as the forming structures (i.e. fibers or particles) travel towards the collector where they will finally deposit [12].

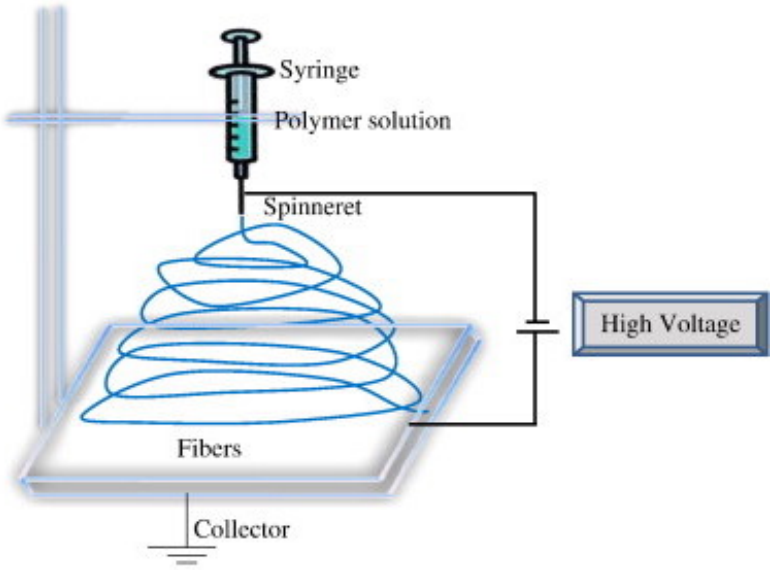

Figure 1.2 The electrospinning set-up. A syringe is loaded with the polymeric solution while a high voltage potential is applied between the spinneret and the grounded collector. Fibers or droplets will then deposit on the collector. Adapted from: [2]

The constant design and improvement of new geometries of the needle and the collector allow for a great versatility and is the reason behind the increase in popularity of these two techniques. The discriminating factor between them is the geometry of the end-product. In fact, while both can produce films, the electrospinning can also produce rods and the electrospraying results in beads. The underlying mechanism and possible applications of these techniques will be discussed more in depth in Chapter 2.

1.3 Research Objectives

The initial hypothesis supporting this work is that controlled drug delivery is able to produce a therapeutic effect on cancerous cells using lower dosages than current conventional treatments. Under this hypothesis, this thesis' main objective was to provide a proof of concept to the feasibility of developing an initial structure produced using the electrospinning or the electrospraying technique, able to deliver active ingredients to the human body in a controlled way with the aim of treating breast cancer.

To produce the structure and tests its capabilities, the following secondary objectives had been identified:
Objective 1: Determine the active ingredient;
Objective 2: Determine the rate and condition of the delivery, the type of structure and the material;
Objective 3: Optimize production parameters, fabricate and characterize the structure (size and morphology);
Objective 4: Characterize the drug delivery (release time, degradation profile) and test the effectiveness of the treatment (cell apoptosis).

Due to delays related to the Covid-19 outbreak, Objective 4 was only partially achieved and this thesis work was not able to test its therapeutic effect on cancerous cells, and confirm or deny the main hypothesis.

1.4 Outline

The text of the thesis is structured as follows:

In the second chapter the state of the art is discussed. The initial part focuses on a more in depth look at how drug delivery can affect cancer treatments and improve the quality of life of these patients. A brief introduction is given to the strategies that can be employed to do so, with a further focus on polymeric structures and which factors should be considered when designing a polymer-based drug delivery system. Following, the used technique, electrospraying, is presented, highlighting its driving mechanisms and looking into the many variables at play and how they may correlate. A brief overlook of competing alternative methods is then given, with a final comparison to the chosen method's advantages and limitations. Finally, some examples of past applications in the field are looked into.

In the third chapter the materials and methods used are displayed. The first section briefly presents the approach taken to the choice of the pharmaceutical agent, as well as

the polymer employed. Afterwards, the methods used during the optimization process are presented, together with some solutions to issues that may have risen during it. What follows is the explanation of the protocol put in place to test the degradation of the produced structure. The conclusion, exposes the method employed for the analysis and characterization of the particles.

In the fourth chapter results are reported and discussed. The first section expands on the choice of the material used, explaining the thought process that brought to the final decisions. Following, are the results from the electrospraying optimization, which underlines the process of trial and error that lead to the final structure, with a focus on how undesired morphologies may arise and be overcome. Later, the results from the degradation tests are presented, particularly observing the changes that the structures went through during a 4 week immersion in Phosphate Buffer Saline (PBS). Finally, a brief overlook regarding the limits of the implemented analysis method is discussed.

In the fifth chapter the conclusions summarize the work performed in the thesis, with a critical eye concerning the technique used and the limitations that the project has faced.

CHAPTER 2 LITERATURE REVIEW

2.1 Cancer drug delivery

As mentioned in Chapter 1, many of the drawbacks of classic chemotherapy as a cancer treatment derive from the systemic way in which the drugs are delivered. The pharmaceuticals usually present very narrow therapeutic windows, i.e. the dosing range in which the drug carries benefits for the disease without toxic effects. At the same time, releasing the drugs on a systemic basis means being aware that an amount of the dosage may be absorbed by other tissues than the desired one or cleared out of the body before it ever reaches the cancerous tissue. This results in a need to sometimes increase dosages with the sole purpose of ensuring that the drugs reach the desired tissue in a sufficient amount to have a therapeutic effect. Moreover, while the pharmaceuticals' mechanism of action may often rely on impairing the multiplication of fast-replicating cells, such as cancerous ones, healthy cells are hit as well. This is what usually causes the many systemic side effects of chemotherapy [3]. Several strategies are being researched and implemented in order to limit the exposure of healthy cells to chemotherapeutic drugs and to better spread out their release over time. For the first objective, targeting has been the leading hypothesis, either passively or actively, with the pharmaceutical being encapsulated by or conjugated with other molecules in order accumulate in the cancerous area. With passive targeting the active agents are usually enclosed in a structure whose physical and/or chemical properties should increase the bioavailability period and lead to an accumulation inside the desired tissue, exploiting its own characteristics. An example of passive targeting is represented by Doxil®, a formulation that uses pegylated liposomes to encapsulate doxorubicin, taking advantage of the Enhanced Permeability and Retention (EPR) effect, which will be better defined shortly. In fact, researchers have been able to verify that Doxil®, with a combined effect from the stealth provided by PEG (Poly(ethylene glycol)), which shields the particles from being cleared out immediately from the body, and the delayed release offered from the liposomal coating, resulted in increased drug payloads delivered to tumors while enhancing the accumulation and reducing toxic effects derived from total life dosage, compared to the free doxorubicin (DOX) [13, 14]. The idea behind EPR is that the fast-paced angiogenesis occurring in cancerous tissues should result in more permeable blood vessels which might present pores big enough to allow the passage of molecules up to 800 nm. Once the molecules are inside the cancer's interstitial space, they are kept there by the defective lymphatic system typical in tumoral areas (Figure 2.1). One of the key challenges faced when using this effect is the heterogeneity between

tumoral tissues due to their different cell types and locations. In particular, different tissues may present dramatically different blood vessel characteristics, meaning that the size requirements that work for an area and type might not in others, rendering the fixation of an ideal particle size a highly debated topic [3, 15]. This fact represents one of the biggest limitations of passive targeting, together with the possibility of the patient developing drug resistance. In fact, targeting the cells in a tumor without any specificity may cause an over-expression of transporter protein in charge with expelling the drug, which will automatically lower the effect of the treatment. Because of this, new strategies based on the co-delivery of two or more chemotherapeutic agents have been proposed, the main idea being releasing the different therapeutics in a staggered manner either by loading the drugs in different domains (for example using core-shell nanorods) or by embedding drugs presenting different hydrophobicity properties in the same nanofiber matrix [16, 17]. Another proposed solution involves the active targeting of specific receptors (Figure 2.1), known to be either peculiar to the tumor cell type or simply over-expressed, with a density depending on the type of receptor, on those type of cells' membrane, for example, a density of 10^5 ErbB2 receptors per cell is needed for anti-ErbB2-targeted formulations in breast cancer, such as the one employed in Trastuzumab. The targeting agents conjugated to the nanocarrier may vary from proteins (such as the anti-HER2 antibody used in the previous example), nucleic acids and ligands such as peptides, vitamins, or carbohydrates.

In regards with the nature of the carrier, the most common are lipid-based and polymeric ones. For the first category, the main advantage are the innate biocompatibility and biodegradability, together with the possibility for easy modification. On the other hand, they have high production costs, some phospholipids are quickly oxidized, they seem to lack controlled-release abilities, showing burst drug releases and long-circulating formulations may not accumulate where intended. As polymers are concerned there are two main possibilities: natural or synthetic [3]. Examples from the former that have been employed successfully in drug delivery are chitosan and alginate, the first having been used for a doxorubicin-dextran conjugate entrapment, the second for applications in oral delivery of insulin [18]. Although natural polymers would be advantageous in terms of biodegradation, their origins might cause issues of reproducibility and might bring upon undesired immune reactions from the body. Moreover, their degradation processes are usually very quick (a few days or weeks if crosslinked), making them unfavourable for longer term delivery. In regards to synthetic polymers, biodegradable ones (such as polycaprolactone (PCL), polylactic acid (PLA), poly(lactic-co-glycolic acid) (PLGA), polyorthoesters and polyanhydrides) are preferred over non-biodegradable for drug delivery purposes, as the elimination from the body is intrinsic. The advantages of synthetic polymers reside mainly in the possibility to consistently syn-

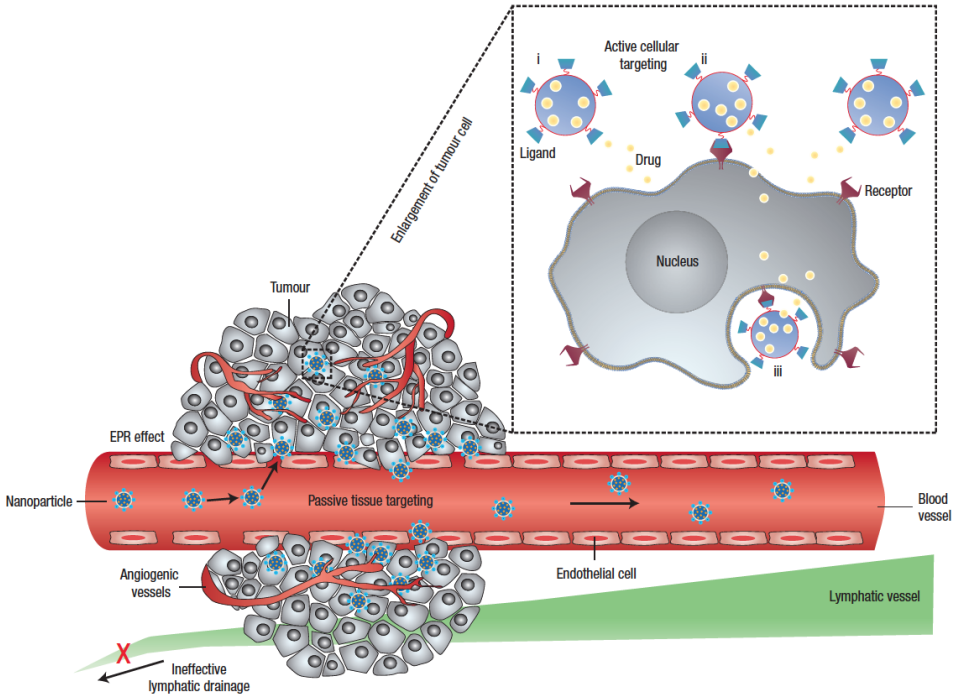

Figure 2.1 Schematic representation of active and passive delivery [3]

thesize and modify them to be tailored to one's requirements. The main aspect to consider while designing a drug delivery system is the type of degradation expected: bulk or surface. The first, present in PLA and PLGA, may be most appropriate when the polymers are used as a shell with the pharmaceuticals as the core, so that these will start diffusing through the polymeric matrix as it degrades and slowly be realeased [19]. The latter, carried out by polyorthoesters and polyanhydrides, may be particularly interesting in structures where the polymer and the active principle are not separated, allowing for a continuous release of the drug as the layers of polymer are degraded. Together with the erosion type, its rate needs to comply with the application's requirements. While changes may be operated, generally the degradation rates of the aforementioned polymers are as follows: polyanhydrides usually erode in a matter of days [20]; on the opposite end of the spectrum are PCL and PLA which can last several months to a couple of years, based on the specific crystallinity of the used polymer; polyorthoesters and PLGA can degrade over a few weeks to a couple months depending on the lactide and glycolide ratio, with the longer erosion times achieved at higher lactide presence [21, 22]. It is to be noted, that, even if the chosen synthetic polymer is biodegradable, one needs to make sure that its byproducts are biocompatible at the concentration levels that will be generated during the degradation. For example, PLA and PLGA will produce acidic low molecular weight by-products (lactic acid for PLA and lactic and

glycolic acid for PLGA) that at certain concentrations may cause tissue inflammation [21]. The morphology in which these polymers are presented, will also influence the degradation rate, for example, an increased erosion rate will be found in nanoparticles, since they expose a high surface area, and porous structures, which allow an easy permeation of biological fluids (Chapter 2 from [23], [24]).

Summing up briefly, the factors to consider in polymer-based drug delivery are: the choice of the polymer, so, its interactions with the pharmaceutical and its degradation characteristics; the drug diffusion pathway, dictated by structural morphology, its partitioning, its diffusivity in the polymer and its solubility in the medium. First of all, the interactions between the polymer and the drug, and the location of the drug in the structure, will be relevant as the drug will have to diffuse inside the polymeric matrix before being able to be released in the medium, at which point the drug solubility in the medium will come into play. The structure's morphology, such as fibers, particles, mono or multi-layered, will also have an important impact on the release profile of a drug as it will mainly define the drug diffusion pathway. Moreover, the choice of a biodegradable or non-biodegradable polymer will heavily determine the delivery mechanism as the first will allow for a release mainly controlled by the degradation rate of the material, whereas in the second case the delivery will depend solely on the drug diffusion pathway in the polymer [16].

2.2 Electrospinning & Electrospraying

As mentioned in Chapter 1, the electrospinning and electrospraying techniques are novel introductions in the biomedical field, even if the process and phenomena used have been studied since the first half of the 20th century [4]. Since the latter technique was chosen to be employed in this work, this section will focus on its theoretical aspects, its strengths and its challenges as well as a review of previously fabricated drug delivery systems found in the literature.

2.2.1 Theoretical mechanism and parameters

The electrospraying set-up is composed by a collector, a syringe pump, a needle (spinneret) and a high voltage power supply. The idea is to apply an electric potential difference between the needle's nozzle and the collecting surface, while a pump slowly injects a conductive solution through said spinneret. The resulting electric field will charge the solution and at the tip of the needle there will be a contrast between the electrodynamic force and the droplet's surface tension. Eventually the electric force will prevail and a construct, called Taylor cone

(Figure 2.2), will form, with a higher free charge density towards the summit of the cone that will originate a highly densely charged jet. Here lies the difference between electrospinning and electrospraying: the former will result if this stream stays intact, maintaining a liquid jet; the latter will be obtained due to instability between the forces at play, the electrostatic repulsion, the surface tension at the interface between the liquid and the gas and the kinetic energy from the Taylor cone's influence, causing a jet breakup and the formation of droplets (Figure 2.2). Once these droplets are released the solvents will tend to evaporate while the electrosprayed material will diffuse inside the structure and form chain entanglements. Droplets in particular, may experience a phenomenon called Rayleigh disintegration or Coulomb fission, where smaller particles are created when, due to the solvent's evaporation and the subsequent increased charge concentration, the primary droplets break up. Finally, dry particles, or filaments in the case of electrospinning, will deposit on the collector [25].

Figure 2.2 Close-up of cone-jet mode electrospraying process. From left to right it's possible to note the formation of the solution jet and its consequent break up into droplets [4].

While the set-up and mechanism are quite simple and straightforward, there are many parameters that contribute to the final product. A first distinction can be made between solution, set-up and environmental parameters; in the following paragraphs these distinctions will be used while briefly explaining the interplay between these variables.

Polymeric solution parameters

The factors related to the solution are highly interconnected as changing something regarding one parameter, will likely influence most of the others. One of the first choices in this regard deals with the chosen material, most likely a polymer, to be electrosprayed, its molecular weight and concentration. It is important to keep in mind, in fact, that in the final steps of electrospraying, multiple events are occurring: the solvent is evaporating, the polymer is

diffusing in the droplets as well as forming chain entanglements. This phenomenon will have an important impact on the size and morphology of the final product. A way to identify this contribution is mentioned by D.N. Nguyen et al. [25] in their review. They explain that the chain entanglement behaviour of a polymer-solution system can be expressed as the number of entanglements per chain in solution ($(n_e)_{sol}$), and that polymers with lower molecular weight should have only 1-2.5 entanglements per chain in the initial solution, to avoid reaching a viscosity high enough to obtain electrospinning. Going back to the impact of the chosen polymer, its molecular weight and concentration, these are the factors determining chain entanglement: in the case of electrospraying, having to find a balance between a too viscous solution and a concentration high enough to be higher than the critical overlap concentration (C^*). For the purposes of electrospraying, polymers with lower molecular weight should not exceed the concentration of thrice C^*, whereas polymers with higher molecular weight should be kept at even lower concentrations.

Conductivity of the solution plays an important role in the size and the dispersion size of the produced particles. While, on one hand, a low conductivity solution tends to the production of more mono-dispersed particles in size, increasing the conductivity is an easy way to reduce the particles' size. In this case one has to be aware of an increased risk in offspring ejection due to the phenomenon of Coulomb fission, that may bring a bimodal size dispersion [24]. Such type of dispersion can also be brought by a high flow rate. This parameter is key in regards to the morphology and the size of the particles, in fact, in order to allow complete solvent evaporation, lower flow rates are preferred (in the order of mL/h or μL/h). If, by the time the droplets deposit on the collector, they are still partially solvated, they will present deformed, non-consistent morphologies once the solvent finally evaporates.

Finally, the solvent represents the last important parameter relative to the solution. As one can easily imagine, the choice of the solvent is crucial to the solution properties, such as: volatility, viscosity, conductivity and miscibility. The first requirement is that the solvent has to be able to solubilize the chosen polymer and eventual additional components. In regards to the volatility, a solvent with a higher boiling temperature (or lower evaporation rate), won't be completely gone by the time the droplets deposit on the collector, possibly causing particle fusion. On the other hand, a too fast evaporation process will bring instability and won't provide enough time to form chain entanglements, producing poly-dispersed particles with porous, hollow, or even collapsed morphology. Volatility has to be balanced with solvent viscosity as this property contributes to the polymer diffusion inside the droplet. If the polymer can distribute uniformly, the droplets will have a smaller chance of collapsing and will be able to retain a spherical shape with a smoother surface once they deposit on the collector. As mentioned earlier, solution conductivity is essential in determining the size

and size dispersion of the particles. In this regard, the solvent's electrical conductivity and dielectric constant are essential properties to consider while choosing the solvent. In order to answer to the many requirements of electrospraying, one may resolve to a mixture of solvents to balance different properties. If one were to choose this path, they must, however, be aware of the solvents miscibility and interactions with each other [25].

Process parameters

As for the set-up parameters, the most important is the applied voltage, that, as mentioned earlier, has to be high enough to overcome surface tension. Once in a working range, increasing the voltage will determine a decrease in particle size, however a too high voltage will lead to elongated particles or even beaded fibers. The distance between the collector and the needle (tip to collector, TTC), contributes to the strength of the electrical field: shorter TTC will result in a higher strength, obtaining smaller particles but reducing the time for solvent evaporation; longer TTC will lead to denser and bigger structures thanks to the higher solidification time but will need higher voltages to reach process stability. According to some researchers the needle gauge comes into play by defining the diameter of Taylor's cone's base, with smaller sizes being related to smaller particle diameters and more consistent processes [25], however others claim that gauge size isn't really relevant in the final morphology or particle size [24]. Moreover, it is possible to create multilayered particles using coaxial needles. This is a key feature employed in many drug delivery applications as it will be later discussed, thanks to the ability to produce a core-shell type particle in a one-step process (Figure 2.3). However, coaxial electrospraying introduces new complexities in the process, as the interactions between the two (or more) solutions and their flow rates will need to be taken into account to obtain the desired morphologies and sizes.

The last set-up contribution is offered by the collector. While many different geometries are available for electrospinning, electrospraying mainly utilizes two types: flat collectors, often covered by aluminum foil for ease of recovery, and collection baths, with a range of media such as water, ethanol, phosphate buffer or mixtures. When using a wet collector, the interaction between particle surface and the collection medium may determine different morphologies and even the chance to act on the electrosprayed material, for example, causing its crosslinking.

Environment parameters

The final category comprises the temperature and humidity where the production takes place. These two parameters can be fundamental in regards to the solvent evaporation, with

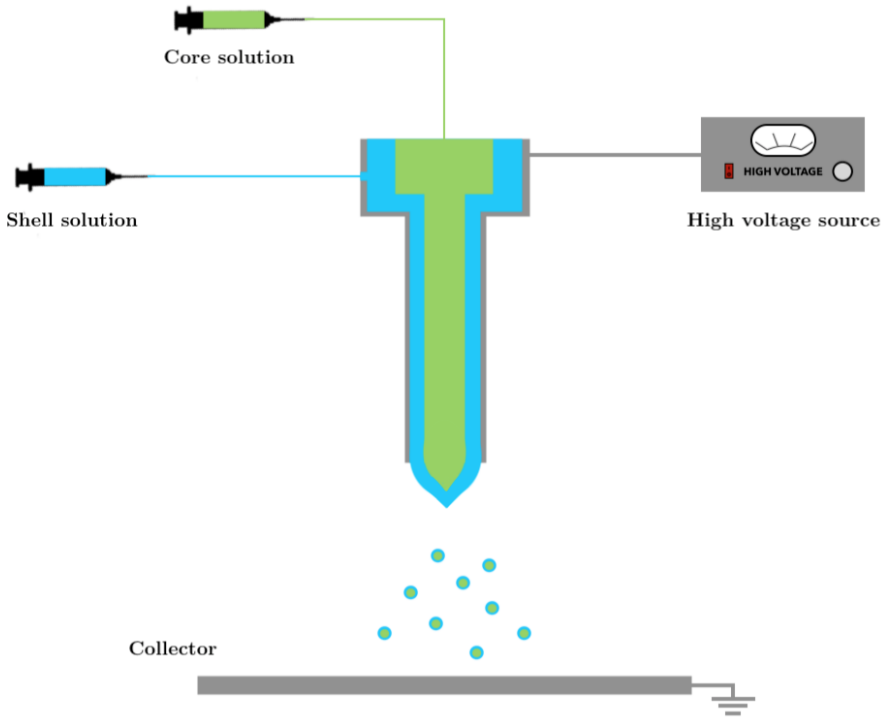

Figure 2.3 Coaxial set-up scheme.

higher temperatures usually favoring the process and higher humidity rates slowing it down. Researchers even report that humidity percentages over 60% RH can completely hinder the process, making it very difficult to obtain successful electrospraying. For this reason, it is advised that the electrospraying process be carried out in isolated structures, with as much control over the local temperature and humidity as possible [26].

2.2.2 Comparison to other methods, advantages and challenges

In order to better discuss the merits of utilizing coaxial electrospraying to produce drug-entrapping capsules, a brief introduction to other methods in use is needed. The first one is nanoprecipitation, preferred for the encapsulation of hydrophobic substances. The principle is to choose two miscible solvents, the first, called "solvent", needs to be able to solubilize the drug and the polymer, while the second, the "non-solvent", needs to not be able to do such thing. Nanoprecipitation into nanoparticles will happen when the solvent solution is added to the non-solvent. Since the non-solvent solution is usually aqueous, this method is not appropriate for hydrophilic drugs, that would tend to escape into the aqueous phase. Moreover, in order to achieve a core-shell structure, the iteration of the process is necessary

[27].

A second common technique is emulsion-diffusion, which can be used to encapsulate lipophilic or hydrophilic substances. Three phases are involved: if the active principle is lipophilic, it will be situated in the organic phase, together with the polymer, oil and an organic solvent, partially miscible with water; in the aqueous phase there will be a stabilizing agent; finally, water represents the dilution phase. At first the organic phase will be emulsified in the aqueous phase, then once water is added, the organic solvent will diffuse into the external phase, triggering particle formation. The organic solvent can then be safely evaporated under reduced pressure [28, 29].

Another, seemingly promising, method is double-emulsion. In a similar way to the previous one, a first emulsion is created and stabilized by using a hydrophobic surfactant. At this point, the emulsion is dispersed in an outer water phase, forming a second emulsion stabilized by a hydrophilic surfactant. The main issue with this technique deals with the challenge to stabilize the different interfaces during processing and storage, explaining why only few products have reached the market [29, 30].

The emulsion-coacervation method has been successfully employed to produce capsules with the use of natural polymers such as sodium alginate, chitosan and gelatine. It, once again, involves the creation of an emulsion of an organic phase, composed by the active substance, oil and sometimes a solvent, and an aqueous phase, with the polymer, water and a stabilizing agent. The following step depends on the chosen polymer as electrolytes, dehydration, temperature or pH change can be used to trigger the coacervation process, which will induce the formation of thin solvated shells. Another strategy employed is depositing a polymer coating onto the pre-formed nanoparticles. Several different methods can achieve this, either by modifying some of the previously presented ones such as nanoprecipitation or double emulsification, or ideating an *ad hoc* one [29].

Finally, layer-by-layer assembly is based on employing electrostatic attraction to envelop a colloidal template in a multi-layered capsule. The basic procedure is to adsorbe a polymeric layer onto a pre-formed colloid and repeating the same process for as many layers as needed. A crucial step is making sure that enough charged groups are present both on the side that will be adsorbed and on the side that will be exposed to the exterior, in order to allow for charge compensation when another layer will be attached. Restrictions regarding the materials used are evident, as an alternation of positively and negatively charged polymers is fundamental. Moreover, the technique presents a high number of complex, time consuming steps, as well as possible undesired interactions during close particle-particle encounters and other difficulties relative to the escape of polyelectrolytes from the capsules and the creation

of contraion aggregates [29].

In comparison to the previously presented techniques, the main advantage offered by the coaxial electrospraying technique is the possibility to obtain core-shell structured particles, double or even multi-layered, in a one-step procedure that requires minimal intervention from the user, once the process parameters are optimized. Moreover, a wide range of materials can be electrosprayed and encapsulated and since the process takes place at room temperature, biological structures, such as proteins, won't be denaturated. The free range in material choice also entails the possibility to combine the drug delivery treatment with other types of therapies with the purpose of increasing the effectiveness. For example, gold nanoparticles could be incorporated in the structure in order to perform an hyperthermal treatment that would bring changes in the cancerous environment benefiting the drug release and efficacy [17]. Other merits come from the simplicity and relative inexpensiveness of the set-up, together with the need for a lower amount of solvents, no requirement for the surfactants sometimes employed in other techniques and a generation of very little residue [31]. Moreover, the different combinations of collectors and needles offer a high versatility regarding the final products obtainable [25]. This adaptability is very useful in the control over the drug encapsulation and release, offering the chance to tailor the produced structure to one's desires. However, the high versatility of this technique doesn't come without issues. The main one being that there are many interlinked variables that come to play in the properties of the final structure, an important part relating to the process' set-up and environmental conditions, requiring an, at times lengthy, optimization period. For these reasons, some researchers rise doubts regarding the actual possibility of eventually scaling-up the production, highlighting that such a process might bring very different structures depending on small processing differences that could be present in an industrial setting [4, 32], thus underlying the need to assess such impact before considering commercialization. Another disadvantage is represented by the small amount of particles one can obtain at a time [31], as the typical feeding flow rates are in the order of mL/h or even $\mu L/h$ and, throughout the process, the collector will be progressively covered and, if the collecting substrate is not periodically changed, the voltage difference perceived by the fluid and the depositing particles, will vary, at best widening the usually narrow size distribution and, at worst, irremediably changing the morphology of the obtained structures. However, the low throughput deriving from the slow feeding flow rates might be solved by employing the technique's flexibility and setting up a multiplexed system with several nozzles acting in parallel [24].

2.2.3 Applications in drug delivery

After discussing the general frame of reference of the electrospraying technique in the production of drug delivery carriers, a few examples will be presented in this section concerning specific applications. While many different active principles have been successfully encapsulated, anticancer drugs are certainly among the most popular ones, with paclitaxel at the forefront of research efforts. Xie et al. report the production of paclitaxel-encapsulating PLGA particles, with diameter sizes ranging from 250 nm to 900 nm. The different dimensions were obtained by combining different sets of parameters such as: voltage, flow rate, concentration of polymer, drug, surfactants and salts, the latter ones responsible for an increase in solution conductivity linked with the smaller particles [33]. Another example of taxol entrapment is brought by Ding et al., who were able to do so employing PCL and successfully obtaining a high encapsulation efficiency together with release over 1 month in a sustained manner and a satisfying *in vitro* cellular uptake. Ding et al. also tried to take on the low production yield found in the electrospraying technique, reporting an improvement of around 80% owed to an increase in ventilation and better discharge of residual charges on the collecting substrate [34]. Two formulations of multi-drug particles obtained with coaxial electrospraying were studied by Nie et al. [35] with brain tumor as the intended application. The compositions differed in the location of paclitaxel and suramin, with the first having a PLA/paclitaxel core and a PLGA/suramin shell and the second swapping the position of the two drugs. While both formulations showed improved tumor inhibition, *in vitro* and in mice inoculated with subcutaneous gliomas, compared to the free drugs, the capsules with suramin in the core presented better apoptosis results over the longer time [35]. Coaxial electrospraying was also employed to produce smart multifunctional TiO_2 capsules (Figure 2.4). The structure involved an outer layer of TiO_2 with an inner core containing Fe_3O_4, for magnetic targeting, and graphene quantum dots, for imaging purposes and paclitaxel. The drug release was triggered by ultrasound stimulation, whose stimulation length was used to control the release profile. Li et al. report that the titanium oxide shell was successful in limiting the initial burst release of the drug [5].

Yin et al. prepared four formulations of PLA particles loaded with gambogic acid, varying in sizes from about 70 nm to 7.5 μm (Figure 2.5). After the samples were injected in mice, it was possible to observe improved liver uptake for the two formulations under 200 nm, a spleen accumulation for the 400 nm one and a collection in the lungs for the microscale one, highlighting the key contribution that size has in particle biodistribution. The second smallest composition (185.6 $\pm$ 33.8 nm), was then tested against model mice hepatocellular carcinoma, showing improved antitumor efficacy due not only to the effective passive targeting

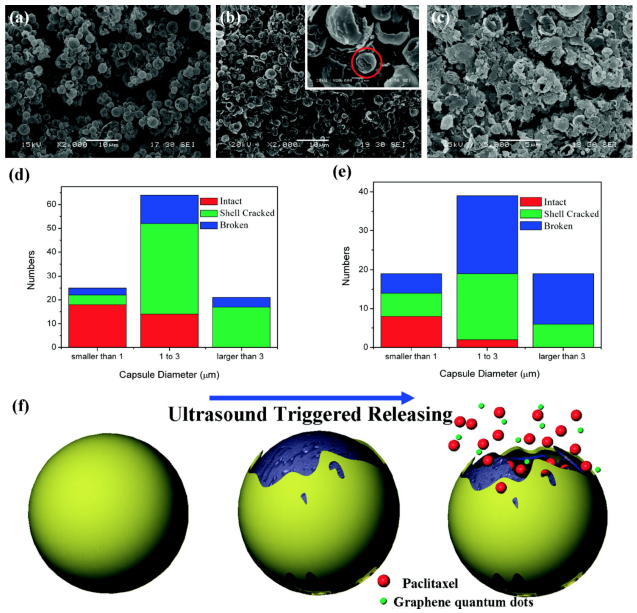

Figure 2.4 Smart multifunctional TiO_2 capsules capable of: magnetic targeting, imaging through quantum dots and paclitaxel delivery. (a) through (c), SEM images of the particles ultrasound for: (a) 5 min; (b) 15 min; (c) 30 min. (d) and (e), size distribution and particles' status of sample ultrasound for: 5 min; 15 min. (f) representation of shell cracking mechanism until drug release from the particles with increasing ultrasound time [5].

but also to higher bioavailability in the body and increased stability of the drug [6].

Another example of multiple delivery comes from Lou et al., who combined DOX and the anti-angiogenesis agent combretastatin A4 (CA4), the first in the shell and the second in the core. Once again, two different formulations were tested, both with a PLGA shell, while the core was PVP in one case and PCL in the other. When tested *in vitro* the first type of particles showed a faster and overall higher release compared to the second, the hypothesis being that the hydrophilic core had more affinity with the incubation media [36]. For what concerns natural polymers, one can look at the work of Songsurang et al., which used the electrospray technique to produce DOX-entrapping chitosan particles of around 300 to 570 nm, then crosslinked into an aqueous solution containing tripolyphosphate (TPP) in order to increase the drug release time. Nevertheless, the particles showed an intial burst release in the first two hours, followed by a slower release for additional five hours [37].

Another interesting application was the use of genetically engineered elastin-like polypeptides (ELPs) as an encapsulating polymer for DOX (Figure 2.6). The ELPs show a pH-dependent solubility so the particles were tested at three pH values to analyze whether the different behaviours could be employed in the drug release. The samples at coacervation

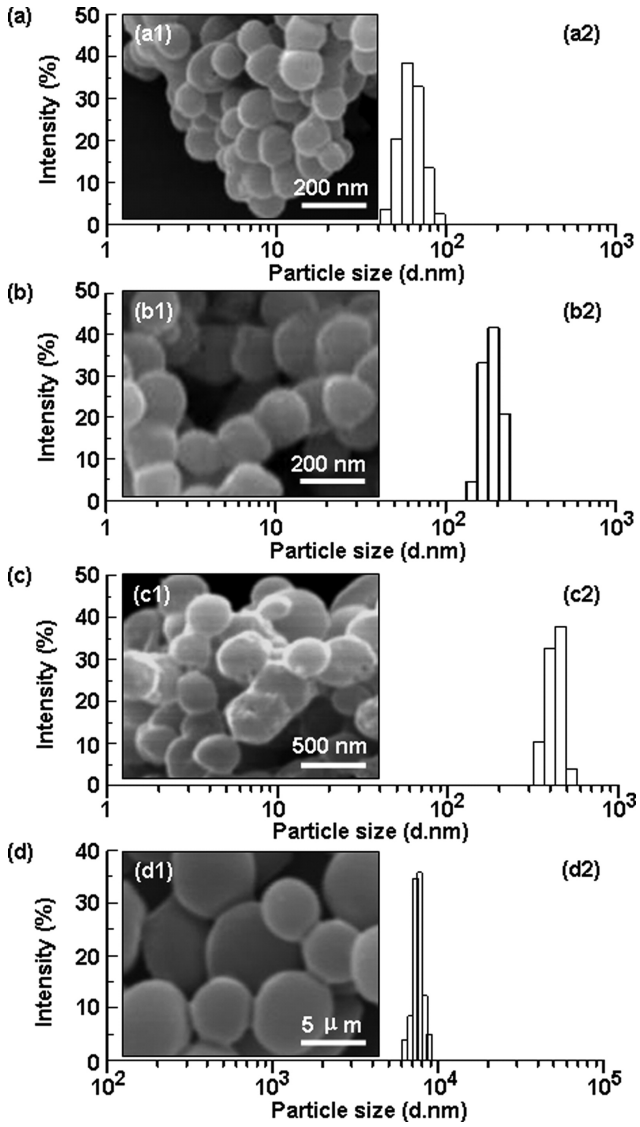

Figure 2.5 PLA particles loaded with gambogic acid. SEM images and particle size distribution of: (a) 70 nm particles; (b) 185.6 nm particles; (c) 358 nm particles; (d) 7.5 μm particles [6].

levels (2.5 pH) showed the lowest initial burst but only 70% of the drug was released in total, while the other two conditions (5.5 and 7.5) had reached complete release after only 15 minutes [7]. Finally, while not strictly involving a drug, an anticancer treatment produced with the electrospraying technique has been studied within the framework of gene therapy. In fact, Park et al. report that they were able to encapsulate adenovirus in alginate beads electrosprayed into a solution containing $CaCl_2$, for crosslinking purposes. The particles were used for the *in vitro* transduction of U343 glioma cells, exhibiting a sustained release over the course of 7 days with high transduction efficiency in cancerous cells. They hypothesize that

this type of formulation would overcome typical issues encountered in gene therapy, such as virus aggregation and accumulation, possible immune responses to the vector and a limited therapeutic effect due to liver accumulation [38].

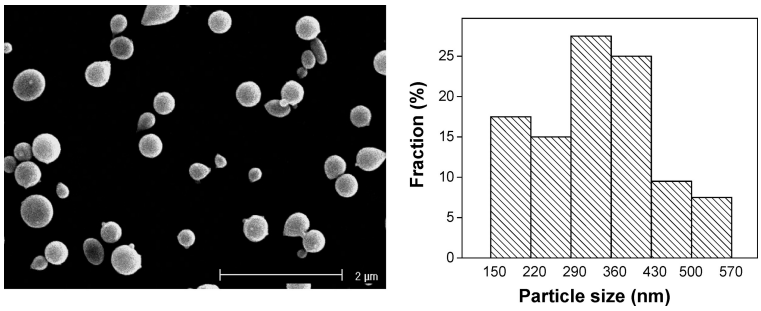

Figure 2.6 Electrosprayed ELP-DOX particles: (a) SEM image and (b) particle size distribution [7].

After a brief overlook on the novelties and achievements brought on by the use of the electrospraying technique, the following chapters will introduce the materials and methods employed in the present work as well as illustrate the process of trial and error that lead to the final formulation. While most of the works mentioned in this chapter were presented to highlight the many promising paths that electrospraying could take, the product of this thesis aimed to combine the innovation of the coaxial set-up, found in Nie et al. and Li et al. [5, 35], with the straightforward application of Xie et al. and Ding et al. [33, 34]. One of the key differences in regards to these examples will be represented by the drug chosen to be encapsulated, an anthracycline, which seem to be less favoured in electrospraying applications compared to taxols, such as the ones employed in the aforementioned works.

CHAPTER 3 MATERIALS AND METHODS

3.1 Choice of materials

In order to define the requirements for an anti-cancer structure intended for breast cancer applications, the literature of available treatments was studied. Once these characteristics were identified, the polymers considered most appropriate were evaluated for the particle's outer shell, specifically in regards to their compliance with the chosen degradation time-frame and process. Finally, a poly(lactic-co-glycolic acid) (PLGA, 30,000 - 60,000 g/mol) copolymer with a lactide/glycolide molar ratio of 50/50 was chosen. Ibuprofen was used as a test drug in place of DOX, in order to reduce the exposure risks and cost while optimizing the electrospraying parameters. The following materials were acquired from Sigma Aldrich: poly(lactic-co-glycolic acid) (PLGA), ibuprofen, doxorubicin (DOX), acetonitrile (MeCN), dimethylformamide (DMF) and tetrahydrofuran (THF).

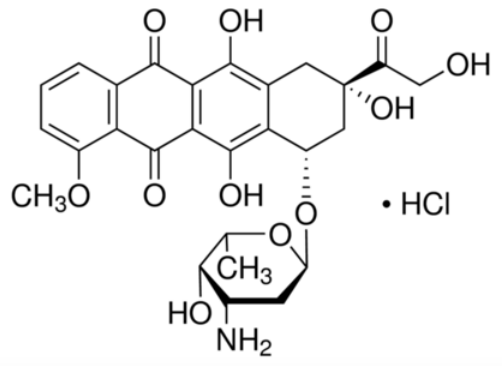

(a)

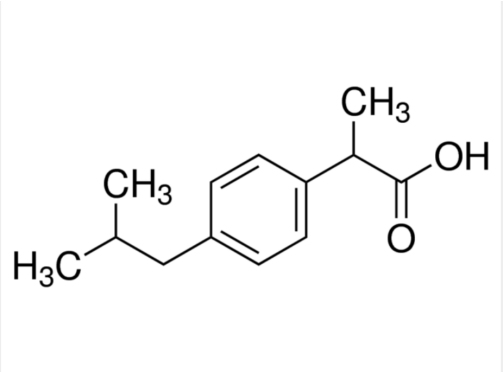

(b)

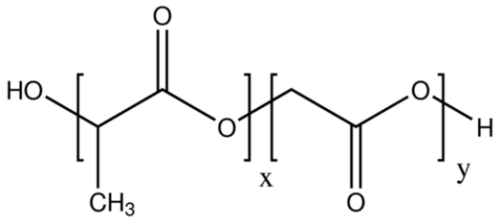

(c)

Figure 3.1 Chemical structures of the materials involved: a) DOX; (b) ibuprofen; c) PLGA [8].

3.2 Electrospraying optimization

Several solution compositions were examined, at first considering the same single solvent for both the inner and outer solution. THF and MeCN were the two solvents considered for this purpose; they were then mixed and tested at various ratios, with a final addition of DMF. It was then decided to employ two different solutions for the outer and inner nozzles, using different combinations for the shell one, in particular. The polymer and drug amounts tested were between 2 and 5 wt%. A balance between evaporation rate and electrical conductivity was finally reached with a solution made up of 5 wt% ibuprofen in 40/60 THF/MeCN for the core and a solution of 5 wt% PLGA in 60/40 DMF/MeCN for the shell. The two solutions were always prepared and left on a mixing plate (PC-420D, CORNING) overnight the day before electrospraying.

Once the solutions were properly mixed, they were loaded in two syringes which where then inserted in their respective slots in the external pumps provided with the Tong Li Electrospinning Unit (Figure 3.2 and 3.3c). At first, the flow rates of the two solutions were kept identical varying from 0.2 to 1 mL/h. As the composition of the two solutions evolved, the flow rates were dissociated, settling on a higher one for the external fluid, from 0.2 to 0.7 mL/h, and a lower one for the core, from 0.1 to 0.2 mL/h. Finally, the two main flow rate combinations tested were: combination A, with the core solution at 0.1 mL/h and the shell one at 0.3 mL/h; combination B, with the inner solution at 0.2 mL/h and the shell one at 0.5 mL/h. The voltage was applied initially with a positive spinneret and a grounded collector, with a range between 7 and 20 kV, later the collector was put at a negative state, with a cumulative applied potential between 9 and 27 kV. The collector had voltages ranging from -4 to -2 kV, while the spinneret was tested between 7 and 24 kV. The needles used throughout the process were a 26G gauge (0.45 mm outer diameter; 0.23 inner diameter) for the inner one and a 19G gauge (1.06 mm outer diameter; 0.70 mm inner diameter) for the outer one. In regards with the TTC distance, it was varied between 2.5 to 38 cm, in compliance to changes in other parameters. Initially, a rotating drum was used to maximize the electrospraying surface area, this was later replaced by the flat collection plate visible in Figure 3.2 and 3.3b. In order to facilitate particle collection, several different substrates were tested to be draped over the collecting surface, such as aluminum foil, non-stick aluminum foil, parchment paper, silicone-sprayed aluminum foil and most notably a wet collection method. This wet set-up, involving an ethanol (acquired from Sigma Aldrich) bath, was created and tested (Figure 3.4), before returning to the dry aluminum foil one as the particle recovery issues were resolved by putting the samples under vacuum for 24 hours before collection. While the final parameters for the Tong Li set-up were as follows, the extensive list of all the parameters used and their

combinations can be found in the tables in Appendix A: core solution of 5 wt% ibuprofen in 40/60 THF/MeCN, shell solution of 5 wt% PLGA in 60/40 DMF/MeCN; combination A for the flow rate; -3 kV at the collector, 12 kV at the spinneret; a 26G needle paired with a 19G one; TTC distance of 21 cm between the spinneret and the flat collector with aluminum foil.

Figure 3.2 Tong Li Electrospinning Unit (Shenzhen Tong Li Tech Co. LTD).

3.2.1 Adjustments and Big box set-up

When the lock-down was put in place, in March, the parameters had been optimized and the particles needed for the degradation tests were about to be produced. Unfortunately, once access to the laboratories was re-established, in July, the environmental conditions had changed, with a spike in the humidity from around 30 RH% to a range between 60-70 RH%. As stated in the literature, such high levels of humidity have a great impact on the electrospraying process and, despite many efforts to keep employing the Tong Li and the previously optimized parameters, a change of set-up was deemed necessary with the hope of being able to quickly proceed towards the following tests.

The new set-up was a combination of the three set-ups available in the laboratory: a high voltage source (ES Series; Gamma High Voltage Research, Inc.) and two pumps (Standard

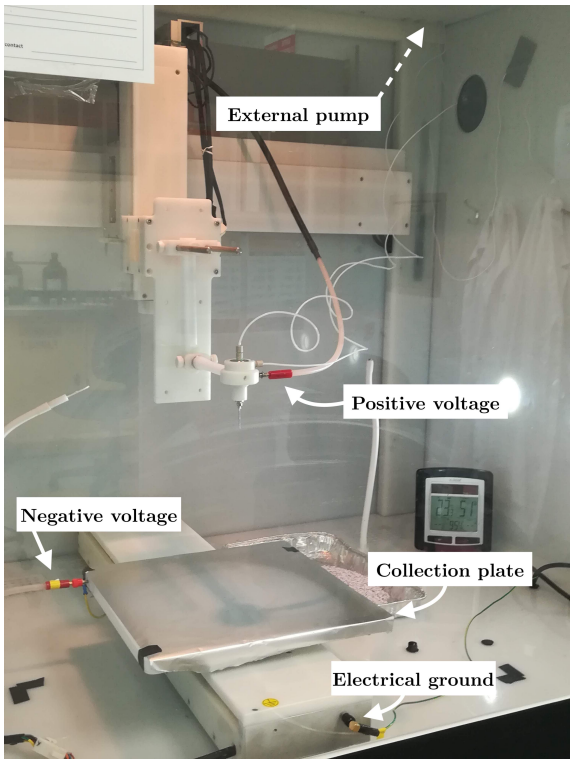

(a)

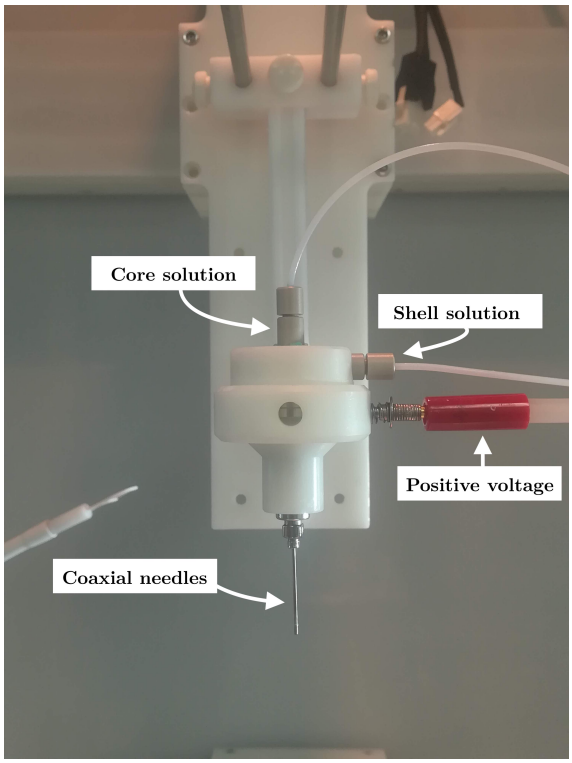

(b)

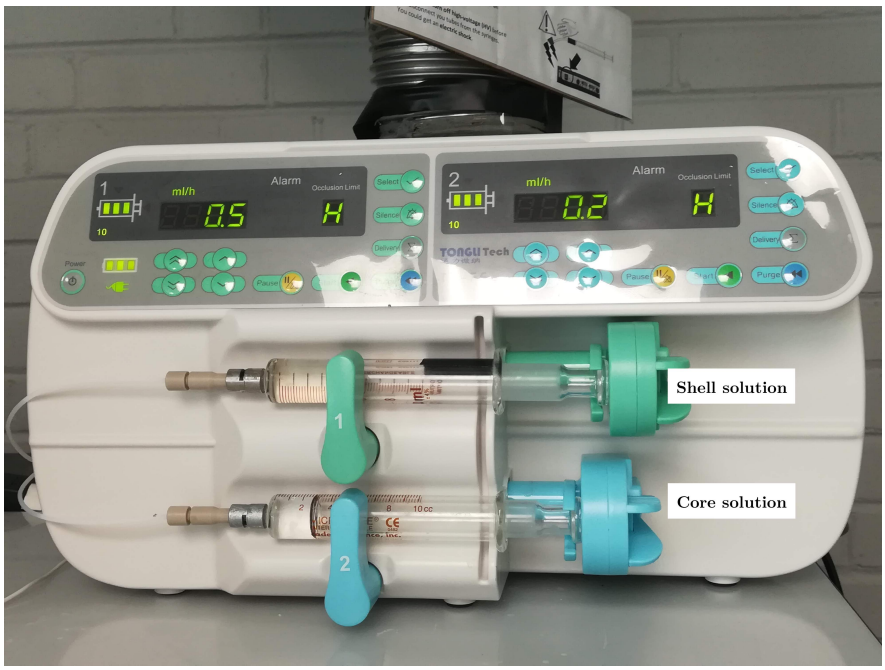

(c)

Figure 3.3 Set-up close-ups of Tong Li Electrospinning Unit (Shenzhen Tong Li Tech Co. LTD): (a) internal Tong Li set-up; (b) coaxial system; (c) external pump.

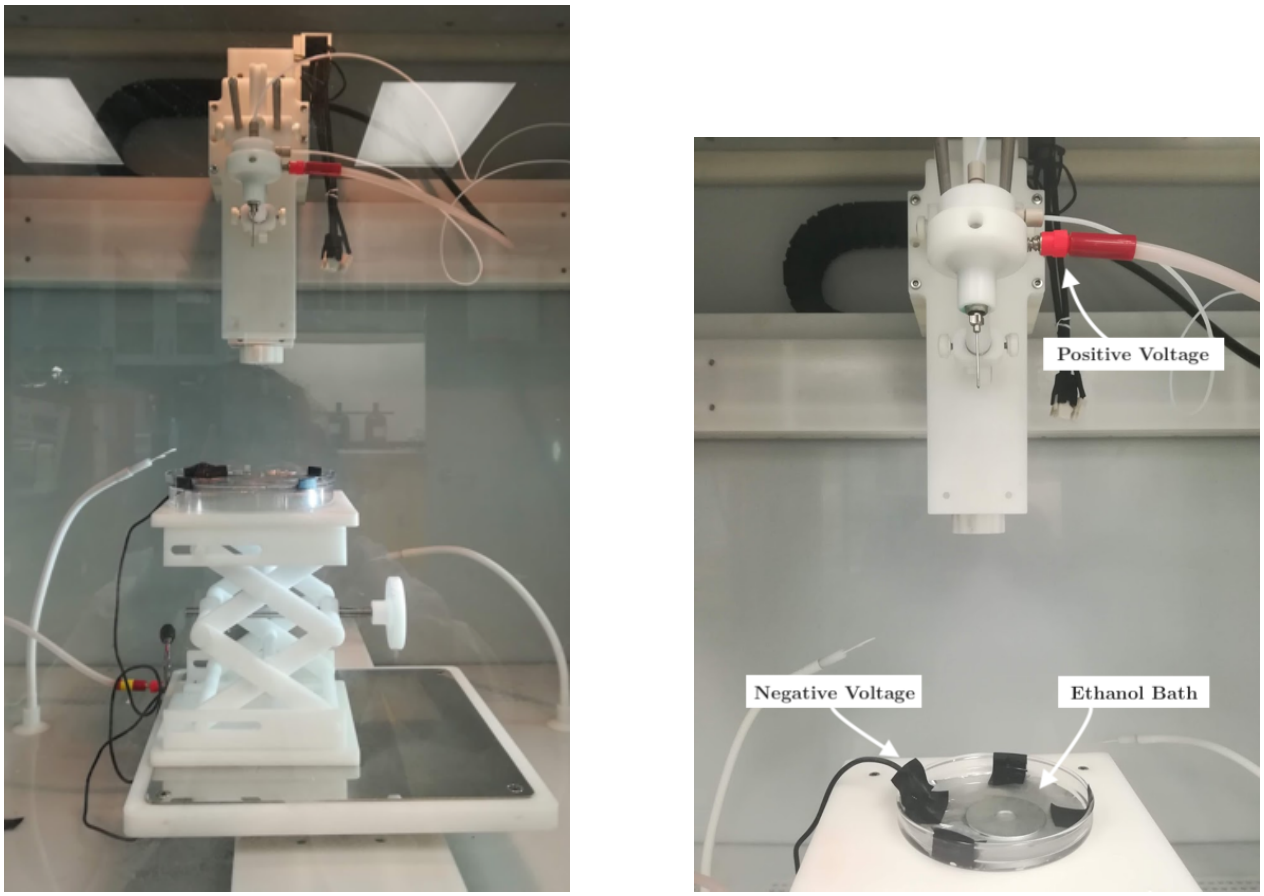

(a) (b)

Figure 3.4 (a) Wet set-up, Tong Li Electrospinning Unit (Shenzhen Tong Li Tech Co. LTD); (b) close up.

Infuse/Withdraw PHD ULTRA^{TM} 4400 Programmable Syringe Pump, Remote Infusion Only PHD ULTRA^{TM} Syringe Pumps; Harvard Apparatus) from two set-ups built in-house from previous researchers in the group, and the coaxial spinneret (Tong Li Tech Co. LTD) from the Tong Li set-up (Figure 3.5). This set-up, referred to as the Big box, was chosen as it had a pre-installed feed of dried compressed air, which was validated in previous projects from the research group as a solution to keep the humidity at operating values. Initially, equivalent parameters to the optimized ones from the Tong Li were tested, however some adjustments were necessary to address the change. The total voltage difference was kept at 15 kV, with the positive electrode connected to the spinneret and a grounded collector, as the new set-up did not offer the possibility to apply negative voltage. The flow rates tested were the two combinations already selected with the Tong Li. The TTC distance was varied in a range from 12 to 30 cm, finally settling at 15 cm. The percentage of PLGA was increased from 5 to 7%. Once more, the list of parameters tested and their combinations can be found in table

A.13 in Appendix A.

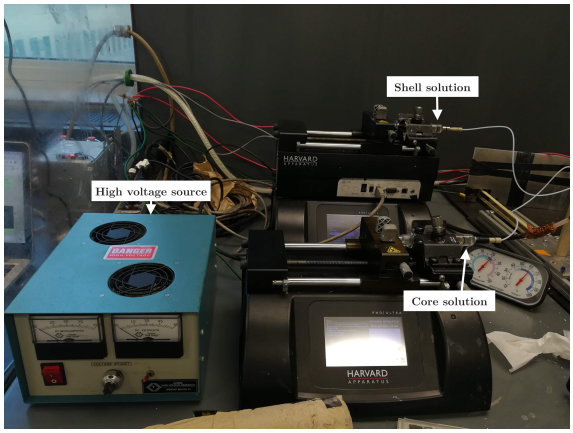

(a)

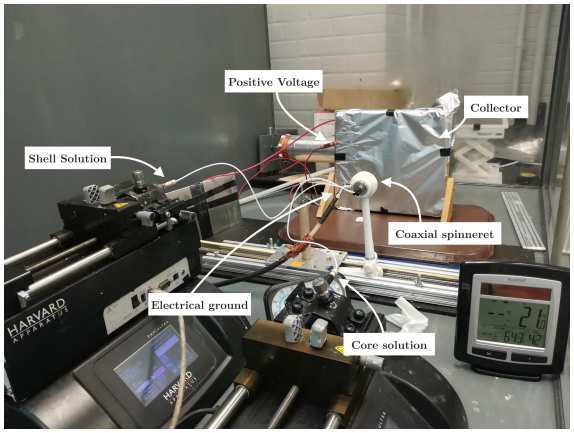

(b)

Figure 3.5 Big box set-up: (a) pumps and high voltage source; (b) coaxial spinneret and collector;

3.3 Particle characterization

3.3.1 Scanning Electron Microscopy (SEM)

The morphology of the particles was observed using Scanning Electron Microscopy (SEM, TM3030Plus tabletop microscope, HITACHI), after depositing a chromium layer of 10 nm thorough sputter coating (Q150T ES, Quorum). The size was then analyzed as mentioned in Section 3.5.

3.4 Degradation tests

The particles for the degradation tests were produced by using the Big box set-up with the following parameters: a solution of 5 wt% ibuprofen in 40/60 THF/MeCN for the core and 7 wt% PLGA in 60/40 DMF/MeCN for the shell, 15 cm as TTC distance, 15 kV as applied voltage and a flow rate of 0.1 mL/h for the core solution and 0.3 mL/h for the shell one. SEM was carried out and the images were analyzed as mentioned in Sections 3.3 and 3.5, in order to confirm the initial morphology and particle size. The particles were then collected and divided between 22 sample vials, where they were submerged by 2 mL of Phosphate Buffer Saline (PBS) solution each. Half of the samples had a PBS solution with a pH of 7.4 (Group A), the other half one of 6.6 (Group B), the latter pH condition being chosen to represent a slightly more acidic, tumor-like environment. The samples and two control vials containing

PBS alone were then put in an incubator (Blue M Model 200A bacteriological incubator – gravity convection) at 37°C for 4 weeks. Pairs of samples from the two groups were taken out each week to be dried for weight monitoring or to be freezed at -20°C for later freeze drying and observation with SEM. Fourier-transform infrared spectroscopy (FTIR) (PerkinElmer, Spectrum 65, FT-IR Spectrometer) was carried out in reflection mode before PBS immersion and at specific time points after (1, 2, 21, 24, 31 hours, then after 8, 15, 22 and 28 days). 10 μL of the solution were released on the FTIR crystal and the spectra were collected both with the liquid and after letting it dry for around 10 minutes. The pH in the samples was also monitored throughout the process with the use of a pH-meter (PC 2700 Benchtop Meter, Oakton).

3.5 Image analysis

The SEM images were processed and analyzed through the open source image processing package Fiji [39]. The treatment was carried out in order to better identify and measure the produced particles. The following steps were performed: the background was subtracted from the image, which was subjected to an Auto-Threshold analysis in order to identify the best threshold to perform a transformation from grayscale to binary. Once the black and white image was obtained, noise removal was carried out by removing black pixel outliers, as defined by Fiji's plugin, and using the despeckle and watershed functions. At this point, particle analysis was run, with a specific interest in the area of the identified particles. From this parameter, further calculations using Excel allowed to gather the particles radii, the average radius and its variance. Initially this process was carried out manually, once the appropriate processing procedure was identified, a macro, which can be found in Figure 3.6, was developed in order to reduce the processing times from 10 to 15 minutes/picture to 2 minutes/picture.

```
dir = File.directory;
name = File.nameWithoutExtension;
selectWindow(name + ".tif");
//setTool("line");
makeLine(512, 978, 1262, 978);
run("Set Scale...", "distance=750 known=20 pixel=1 unit=um");
//setTool("rectangle");
makeRectangle(0, 2, 1278, 954);
run("Crop");
run("Subtract Background...", "rolling=50 sliding disable");
run("Auto Threshold", "method=[Try all] show");
waitForUser("Select threshold, then ok");
run("Convert to Mask");
run("Remove Outliers...", "radius=2 threshold=50 which=Dark");
run("Despeckle");
run("Watershed");
run("Analyze Particles...", "size=0.02-Infinity circularity=0.30-1.00 exclude clear summarize add");
roiManager("Show All without labels");
waitForUser("Check if parameters are ok, if not run Analyse Particles, then ok")
selectWindow("ROI Manager");
run("Select All");
roiManager("Measure");
selectWindow("Results");
Table.sort("Area");
selectWindow(name + ".tif");
saveAs("Tiff", dir + name + "_bin.tif");
saveAs("results",  dir + name + ".csv");
```

Figure 3.6 Code developed to improve the image processing and analysis time.

CHAPTER 4 RESULTS AND DISCUSSION

4.1 Choice of materials

Since the prospective application that is considered in the present thesis work was breast cancer, the most common chemotherapeutic agents in use were considered as potential drugs for this research. Ultimately, the choice fell on the class of anthracyclines, more specifically on DOX, as it provided the chance for comparison with non-polymeric controlled delivery formulations while not being as commonly encapsulated through electrospraying as taxol-based drugs. Moreover, DOX is known to increase the risk of long-term cardiomyopathies in patients taking even very limited dosages, with a maximum lifetime dose set at 500 mg/m^2 [40]. Taking inspiration from classical therapies and liposome-based approved drugs, the timeframe of the delivery was identified to be over the course of 3-4 weeks. By looking into the literature, such release period, at a dimensional scale under the microscopic one, was achievable either by employing crosslinked chitosan or 50/50 PLGA of a molecular weight around 45 kDa [21, 41]. PLGA was preferred over chitosan for the possibility to avoid the crosslinking step, which would have been necessary as to increase the release period and to ensure the entrapment of the slightly positively charged DOX into a positively charged polymer. Ibuprofen was chosen as the test drug as it was solvable in the solutions prepared for DOX and it would allow to safely and cheaply optimize the electrospraying parameters.

4.2 Electrospraying optimization

4.2.1 Initial optimization

The initial optimization tests were focused on finding the optimal combinations for the solutions, the flow rate and the applied voltage. In fact, the TTC distance was kept constant at around 10 cm, while three flow rates (0.5, 0.7 and 1 mL/h) and three applied voltages (7, 10, 15 kV) were tested against each other and the different solutions produced. As to avoid mentioning the parameters for each result referenced, appropriate tables are reported in Appendix A. Moreover, considering the large amount of trials carried out throughout the optimization process, only the most significant results from each test group will be presented in this work.

The first tests utilized THF as the sole solvent, the reasoning was to reduce the number of solvents used and hopefully be able to employ the same solvent for both solutions, which

would allow to disregard interface interactions between different liquids, and keeping an identical flow rate for both. While it is to be noted that the partially formed spheres may be due to the fact that the polymer and drug concentrations were only of 2 wt% (Figure 4.1a), the particles still present a rough, highly porous morphology. Moreover, the sizes of the more full spheres, are usually in the microscale, around 1-4 μm. During the same tests, 0.7 mL/h was identified as the maximum flow rate able to obtain distinct, separated particles, as the tested 1 mL/h resulted in highly connected structures lacking any specific shape (Figure 4.1b). The source of the particles' porosity was identified in a too quick evaporation of THF, which was replaced by MeCN in the next experiments. The use of MeCN alone, however did not bring about any improvements, as, while the evaporation was supposed to be longer, MeCN is more conductive than THF, which resulted, in the best case, in slivers of polymer to be delivered upon the collector (Figure 4.2).

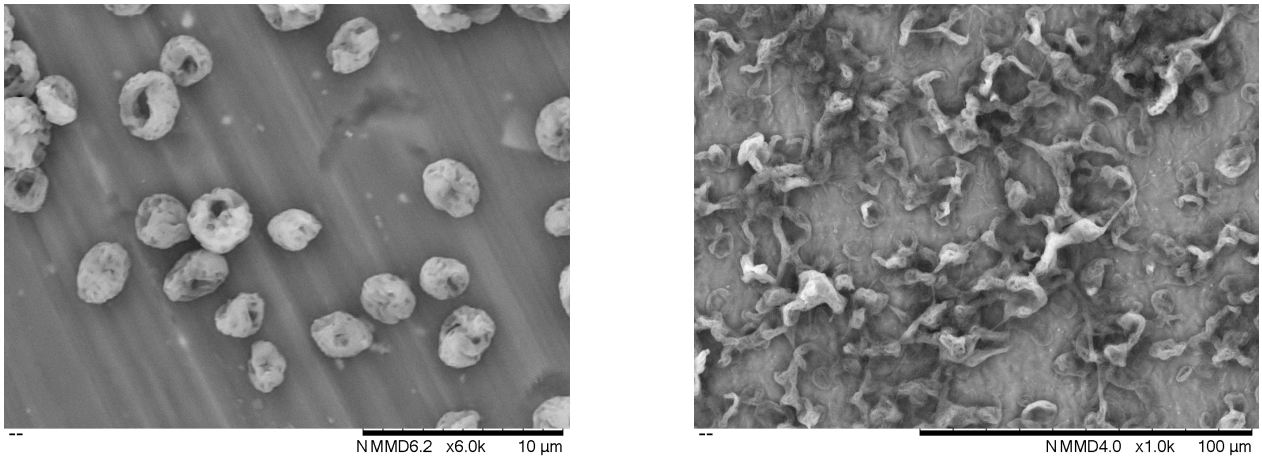

(a) (b)

Figure 4.1 Examples of tests with the use of THF as lone solvent with 2 wt% for both the drug and the polymer: (a) Porous incomplete particles; (b) Inconsistencies caused by a too high flow rate of 1 mL/h; Scale bar: (a) 10 μm; (b) 100 μm.

It was then decided to mix the two solvents in a 50/50 ratio in order to reach a mid-point between THF's too fast evaporation and the increased conductivity from MeCN. These trials showed a more consistent spherical shape than previous ones but the particles continued to be incomplete despite a reduction in size by half brought by the increased solution conductivity (Figure 4.3).

For this reason, the following experiments focused on increasing the polymer and drug contents in the solution, at first to 3 wt% and then to the final 5 wt%, value at which the fully formed particles were obtained. As reported in Figures 4.4a and 4.4b, the 3 wt% particles

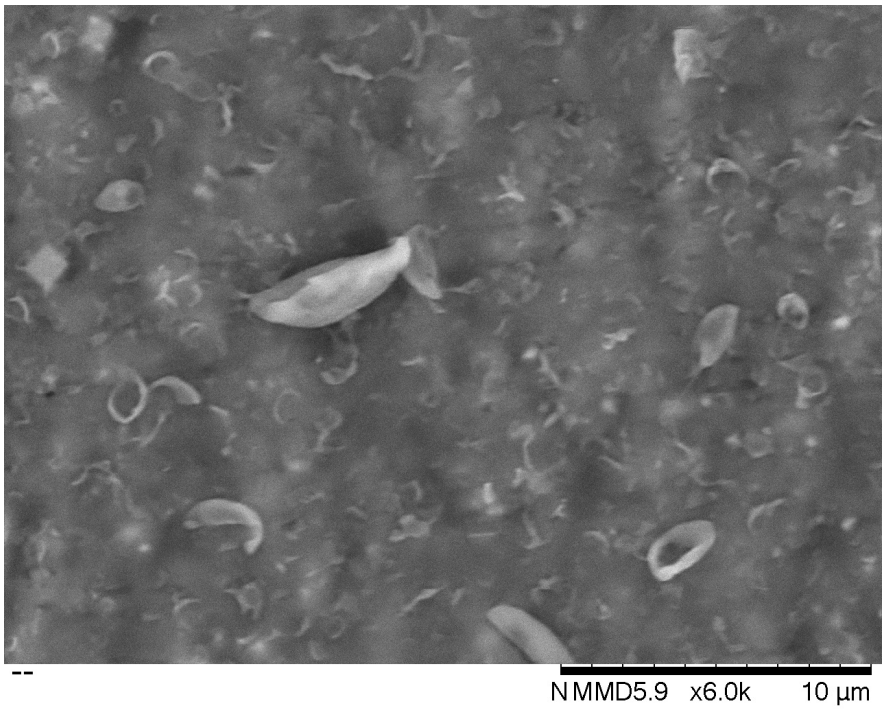

Figure 4.2 Example of tests with the use of MeCN as lone solvent with 2 wt% for both the drug and the polymer. Scale bar: 10 μm.

had a reduced porosity in comparison to the ones obtained from THF alone while being still not fully complete. On the contrary, once the polymer and drug concentrations were brought up to 5 wt%, the particles were finally rid of the holes and dips previously observed (Figure 4.5). The following test (test 13, see Table A.2), was focused on evaluating the reproducibility of the parameters from test 12, as well as introducing a lower flow rate of 0.2 mL/h. The main takeaway from this experiment was brought by the observation of the needle tip at a flow rate of 0.7 mL/h. In fact, this configuration lead to the formation of a multi-jet cone, which explains the presence of bigger particles (Figures 4.5 and 4.6). Moreover, the presence of multi-jets introduces inconsistencies in dimension and morphology between trials using the same parameters, as can be seen in Figure 4.7, trial 13H shows a higher average size in comparison to trial 12B, whilst the opposite happens for trial 13G and 12H (Parameters from both sets of trials are available in Table A.2, Appendix A).

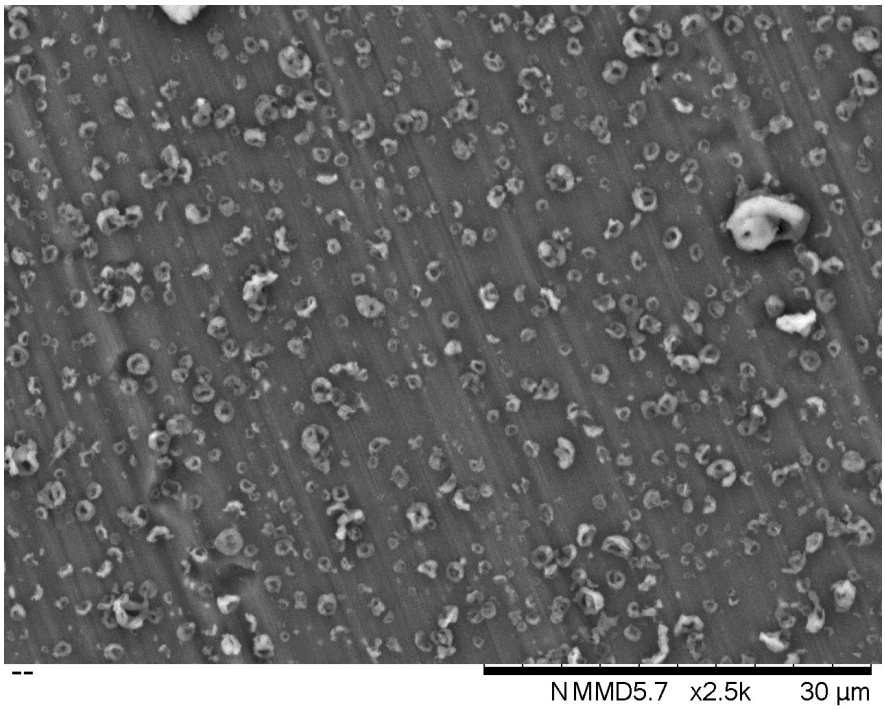

Figure 4.3 The first results from the 50/50 combination of THF and MeCN (test 10C, see Table A.1, Appendix A). Scale bar: 30 μm.

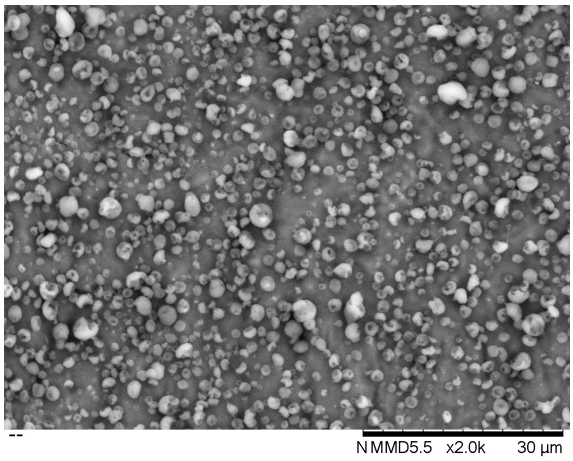

(a)

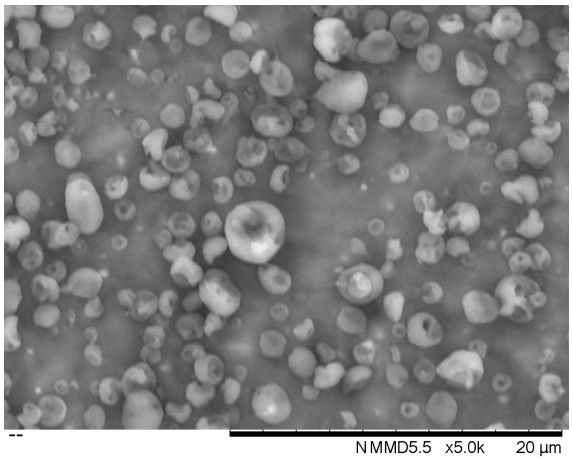

(b)

Figure 4.4 THF and MeCN with 3 wt% polymer and drug (test 11A, see Table A.1, Appendix A). (a), (b): particles with a reduced porosity in comparison to ones obtained from THF alone but not fully complete. Scale bar: (a) 30 μm; (b) 20 μm.

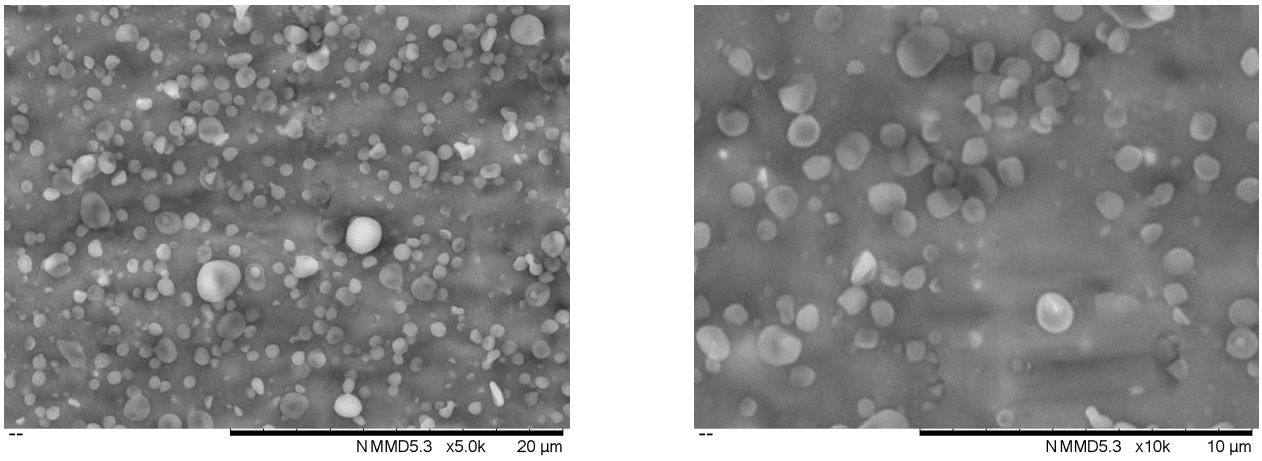

(a) (b)

Figure 4.5 THF and MeCN with 5 wt% polymer and drug (test 12B, see Table A.2, Appendix A). The particles show no evident porosity. Scale bar: (a) 20 μm; (b) 10 μm.

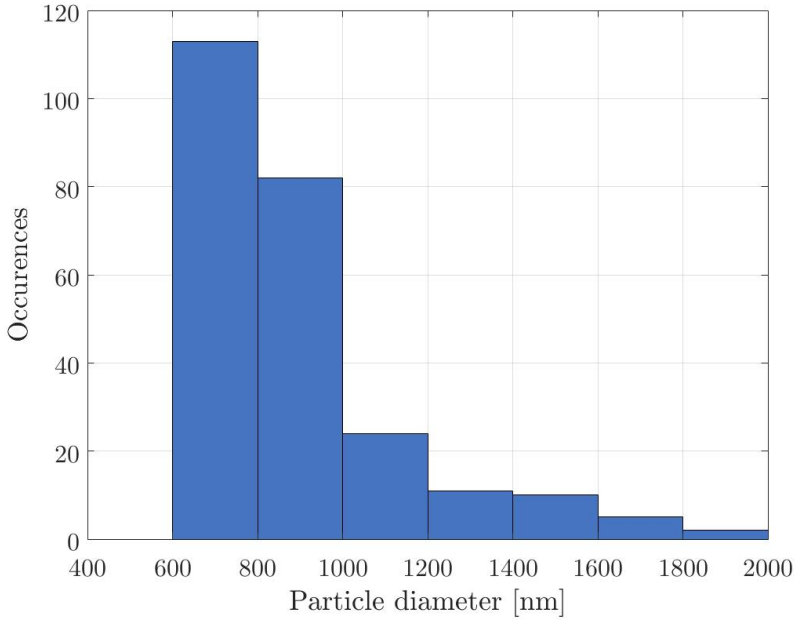

Figure 4.6 Distribution size of the particles obtained in test 12B (For parameters, see Table A.1, Appendix A).

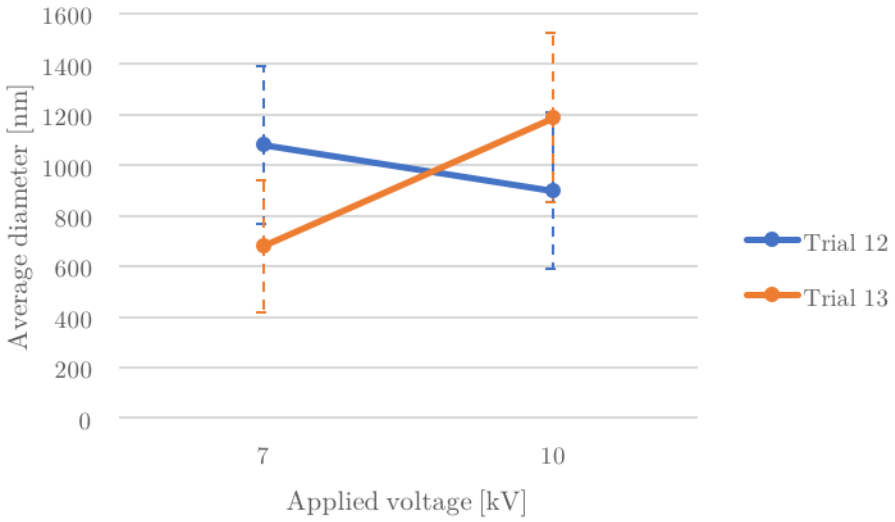

Figure 4.7 Comparison between the average values for the particles obtained with 0.7 mL/h as flow rate in trial 12 and 13. In order from left to right: 12H, 13C, 12B, 13H. (For parameters, see Table A.1, Appendix A).

4.2.2 Size optimization

Once the solution composition had reached a first optimization (i.e., 5 wt% of ibuprofen and PLGA in 50/50 THF/MeCN), the focus shifted on reducing particle size under the 800 nm threshold. Different trials (15, 16, 17) attempted to do so by reducing TTC distance (for parameters, see Table A.4, Appendix A). Trial 15 involved a TTC distance of 2.5 cm, the shortest distance tested in this work, whereas trial 16 and 17 had one of 4.5 cm. The results were a highly connected, almost mat-like structure for trial 15 (Figure 4.8a), and particles with inconsistent dimensions and morphologies, connected by thin filaments for trial 16 and 17 (Figure 4.8b). These findings are related to a reduced evaporation time, which leads the droplets to deposit with solvent still present in the structures. The liquid will consequently increase the cohesion between particles and form interconnected morphologies, the more solvent is present, the bigger will be the effect.

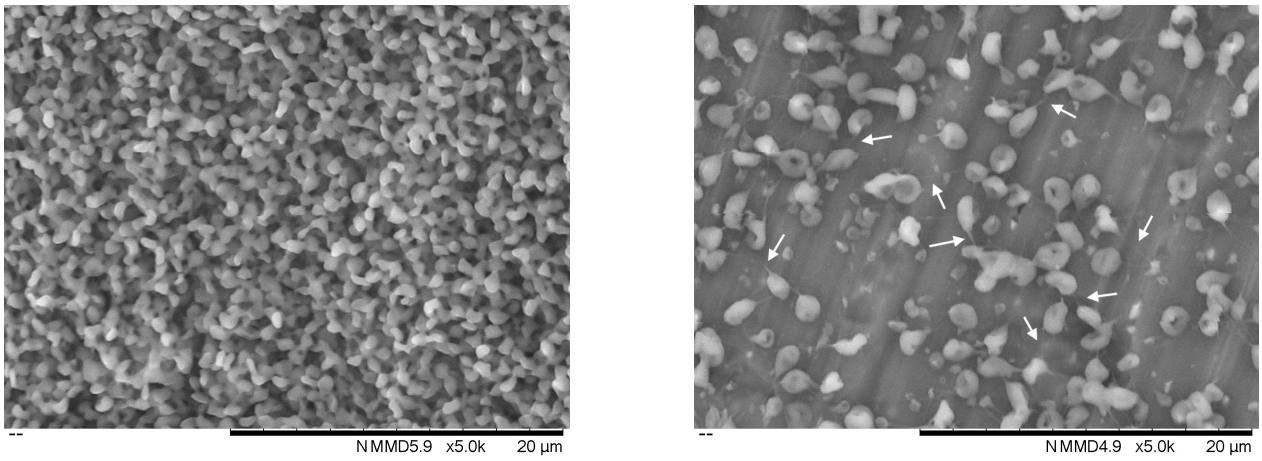

(a) (b)

Figure 4.8 Results from the reduction of TTC distance: (a) connected mat-like particles (Test 15E); (b) particles with several shapes and sizes, connected by thin filaments, some of these filaments are highlighted by the white arrows (Test 16H); Scale bar: (a), (b) 20 μm. (For parameters, see Table A.4, Appendix A).

Another route considered to reduce particle size, was investigating further solution optimization. As mentioned earlier, MeCN is more conductive than THF, and increasing solution conductivity is a way to obtain smaller particles (see Chapter 2). This inspired trials 14 and 18 through 20 (for parameters, see Tables A.3 and A.5, Appendix A): the first with a 30/70 THF/MeCN ratio, the following with a 40/60 split. In the first case (Figure 4.9a), the conductivity increased to the point that the droplets reached the collecting plate before they could form the entanglements necessary to form and hold a consistently spherical shape. For

the 40/60 ratio, most of the parameter combinations tried resulted in fragments and slivers being deposited, often presenting multiple-jet cones at the nozzle of the coaxial system. An exception was reported when the TTC distance was set to 2.5 cm (Figure 4.9b). While there were still some particles over 1000 nm, the majority was under the desired limit of 800 nm, with an average size of around 700 nm (Figure 4.10).

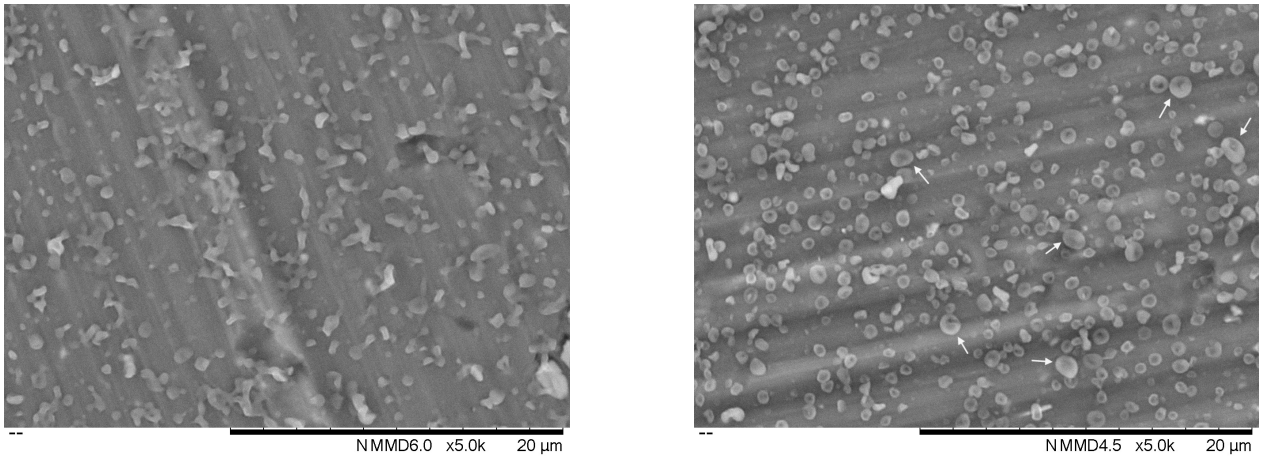

(a) (b)

Figure 4.9 Results from the reduction of TTC distance: (a) particles with several shapes and sizes, with 30/70 THF/MeCN as solvent (Test 14C, see Table A.3, Appendix A); (b) spherical particles, average diameter 700 nm, standard deviation ±240 nm, with 40/60 THF/MeCN as solvent (Test 19H, see Table A.5, Appendix A). The arrows highlight some of the particles with a diameter over 1000 nm; Scale bar: (a), (b) 20 μm.

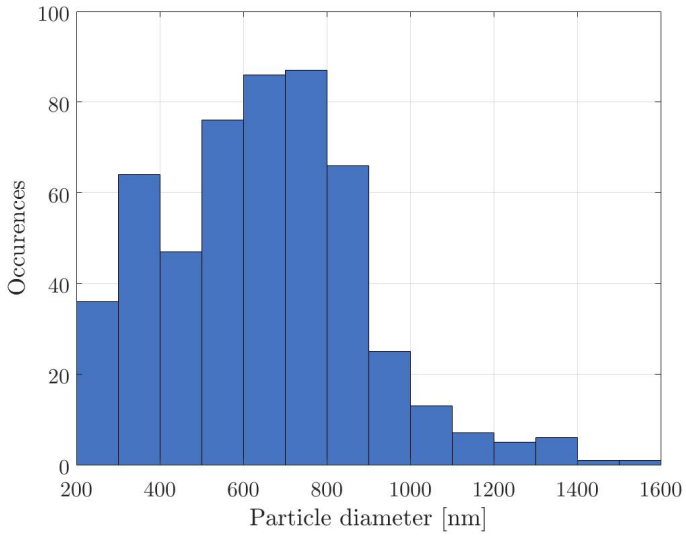

Figure 4.10 Distribution size of the particles electrosprayed in test 19H (see Table A.5, Appendix A).

4.2.3 Different solutions for core and shell

In an effort to look for a more consistent set of parameters that would allow for the totality of the particles to be under the 800 nm threshold, it was decided to test the use of different formulations for the core and shell solutions. The inner solution was kept constant as 40/60 THF/MeCN, while several options were explored for the outer one (see Tables A.6 through A.9). The first change made to this solution was the introduction of DMF as tertiary solvent, in a 10/30/60 ratio with, respectively, THF and MeCN. The first test was carried out by keeping the flow rates of the solutions at the same values of either 0.2 mL/h or 0.5 mL/h, with TTC distances of either 6 or 10 cm. For what concerns the tests that used TTC distance of 6 cm, the particles produced showed similar morphology issues as reported earlier Section 4.2.2 (Test 14, see Table A.3, Appendix A), irregularly shaped and lacking uniformity. The other combinations instead, showed an interesting difference between the 0.2 mL/h particles (21E-21H), and the 0.5 mL/h ones (21A-21D) (for parameters, see Table A.6, Appendix A). In fact, while the latter show a collapsed spherical morphology (Figure 4.11a), the former appear to be smaller and denser, although their shape is not uniformly spherical (Figures 4.11b and 4.12). To explain the collapsed morphology, it was hypothesized that the faster feeding rate (i.e. 0.5 mL/h) contributed to a faster deposit of the particles, which would effectively trap some of the solvent inside them. The slow evaporation of this liquid would then bring about the collapse of the dried structures [24].

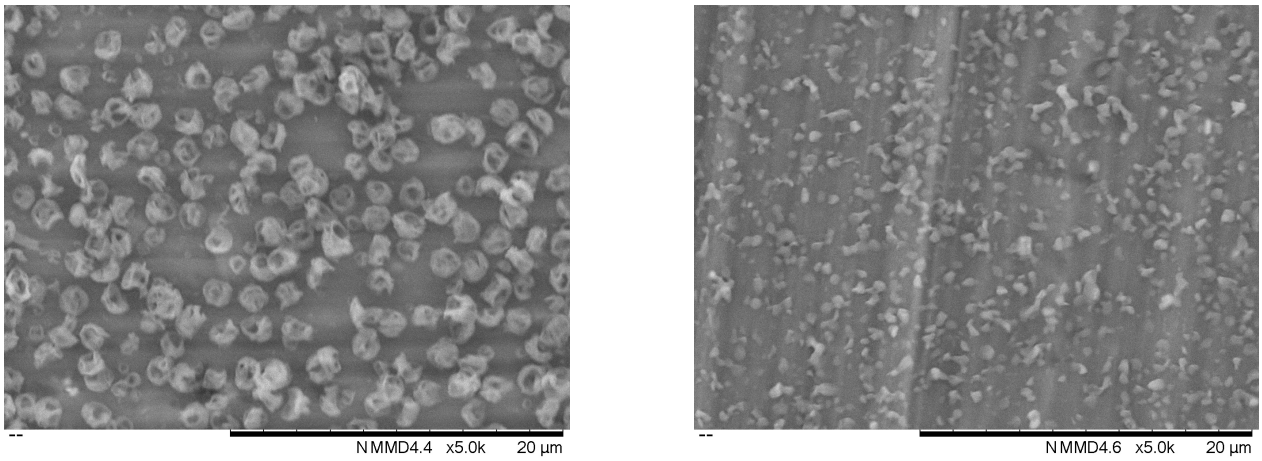

(a) (b)

Figure 4.11 Results from inner solvent 40/60 THF/MeCN, outer solvent 10/30/60 DMF/THF/MeCN: (a) collapsed particles, paired flow rate of 0.5 mL/h (Test 21B); (b) particles, average diameter 570 nm, standard deviation ±166 nm, paired flow rate of 0.2 mL/h (Test 21H); Scale bar: (a), (b) 20 μm. (For parameters, see Table A.6, Appendix A).

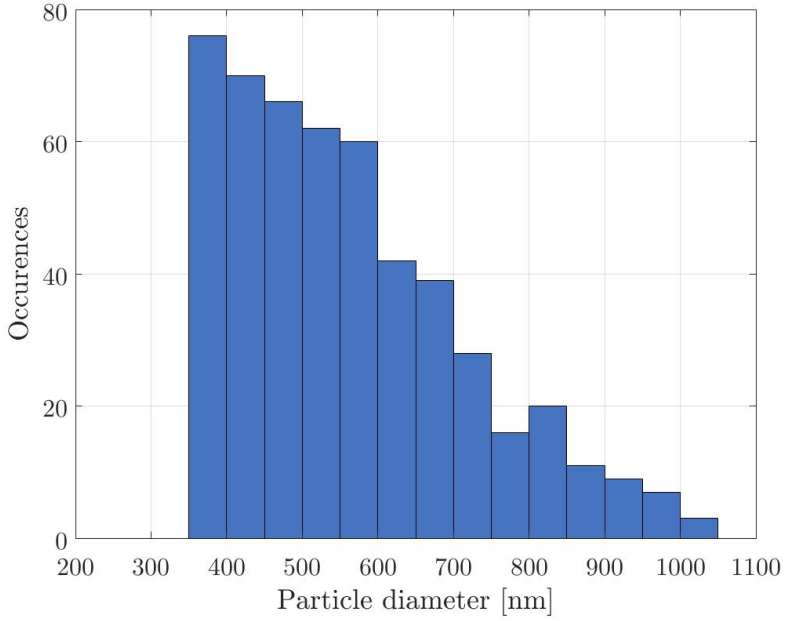

Figure 4.12 Distribution size of particles obtained in test 21H (for parameters, see Table A.6, Appendix A).

Keeping the solution combination to 40/60 THF/MeCN for the core and 10/30/60 DMF/ THF/MeCN, it was decided to uncouple the flow rates in order to account for the interface interactions between different fluids, putting the inner one at 0.2 mL/h and the outer at 0.5 mL/h. With this new combination, shorter TTC distances were not as effective in reducing the size as previously shown (as in Figure 4.12), with the most successful being 15 and 20 cm. An example of this is trial 24F (for parameters, see Table A.6, Appendix A), in which particle size was in the nanometric scale, with an average size of 547 nm (Figures 4.13a and 4.14a). It is also possible to compare the effect of coupled and uncoupled flow rates; in fact, trial 25F (for parameters, see Table A.6, Appendix A), which kept the same parameters as 24F save for the flow rates, shows the presence of bigger more porous particles (between 400 and 2000 nm, with an average size of 670 nm; Figures 4.13b and 4.14b). This behaviour is consistent with observations found in the literature in which a slower inner flow rate compared to a faster outer one is linked with a decrease in size [24]. Moreover, it is interesting to point out the differences between test 24D and 26C. The same parameters have been used for the two, with the exception of the TTC distance (see Table A.6, Appendix A, for 26C reference 25I). While test 24D (Figure 4.15a) resulted in collapsed misshapen particles using a TTC distance of 15 cm, increasing this parameter to 20 cm lead to much more regularly shaped particles. An explanation could be found in an insufficient evaporation time for test 24D, as wet spots were visible with the naked eye during the test. The opposite could be postulated

for test 26C in regards with evaporation time. In fact, in Figure 4.15b, the presence of larger particles, up to 1100 nm, and much smaller ones is also noticed. This could be an example of Rayleigh disintegration which, as mentioned in Section 2.2.1 of Chapter 2, involves the dismembering of bigger droplets into smaller particles due to solvent evaporation and a change in the droplets' electrical charge.

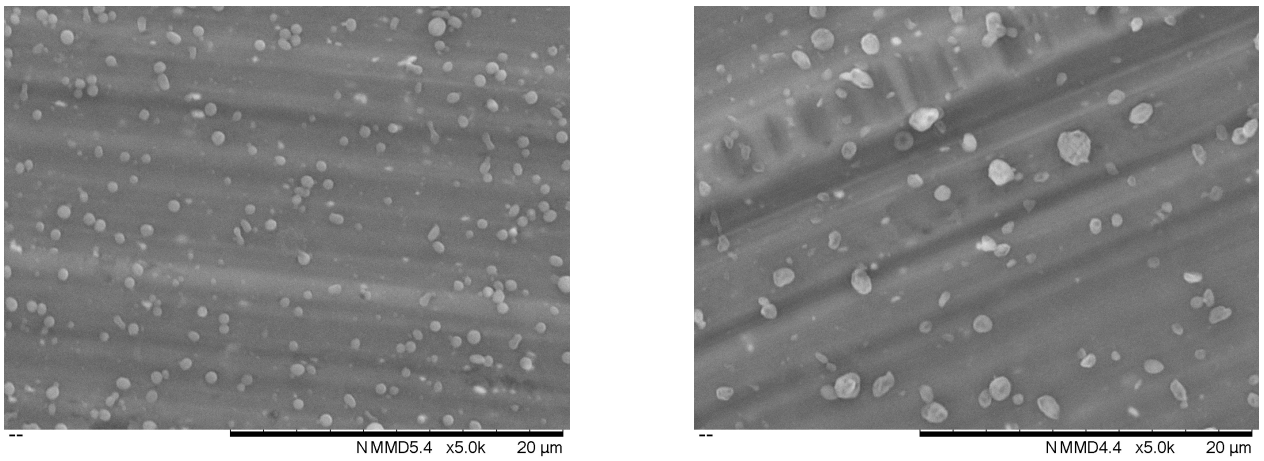

(a) (b)

Figure 4.13 Comparison between uncoupled and paired flow rates: (a) particles, average diameter 547 nm, standard deviation ±164 nm, inner flow rate of 0.2 mL/h, outer flow rate of 0.5 mL/h (Test 24F); (b) particles, average diameter 670 nm, standard deviation ±348 nm, paired flow rate of 0.5 mL/h (Test 25F); Scale bar: (a), (b) 20 μm. (For parameters, see Table A.6, Appendix A).

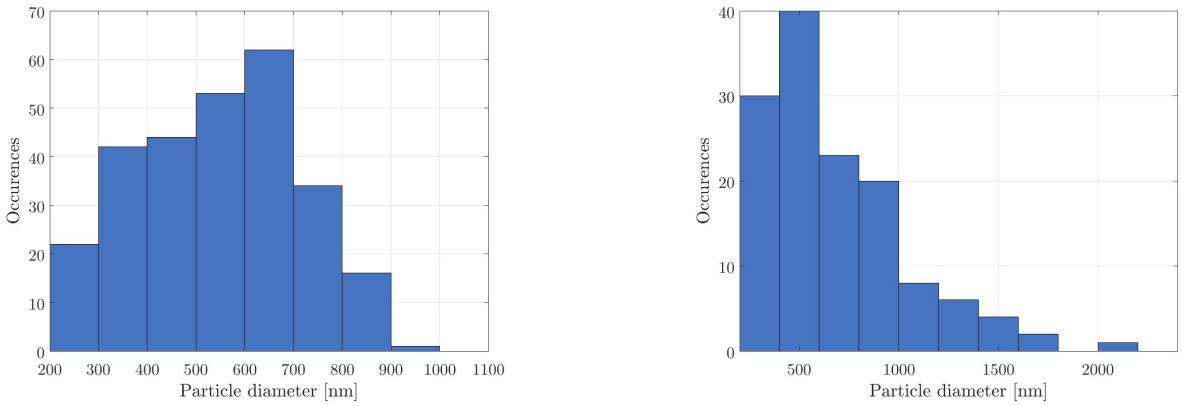

(a) (b)

Figure 4.14 Distribution size comparison of particles obtained in two different trials: (a) 24F; (b) 25F. (For parameters, see Table A.6, Appendix A).

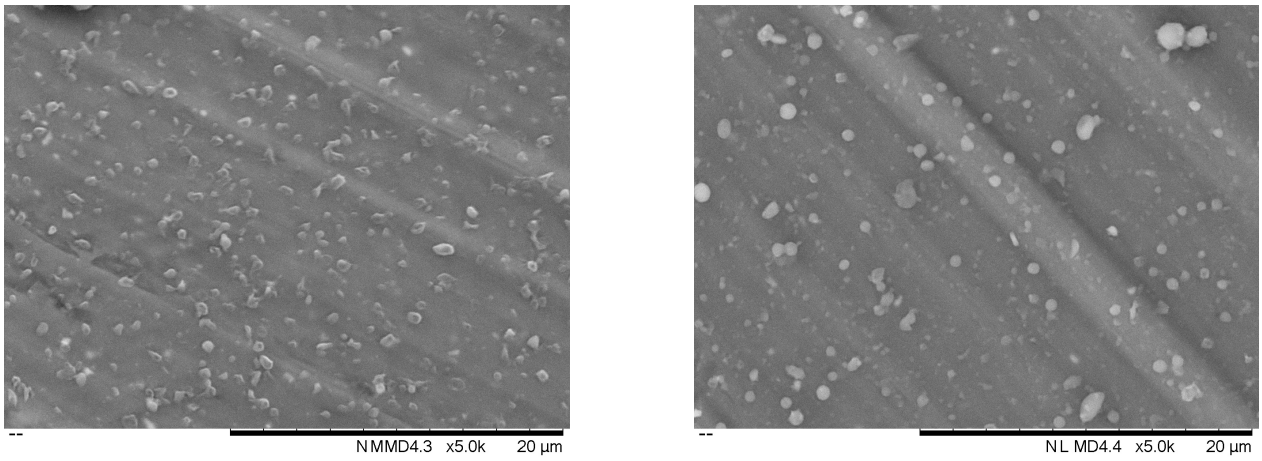

(a) (b)

Figure 4.15 Comparison between same parameters except TTC distance: (a) collapsed misshapen particles, TTC distance 15 cm (Test 24D); (b) particles, it is possible to notice the effect of the Rayleigh disintegration thanks to the presence of larger and smaller particles, TTC distance 20 cm (Test 26C, for parameters see 25I); Scale bar: (a), (b) 20 μm. (For parameters, see Table A.6, Appendix A).

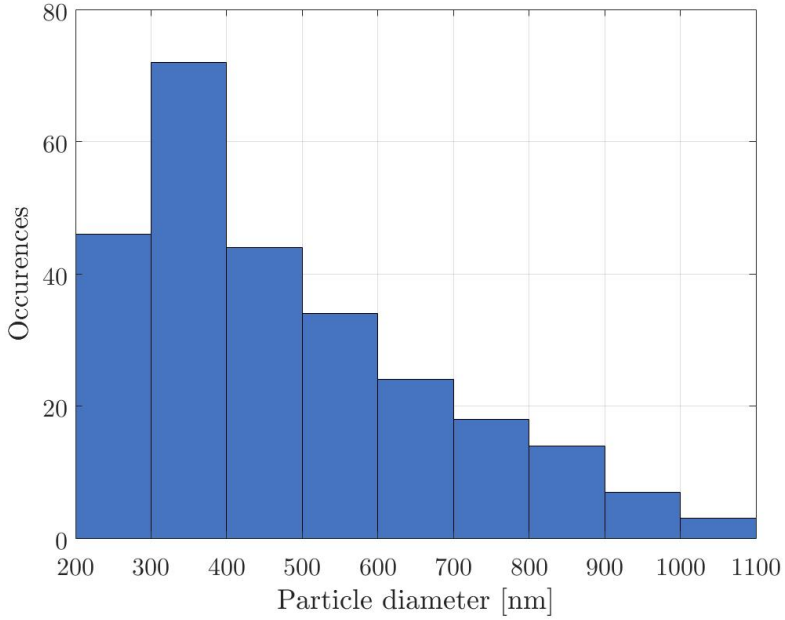

Figure 4.16 Distribution size of particles obtained in test 26C. (For parameters, see 25I, Table A.6, Appendix A)

Once again the core solvent was kept to 40/60 THF/MeCN while the shell solvent was changed to 15/35/50 DMF/THF/MeCN. This solvent combination was used for trials 29, 30 and 31 in which several parameter variations were tested (see Tables from A.7 through A.9), with changes to the applied voltage, TTC distance and polymer and drug concentrations. Nevertheless, the common results obtained with this solution combination were overall undesirable: instances of multi-jet cone formations were observed, resulting in particles of random sizes (Figure 4.17) that often aren't consistently reproducible due to their erratic formation, both from what has transpired over the course of this thesis but also according to the literature [24]; Moreover, despite the reduced amounts of solutes, the increased solution conductivity often lead to stretched, elongated particles, in some cases leaning towards the typical beaded filament structure that can be observed in mid-way conditions between electrospraying and electrospinning (Figure 4.18). This behaviour seems to be overall in accordance with the literature, which reports that while higher electrical conductivity might lead to reduced particle sizes, it also affects the electric field range in which a stable cone-jet can be achieved, both making it narrower and moving it to lower values [24].

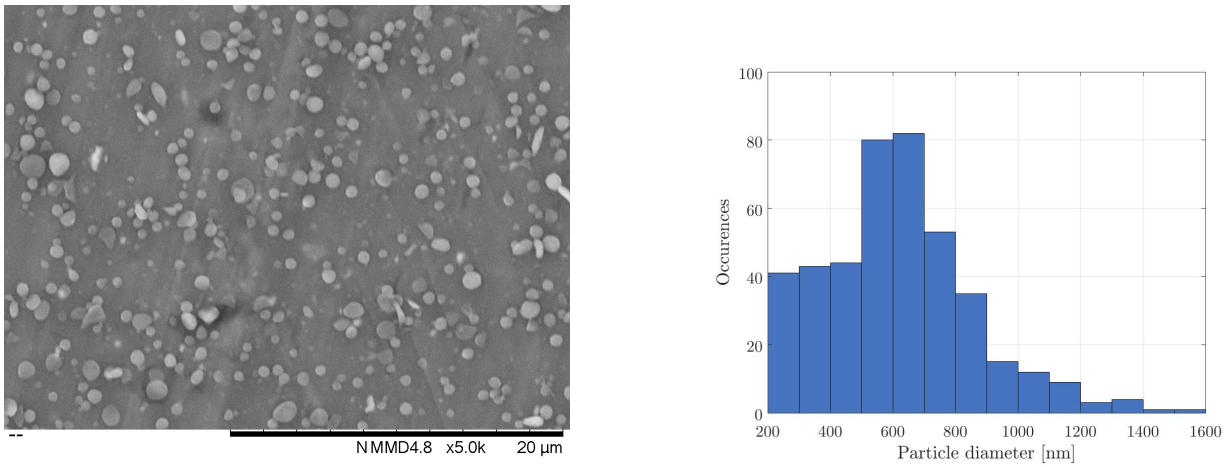

(a) (b)

Figure 4.17 Effect of multi-jet cone: (a) particles of several sizes (Test 29E); (b) distribution size of test 29E. The effect of a multi-jet cone can be noticed in the wide range of sizes; Scale bar: (a) 20 μm. (For parameters, see Table A.7, Appendix A).

With the intention of reducing the number of solvents used, other combinations were tested. The solvent mix of 40/60 THF/MeCN was still used for the core, while THF was eliminated from the shell solution, leaving it as 50/50 DMF/MeCN for test 32 (for parameters, see Table A.9, Appendix A) and as 60/40 DMF/MeCN for test 33 (for parameters, see Table A.12, Appendix A). The first combination showed similar issues encountered with previous shell solutions with high MeCN (ex. 30/70 THF/MeCN from test 14 in Section 4.2.2): some

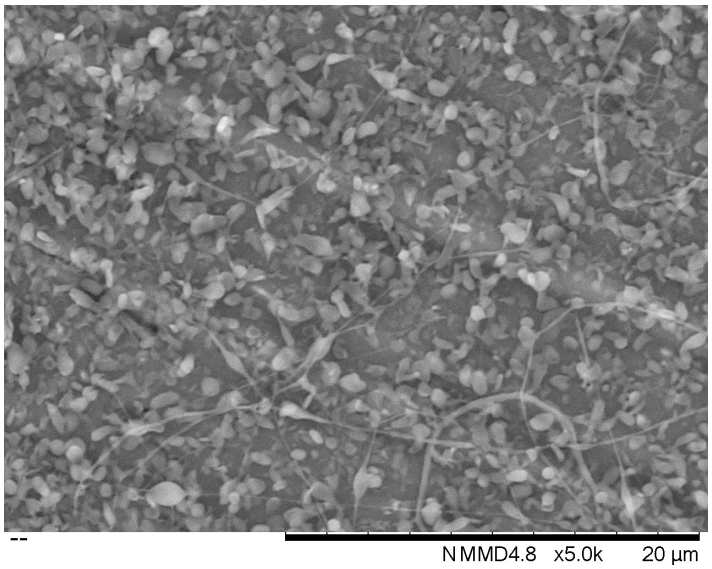

Figure 4.18 Beaded filaments structure (Test 29D); Scale bar: (a) 20 μm. (For parameters, see Table A.7, Appendix A).

trials resulting in multimodal size distributions, others having elongated particles, or even a mid-point between the two. The second solution combination, using 60/40 DMF/MeCN for the shell, showed a much more consistently spherical morphology, especially when the test involved a TTC distance of 20 cm (Figures 4.19a and 4.20a). For what concerns tests made with a TTC distance of 26 cm, it was once again noticed the presence of groups of particles of different sizes that, due to the lack of multi-jet cones, were attributed to the Rayleigh disintegration effect (Figures 4.19b and 4.20b). The differences between the tests with the two TTC distances can be appreciated in Figures 4.19, 4.20 and 4.21, where the longer distance, 26 cm, provided overall larger particles with wider size distributions. Although other solution combinations (such as 40/60 THF/MeCN for the core and 10/30/60 THF/DMF/MeCN for the shell) yielded much smaller particles, this, with a core solution of 40/60 THF/MeCN and a shell one of 60/40 DMF/MeCN, was chosen as the final one, as it proved to be more reproducible in terms of particle sizes and morphology even across electric fields of different strengths (Figure 4.21).

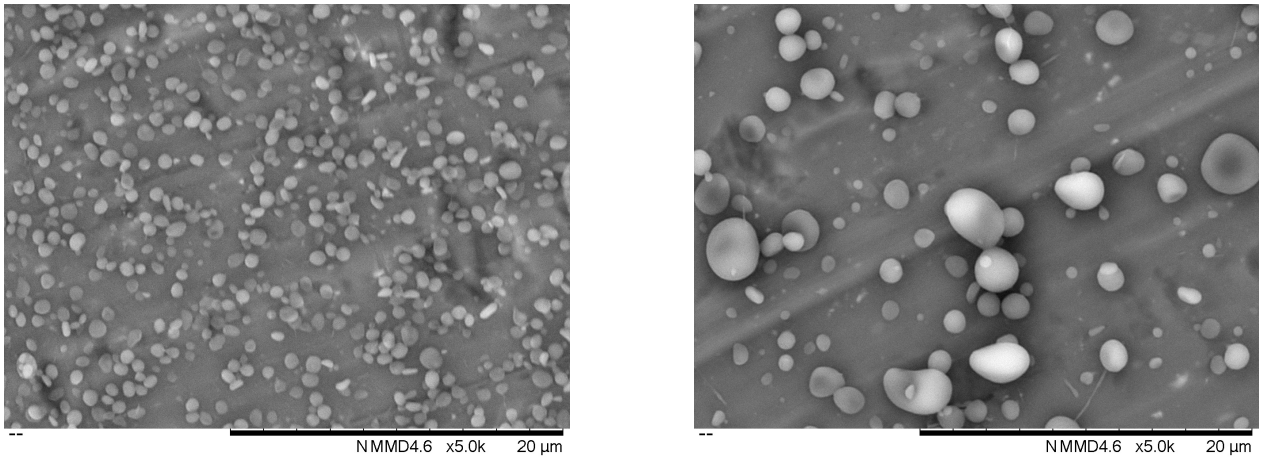

(a) (b)

Figure 4.19 Effect of TTC distance on size: (a) spherical particles (Test 33C); (b) particles of several sizes (Test 33F); Scale bar: 20 μm. (For parameters, see Table A.12, Appendix A).

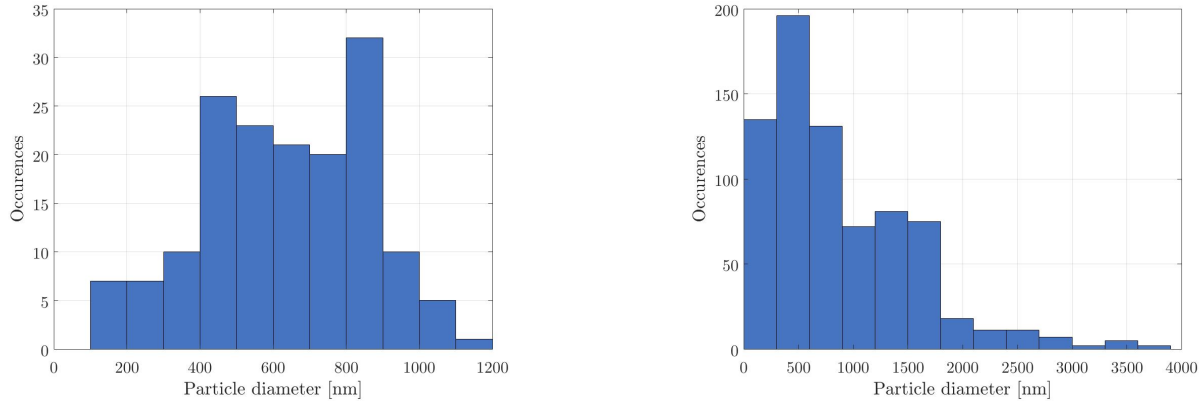

(a) (b)

Figure 4.20 Effect of TTC distance on distribution size: (a) particles produced in test 33C; (b) particles produced in test 33F. (For parameters, see Table A.12, Appendix A).

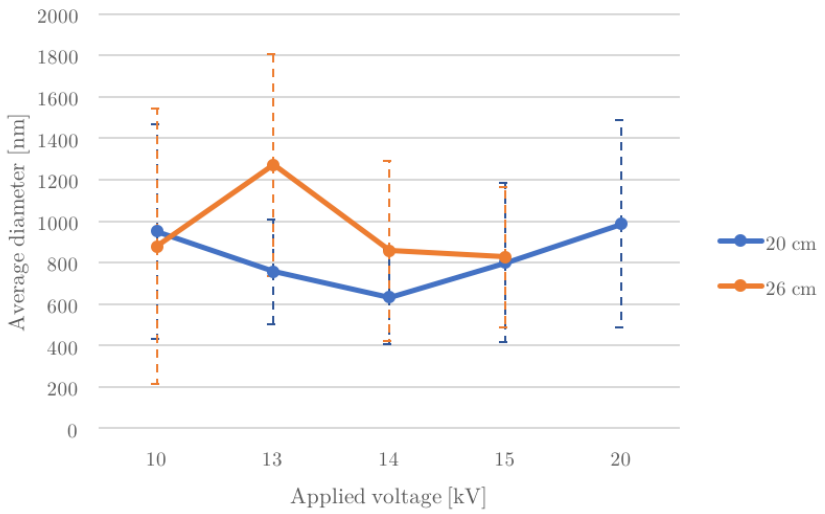

Figure 4.21 Test 33 comparison between different voltages at different TTC distances. In order from left to right: 33A, 33F, 33B, 33G, 33C, 33H, 33D, 33I, 33E. For parameters, see Table A.12, Appendix A.

4.2.4 Final Tong Li optimization

Through the optimization of the solution, the array of possible parameters had been restricted: the TTC distance was set at 21 cm; the preferred total voltage ranged between 13 and 15 kV; and the flow rate combinations had been set as either 0.1 mL/h for the core and 0.3 mL/h for the shell or 0.2 mL/h for the core and 0.5 mL/h shell. During tests 38, 39 and 42 (Table A.12, Appendix A) the applied voltage was set as -3 kV for the collector and 12 kV for the spinneret. As shown in Figures 4.22 and 4.23, the two flow rate combinations were put to the test as well. The lower one was then selected, as, even if the higher showed a more normal distribution, its particles were more consistently under the microscopic scale (see Table 4.1 for the optimized parameters of the Tong Li set-up). The more spread-out size distribution was also considered interesting in terms of the application, as it would allow for a staggered delivery not only based on paths created through the shell as the polymer degradates, but also differentiated by the array of dimensions. In fact, it was hypothesized this variety would act as an intrinsic degradation gradient, with smaller particles exposing a bigger surface area and thus degradating in a quicker manner, while bigger ones would go through a lengthier process, thus ensuring a continuous release [24].

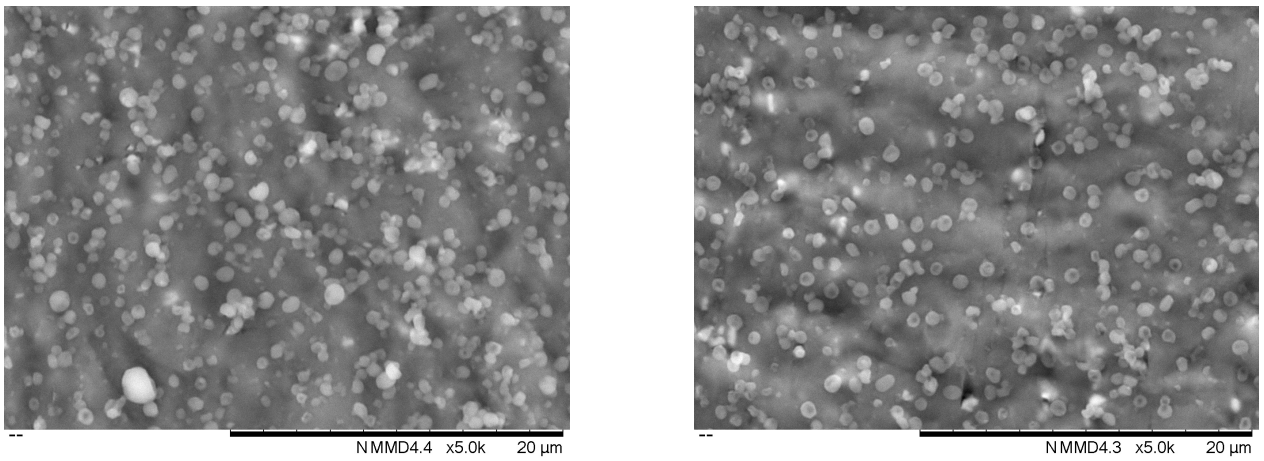

(a) (b)

Figure 4.22 Effect of flow rate: (a) particles, average diameter 570 nm, standard deviation ±292 nm, core flow rate of 0.2 mL/h, shell flow rate of 0.5 mL/h, total applied voltage 15 kV, TTC distance 21 cm (Test 38B); (b) particles, average diameter 598 nm, standard deviation ±286 nm, core flow rate of 0.1 mL/h, shell flow rate of 0.3 mL/h, total applied voltage 15 kV, TTC distance 21 cm (Test 38C); Scale bar: 20 μm. (For parameters, see Table A.12, Appendix A).

Of note is that the distribution sizes of the two tests (38B and 38C) here presented are slightly skewed towards higher values due to image processing errors of the used software, which has trouble distinguishing between different nearby particles especially in the presence of speckles, as will be later discussed in section 4.4.

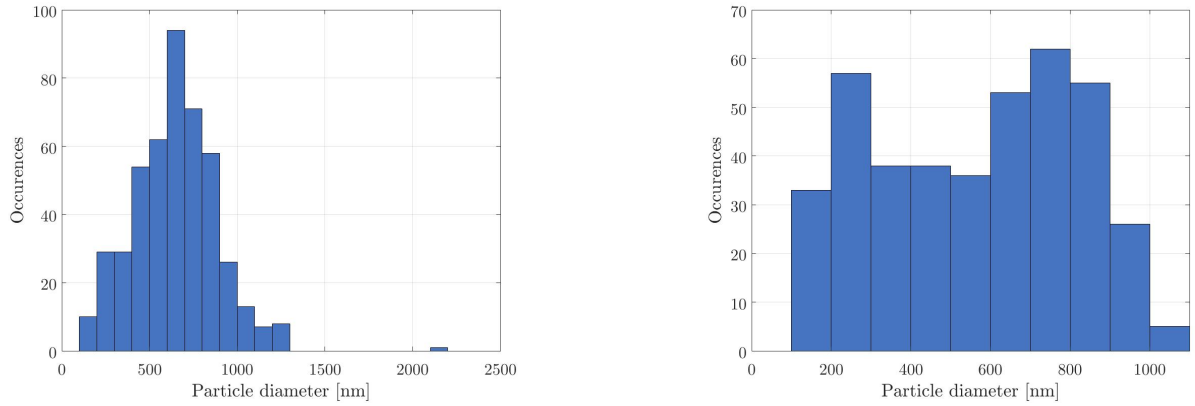

(a) (b)

Figure 4.23 Effect of flow rate on distribution size: (a) test 38B; (b) test 38C. For parameters, see Table A.12, Appendix A.

Table 4.1 Final optimized parameters for the Tong Li set-up.

Core solution	5 wt% ibuprofen in 40/60 THF/MeCN
Shell solution	5 wt% PLGA in 60/40 DMF/MeCN
Inner flow rate	0.1 mL/h
Outer flow rate	0.3 mL/h
Positive applied voltage	12 kV
Negative applied voltage	-3 kV
TTC distance	21 cm

4.2.5 Particle collection

Over the course of the optimization process, several methods to facilitate the particles' collection from their aluminum substrate were tested. Among the tested strategies, the most innovative one for the project was the implementation of a wet set-up, that would allow the particles to collect into an ethanol bath. The choice of ethanol was made as it was identified as non-solvent for the materials involved (PLGA, ibuprofen and DOX). Nonetheless, this approach did not bring the desired results. The trials showed particles merging together (Figure 4.24a, test 36B, see Table A.10 for parameters), or forming aggregates of differently

sized spheres (Figure 4.24b, test 37F, see Table A.10 for parameters). Moreover, the obtained particles tended to be well over the size of ones produced in dry conditions (1.35-5 μm). An hypothesis for this behaviour is that the homemade wet set-up may present losses in the electric arrangement that resulted in a reduced electric field in comparison to what was configured. This set-up was then abandoned as leaving the particles under vacuum for a 24h period proved to be enough to ease the collection.

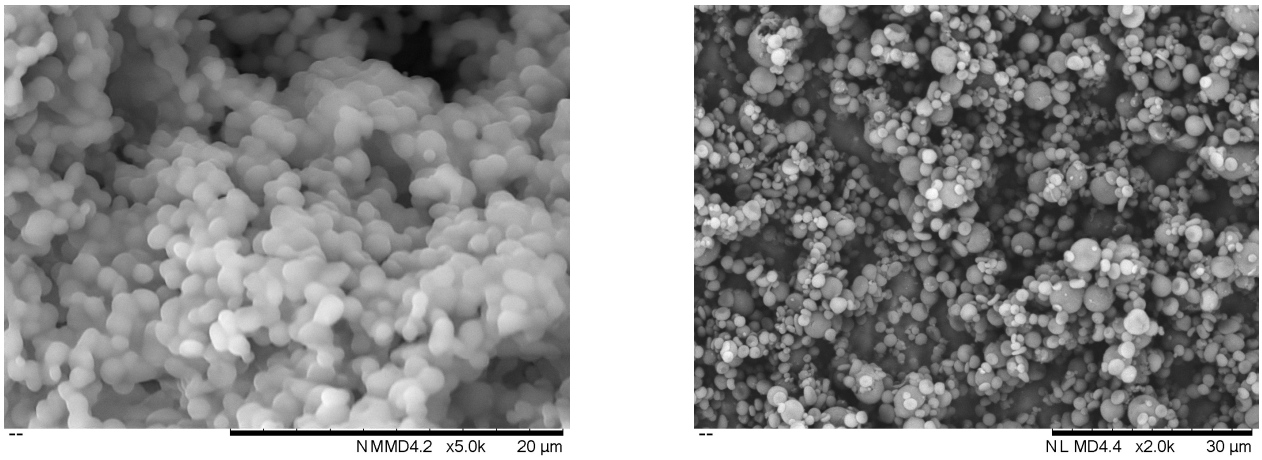

(a) (b)

Figure 4.24 Wet set-up results: (a) merged particles (Test 36B); (b) aggregated particles (Test 37F); Scale bar: (a) 20 μm; (b) 30 μm. (For parameters, see Table A.10, Appendix A).

Other strategies involved using parchment paper as a collecting substrate or covering the aluminum sheets with a silicone spray, as well as employing non-stick aluminum. The first method was discarded as it rendered impossible to visualize the deposition of the particles, as well as not improving the ease of collection from the substrate. The second was a poor choice from the start as silicone is commonly known as an insulating material, thus its contribution in an electrical-based process such as electrospraying would clearly be detrimental. Non-stick aluminum instead, proved to ease the particle collection and was then used as the standard collecting substrate.

4.2.6 Adjustments and Big box set-up

As mentioned in Chapter 3, before it was possible to produce the final particles and initiate the following phase of this thesis, access to the Polytechnique Montréal laboratories was revoked, in line with the Canadian and Québécois governments' safety procedures to contain the spread of Covid-19. As a consequence, the experiments needed to complete this thesis were delayed, moving them well into summer, season in which the humidity rates in the laboratory are well over the levels at which the parameters had been optimized (Figure 4.25).

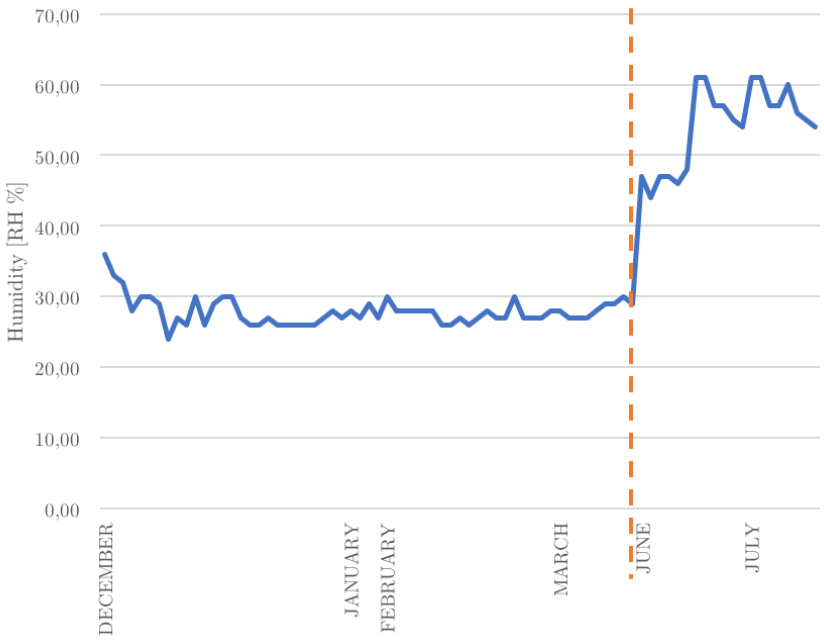

Figure 4.25 Relative humidity values in the electrospraying laboratory from December to July. The dashed line represents the closing period, from mid-March to mid-June.

This increased humidity (+20-30 %) had a noticeable impact over the output of the previously optimized parameters. In fact, the results had regressed to morphologies resembling that of test 21B (Figure 4.11a), if not worse, with crumpled, interconnected and poorly defined particles (Figure 4.26). The hypothesis made to explain this phenomenon is that the augmented surrounding humidity increases the evaporation time needed for the solvents to abandon the structures, thus leading particles to land on the collector with an increased amount of trapped liquids [26]. These would then slowly evaporate causing the collapse of the structures. As mentioned in Section 4.2.2, the solvent presence once the particles have deposited on the collector, also tends to favour their cohesion with one another, leading to interconnected structures. After a phase consisting on trying to modify the parameters to

fit with the new conditions, several strategies were put in place to reestablish the humidity conditions of the optimized parameters. The first relied on the use of a dehumidifier system provided with the Tong Li Electrospinning Unit (Shenzhen Tong Li Tech Co. LTD). While this solution succeeded in reducing the relative humidity in the electrospraying environment, it did so by increasing the temperature by 10°C, from the usual 19-22°C, which in turn affected the evaporation times resulting in irregular, elongated polymeric fragments (Figure 4.27). This morphology is a consequence of the solvents leaving the droplets before a sufficient number of chain entanglements could be formed within the polymeric matrix [24]. One more attempt was made by employing Indicating DRIERITE (mesh size 8, from W. A. HAMMOND DRIERITE CO. LTD.), a composite of calcium sulfate ($\geq$ 98%, $CaSO_4$), commonly used as a desiccant, and cobalt dichloride (<2%, $CoCl_2$) which turns from blue to pink upon absorption of moisture. With the use of DRIERITE the relative humidity in the electrospraying unit went from about 60 RH% to 47 RH% which proved to be still too high for the optimized parameters, as can be seen in Figures 4.28 and 4.29. In fact, test 48D, which employed the faster flow rate combination (core: 0.2 mL/h; shell: 0.5 mL/h), showed two different behaviours, one at a higher scale, with millimetric (0.10-1.00 mm) fragmented and frayed filaments that could easily be detected even with the naked eye (Figure 4.28b), and one at a much smaller scale with few particle-like structures of micrometric and nanometric levels (200-1000 nm). Test 48F instead, showed a morphology similar to test 15E, with slightly interconnected particles that lack a specific and consistent shape (Figure 4.29).

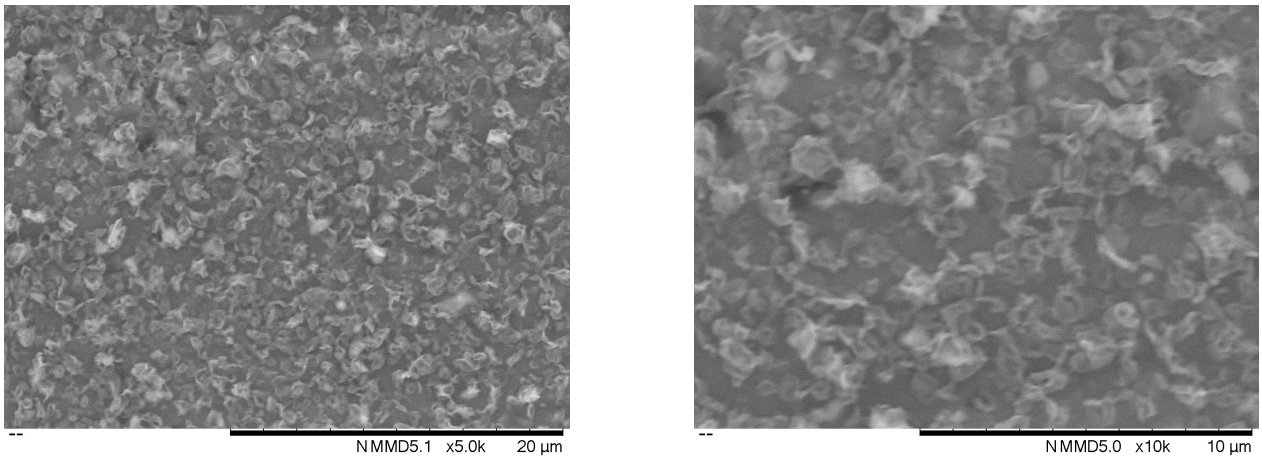

(a) (b)

Figure 4.26 Effect of increased relative humidity on the optimized parameters (Test 45E, see 38B for parameters, Table A.12, Appendix A): (a) test 45E; (b) Test 45E, close-up; Scale bar: (a) 20 μm; (b) 10 μm.

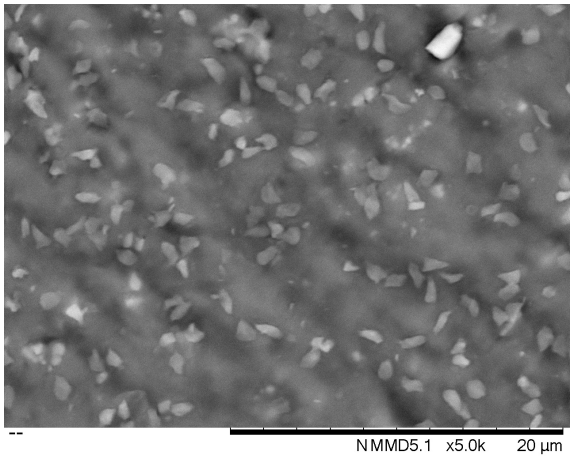

(a)

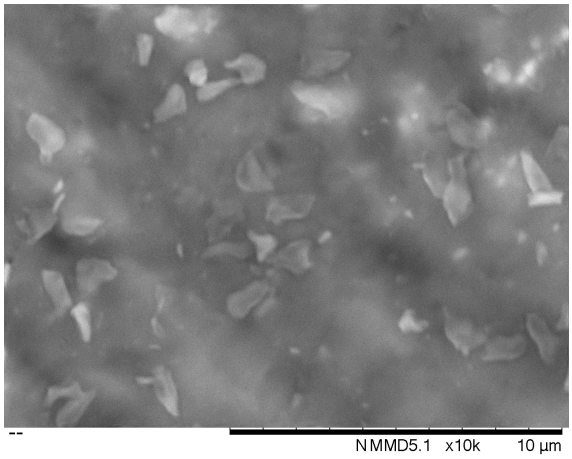

(b)

Figure 4.27 Effect of increased temperature on the optimized parameters (Test 46F, see 38C for parameters, Table A.12, Appendix A): (a) test 46F; (b) test 46F, close-up; Scale bar: (a) 20 μm; (b) 10 μm.

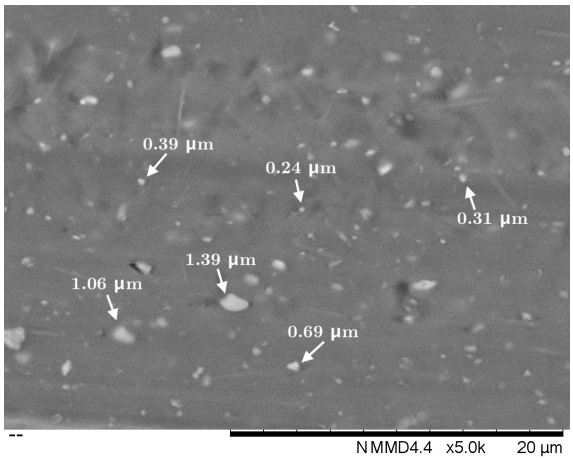

(a)

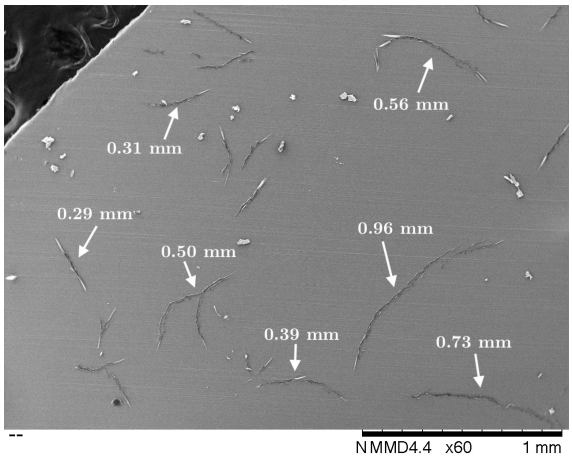

(b)

Figure 4.28 Effect of Indicating DRIERITE (Test 48D, see 38B for parameters, Table A.12, Appendix A): (a) test 48D; (b) Test 48D, lower magnification; Scale bar: (a) 20 μm; (b) 1 mm.

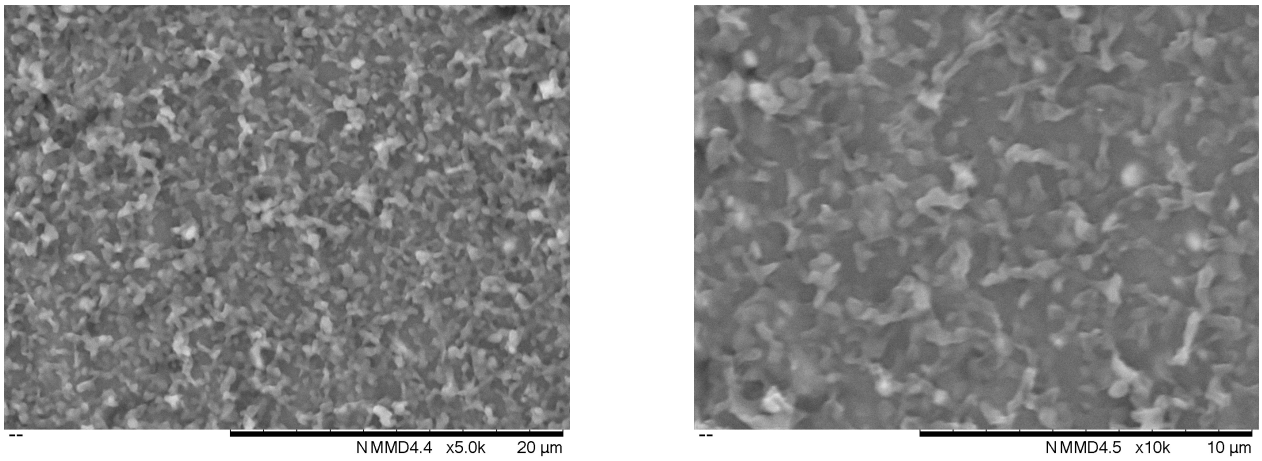

(a) (b)

Figure 4.29 Effect of Indicating DRIERITE (Test 48F, see 38C for parameters, Table A.12, Appendix A): (a) test 48F; (b) Test 48F, close-up; Scale bar: (a) 20 μm; (b) 10 μm.

In an effort to quickly proceed with the next steps of the project, it was decided to move the production to the Big box set-up (see Section 3.2.1). The reasoning was that this other set-up was equipped with a system that, by pumping dried compressed air into the unit, is able to reduce by 20-25% the relative humidity of the environment. The downside to this approach was that new parameters had likely to be implemented for this set-up. With the knowledge gained through the optimization of the Tong Li conditions, the optimization of the Big box set-up was reached more quickly, with a smaller number of experiments and a process more based on immediate empirical observations and modification of the parameters. The first ones tested were equivalent to those for the Tong Li set-up: the TTC distance was set at 21 cm; the total applied voltage was 15 kV with a grounded collector and a positive spinneret, instead of a collector at -3 kV and a spinneret at 12 kV; for the flow rate, it was decided to test both combinations that had reached the final steps of the previous optimization with 0.1 mL/h for the core and 0.3 mL/h for the shell or 0.2 mL/h for the core and 0.5 mL/h shell (see tests 44A and 44B in Table A.13, Appendix A). These first trials confirmed that the parameters would need a second optimization. In fact, the test involving the lower flow rate combination resulted in slightly elongated fragments of polymer, in shapes and dimensions overall non-uniform from one another (Figure 4.30b). For what concerns the trial with the higher flow rate configuration (i.e. 0.2 mL/h for the core and 0.5 mL/h shell), these parameters brought, once again, randomly shaped particles together with some more polymer fragments and an overall poor yield (Figure 4.30a).

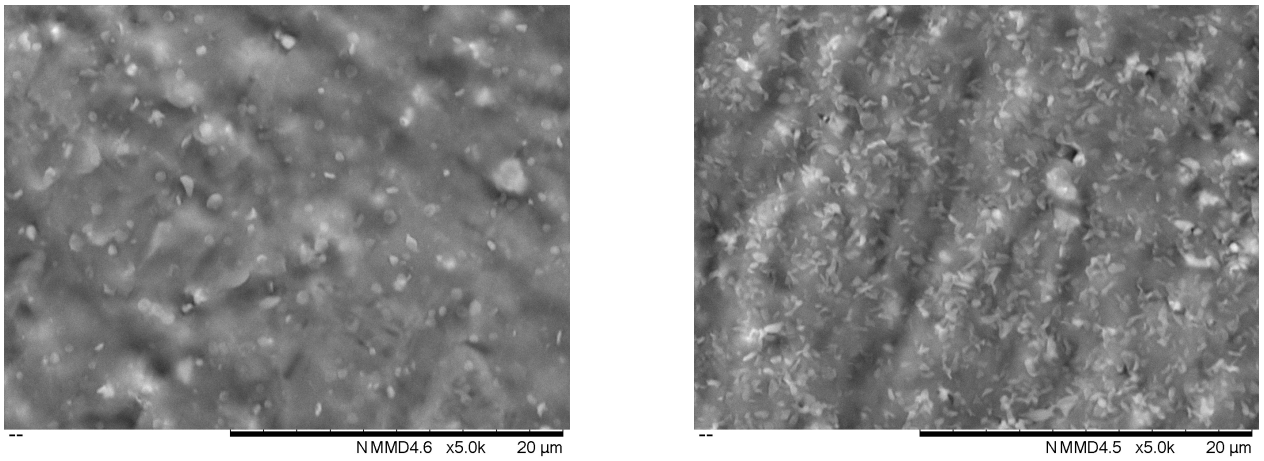

(a) (b)

Figure 4.30 Tong Li optimized parameters tested in Big box set-up: (a) fragments and a few particles (Test 49E, see 44B for parameters, Table A.13, Appendix A); (b) elongated random fragments (Test 49F, see 44A for parameters, Table A.13, Appendix A); Scale bar: (a), (b) 20 μm.

For the next set of tests the focus shifted on finding the correct TTC distance, keeping the other parameters as mentioned earlier (for a more throughout look, see Table A.13, Appendix A). This thought process led to increasing the parameter to 34 cm. In this case, both combinations of flow rates brought to overall spherical particles, although they presented a similar morphology to test 10C, crumpled and seemingly incomplete (Figure 4.31).

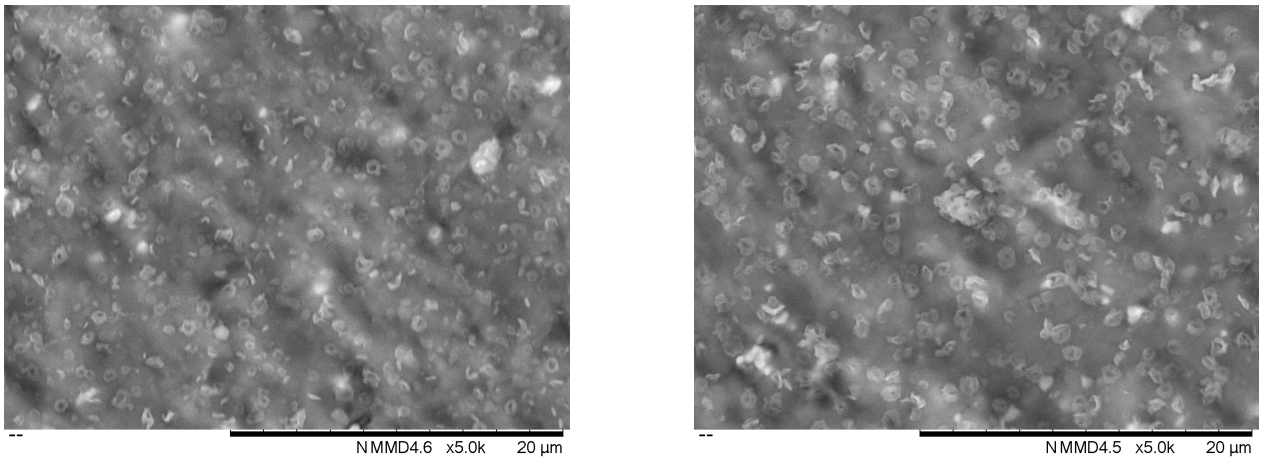

(a) (b)

Figure 4.31 Big box set-up with TTC distance of 34 cm: (a) crumpled incomplete particles (Test 50A); (b) crumpled incomplete particles (Test 50C); Scale bar: (a), (b) 20 μm. (For parameters, see Table A.12, Appendix A).

From this observation, it was decided to increase the polymer's concentration in the solution, from 5 wt% to 7 wt%. In fact, according to the literature, increasing the polymer concentration in a solution is a way to resolve issues of wrinkling and incompleteness [24]. When test 52 began, the TTC distance was set at 30 cm but the collector lacked any of the macroscopic signs of successful electrospraying that would usually appear. For this reason, the distance was progressively shortened, each new value was tested for a few minutes while the user observed the system's behaviour. Through this process the TTC distance of 15 cm was tested. This value, with a flow rate combination of 0.1 mL/h for the core and 0.3 mL/h for the shell, finally showed the same macroscopic phenomena at the collector that had been experienced in the previous experiments. The particles obtained with these parameters (Table 4.2) were bigger than desired initially (>800 nm), with a minority even in the order of few micrometers, but overall presented the correct morphology and were regarded as acceptable to proceed to the following steps of the project (Figure 4.32). The increase in size was to be expected, as it can be a known consequence of increasing the solute's concentration in the solution as well as lowering the TTC distance [24]. It is to be noted that these parameters could have been further optimized to achieve more desirable dimensional features, but the choice of moving on was taken in consideration of the reduced available time to access the facilities, as well as the increased time that each test required in order to comply with the safety measures put in place to limit the spread of Covid-19.

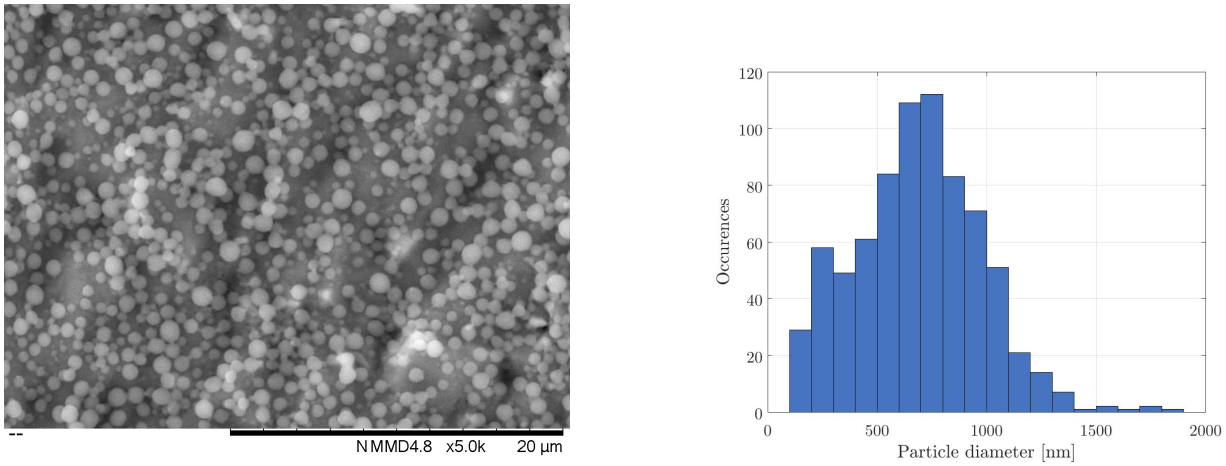

(a) (b)

Figure 4.32 Final particles with Big box set-up (Test 53E, see 52C for parameters, Table A.12, Appendix A): (a) particles, average diameter 685.9 nm, standard deviation ±286 nm, core flow rate of 0.1 mL/h, shell flow rate of 0.3 mL/h, total applied voltage 15 kV, TTC distance 15 cm; (b) distribution size of particles obtained in test 53E. Scale bar: (a) 20 μm.

Table 4.2 Final optimized parameters for the Big box set-up.

Core solution	5 wt% ibuprofen in 40/60 THF/MeCN
Shell solution	7 wt% PLGA in 60/40 DMF/MeCN
Inner flow rate	0.1 mL/h
Outer flow rate	0.3 mL/h
Applied voltage	15 kV
TTC distance	15 cm

4.3 Degradation tests

Before delving into the specifics of the degradation tests, a more general commentary upon their organization is needed. The particles involved were prepared with the Big box set-up (see Section 4.2.6), and can be observed in Figure 4.32a. A combination of limited available time in the electrospinning laboratory and the technique's intrinsic poor yield meant that only a small array of samples could be produced (22 in total), thus rising the issues of a lack of time-points over the course of the experiment and of reproducibility in regards to tests such as SEM and weight loss, as well as impacting tests as the encapsulation efficiency, which was eliminated from the protocol. Instead of having duplicate samples, testing the degradation in two different pH conditions (6.6 and 7.4) was prioritized, as the biological correlation to the application was deemed more valuable. From now on, the samples tested at a pH of 7.4 will be referred to as Group A (11 samples), and the ones tested at a pH of 6.6 will be called Group B (11 samples). Moreover, lack of access to the laboratory where these tests took place whilst planning the experiments, meant that some issues, specifically concerning the FTIR analysis set-up, only came to light while the testing had already begun.

For these reasons, the general consideration is that the degradation tests should be carried out again with the following improvements: a larger array of samples, allowing for more frequent SEM time points as well as triplicates for each test to be made; a higher frequency of time-points, especially in the first stages of the experiment; and finally, the introduction of new tests or the exchange of some with more appropriate ones. The specific instances where these changes could come into play in future improvements, will be discussed where relevant in the following sections.

4.3.1 Fourier-transform infrared spectroscopy (FTIR)

FTIR spectrometry was chosen to be used to track the drug release over the course of the degradation tests. At first, the spectra of the pure materials involved, PLGA, ibuprofen and PBS, were acquired, as well as the one of the PLGA-Ibuprofen particles. For what concerns

PLGA (Figure 4.33 and Table 4.3), the peaks between 850 and 1450 cm^{-1} are normally attributed to the bending of single bonds between C and H; the intense peaks in the bands between 1089 and 1186 cm^{-1} are attributed to the stretching of single bonds between C and O; the most prominent peak around 1720 cm^{-1} is often attributed to the stretching of double bonds between C and O; finally, the stretches of single bonds between C and H are responsible for the peaks between 2900 and 3000 cm^{-1} [1, 42]. For the interpretation of the ibuprofen spectrum (Figure 4.34, Table 4.4), the high density of peaks between 500 and 1500 cm^{-1} can generally be attributed to bonds involving C and H, as well as C and other C atoms; the intense peak at around 1720 cm^{-1} is once again caused by the stretching of double bonds between C and O; finally, the peaks between 2869 and 3045 cm^{-1} are usually attributed to the stretch of C and H single bonds [43]. In regards with the spectrum from the PLGA-Ibuprofen particles (Figure 4.35 and Table 4.5), it can be noticed that it mostly resembles the PLGA one dampened down. In fact, we can see the same peaks discussed earlier at 850-1450, 1089-1186 and 1700 cm^{-1}, with the first and the latter noticeably reduced in intensity. A smaller peak can also be noticed at around 3300 cm^{-1}; this could be the peak found around 2900-3000 cm^{-1} shifted due to the encapsulation.

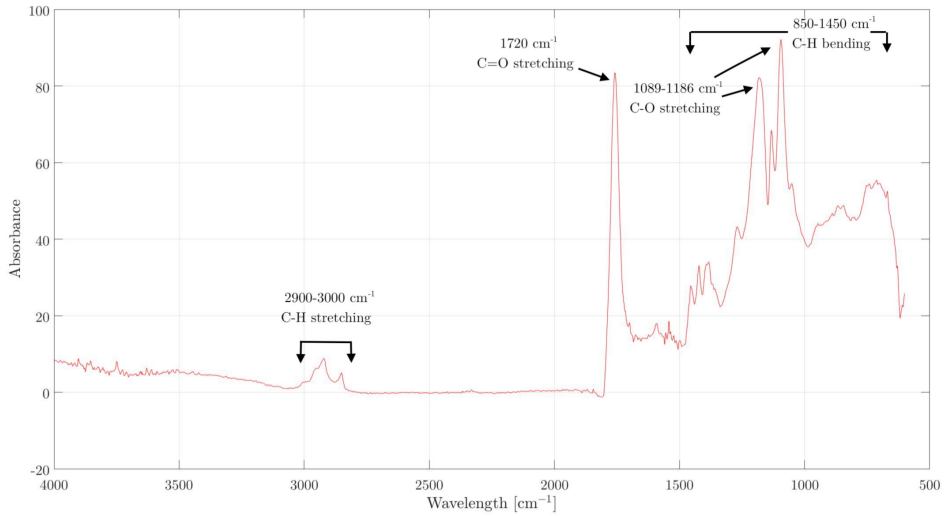

Figure 4.33 FTIR spectrum of PLGA obtained in reflection mode.

Table 4.3 Breakdown of the main peaks from the PLGA spectrum [1].

Wavelength [cm^{-1}]	**Attributed bond**
850-1450	C-H bending
1089-1186	C-O stretching
1720	C=O stretching
2900-3000	C-H stretching

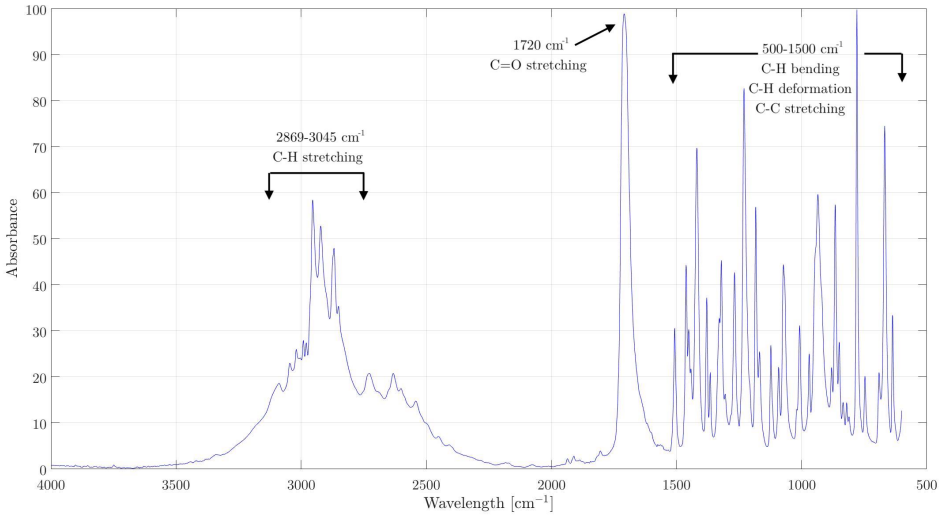

Figure 4.34 FTIR spectrum of ibuprofen powder obtained in reflection mode.

Table 4.4 Breakdown of the main peaks from the ibuprofen spectrum.

Wavelength [cm^{-1}]	**Attributed bond**
500-1500	C-H bending
500-1500	C-H deformation
500-1500	C-C stretching
1089-1186	C-O stretching
1720	C=O stretching
2869-3045	C-H stretching

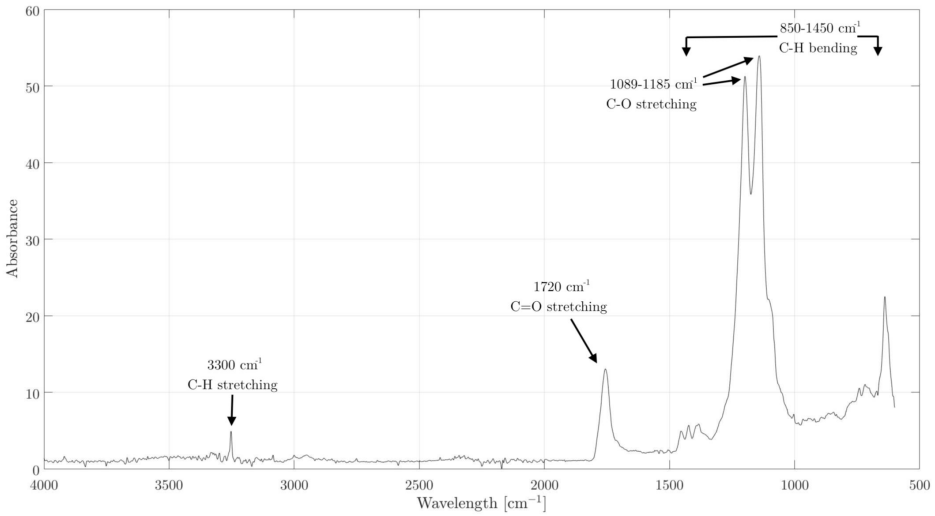

Figure 4.35 FTIR spectrum of PLGA-Ibuprofen particles obtained in reflection mode.

Table 4.5 Breakdown of the main peaks from the PLGA-ibuprofen particles spectrum.

Wavelength [cm^{-1}]	**Attributed bond**
850-1450	C-H bending
1089-1186	C-O stretching
1720	C=O stretching
3300	C-H stretching

As FTIR spectra of solutions with PBS and ibuprofen at different concentrations were being acquired, it was noticed that, for all of the molarities tested (up to 3 M) the spectra were identical to the ones of PBS alone. This posed the question of how to try and track the drug release without being able to change the technique used. An hypothesis was made that, since the scanning mode used was reflection, which only considers the superficial layer in contact with the FTIR crystal, the issue might be solved through switching to FTIR spectroscopy in transmission mode. Once again the project was faced with limitations determined by the available set-up, as the FTIR spectrometer was not equipped with an holder compatible with liquids. An alternative strategy developed to asses the presence of ibuprofen was to let the liquids evaporate from the crystal's surface. However, this meant that the analysis done could only be a qualitative assessment of free ibuprofen in the solution and the information provided cannot be used to define the release profile of the drug from the particles. To validate this hypothesis, a droplet of 10μL of PBS with 0.05 M ibuprofen was analysed, before and after PBS evaporation. As can be seen in Figure 4.37, in the dried state two new peaks appear

in the 1000-1200 cm^{-1} region. These peaks were then taken as fiducial points to assess the presence of free ibuprofen, as the drug itself presents a high density of peaks in the region. Unfortunately, this strategy was not developed until day 9 of testing and for this reason, no assumption can be made regarding a possible burst release of the drug in the first hours of immersion in PBS.

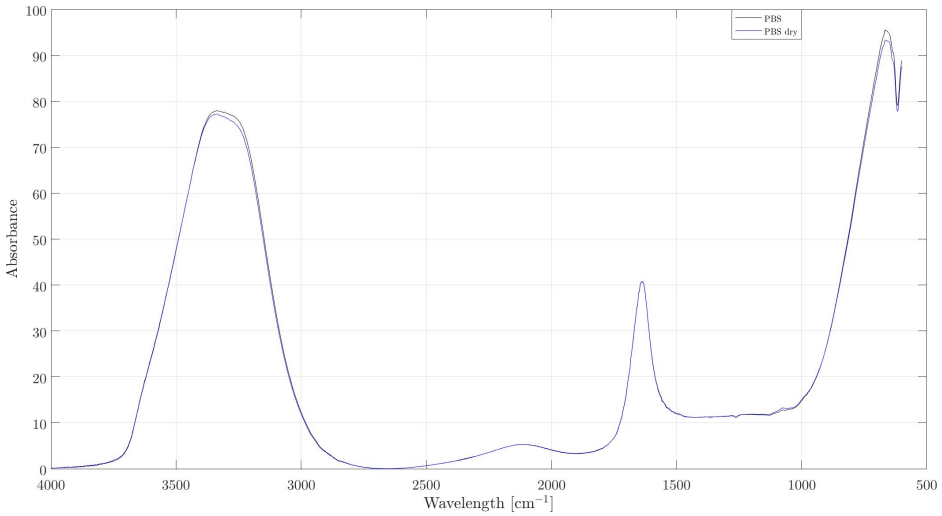

Figure 4.36 Comparison of FTIR spectra of 1μL droplet of PBS and the same droplet dried on the crystal obtained in reflection mode.

Following this process, it can be noted that the spectra for both groups, relative to the first 8 days of testing, closely resemble the PBS spectrum acquired in the same day as the sample spectra (Figures 4.38 and 4.41). In fact, even the smaller peak present in the region of the 3000-3500 cm^{-1} peak, for both groups, found in the acquisition at the beginning and after an hour of immersion in PBS, can be seen in the PBS spectra recorded on the same day. This similar behaviour between the droplets with and without PLGA-Ibuprofen particles continued for the duration of the whole experiment (Figures 4.39 and 4.42). The same does not happen when spectra acquired after PBS evaporation from the sample are concerned. In fact, as soon as the new procedure was put in place, the peaks observed in the 1000-1200 cm^{-1} region with only ibuprofen in PBS appeared (Figures 4.40 and 4.43). This should confirm the presence of free drug in the solution. As it was mentioned earlier, there is no clear way to know whether the ibuprofen that seems to have been released by day 9 was a consequence of a burst release of the drug in the first hours of testing or if it had been caused by a more gradual process. Moreover, it cannot be disregarded that, despite ibuprofen having shown peaks in the considered area when dispersed in PBS, both the drug and PLGA have

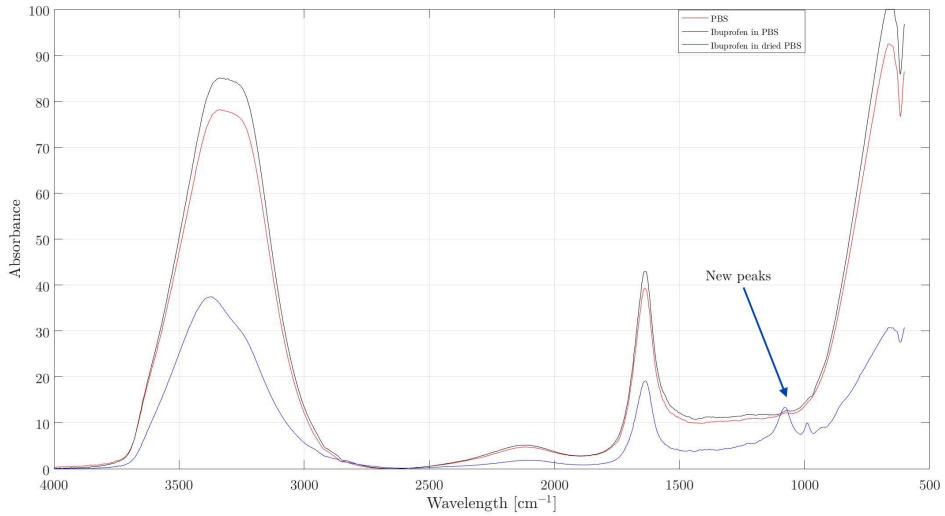

Figure 4.37 Comparison of FTIR spectra of a 1μL droplet of PBS, a 1μL droplet of PBS with 0.05 M ibuprofen and the same droplet dried on the crystal obtained in reflection mode. It can be noticed that the spectra of the two droplets are equivalent, safe for a small difference in intensity. The dried PBS with ibuprofen however present some peaks in the 1000-1200 cm^{-1} region.

highly absorbing bonds in the 1000-1200 cm^{-1} region and it can't be excluded that what is being seen in these spectra is, in fact, PLGA from the particles' shell. As it will be later discussed in section 4.3.4, the particles went through an agglomeration process, which could have greatly delayed the degradation of PLGA and, consequently, the release of ibuprofen.

Due to the qualitative aspect of the analysis performed in this work, no comment of note can be made regarding any difference in release behaviour of the drugs in the two groups. In order to be able to more confidently assess the release of the drug in a future reiteration of the experiment, alternative methods that could provide quantitative information need to be discussed. The easier adjustment would be employing FTIR holders specifically made for liquid samples, which could allow the use of transmission FTIR spectroscopy, such as mentioned by Rescignano et al. [1, 44]. Another option could be the use of UV spectroscopy to detect the drug release over time. All the methods mentioned (i.e. FTIR and UV) would require a calibration process with known amounts of the drug to extrapolate quantitative information from the results.

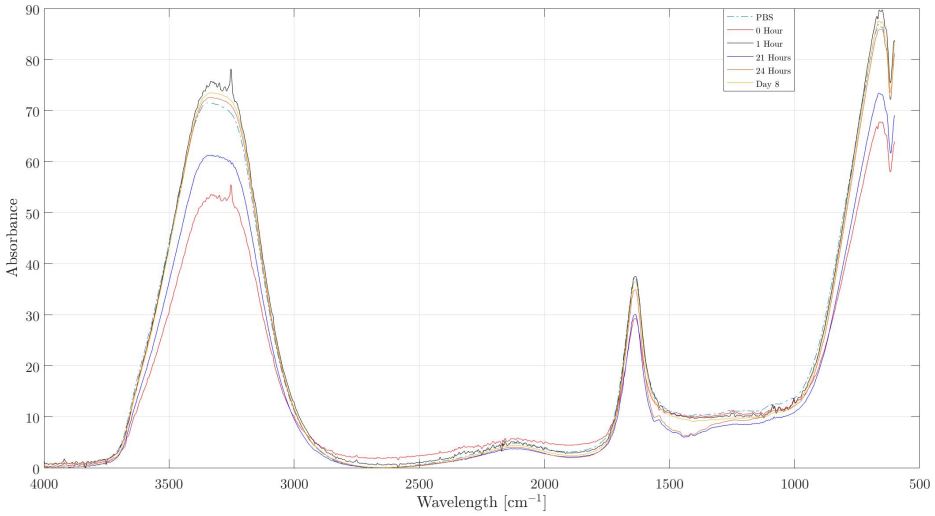

Figure 4.38 FTIR spectra of Group A obtained in reflection mode [Part 1]. No significant difference can be noticed between the spectra of the sample and PBS. The noise present for 0 and 1 Hour, noticeably the smaller peak in the midst of the 3000-3500 cm^{-1} peak was also there in the plain PBS spectra recorded on the same day and never reappeared over the course of the experiment.

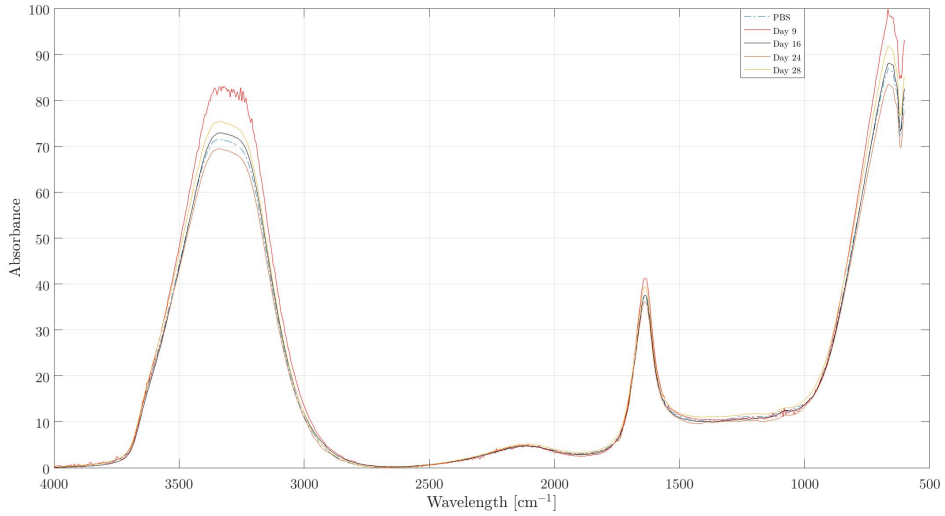

Figure 4.39 FTIR spectra of Group A obtained in reflection mode [Part 2]. No significant difference can be noticed between the spectra of the sample and PBS.

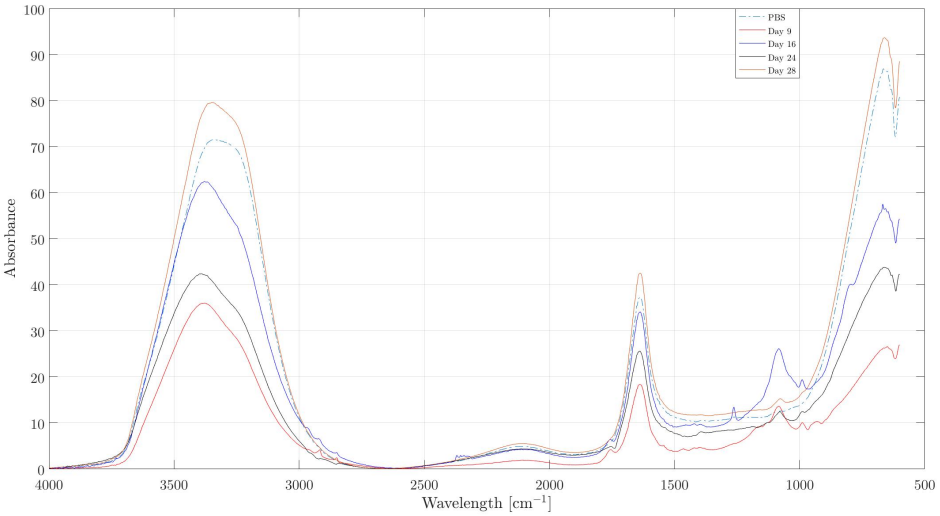

Figure 4.40 FTIR spectra of Group A obtained in reflection mode after a 10μL droplet of the sample was dried on the FTIR crystal. In the dried state new peaks appear in the 1000-1300 cm^{-1} region.

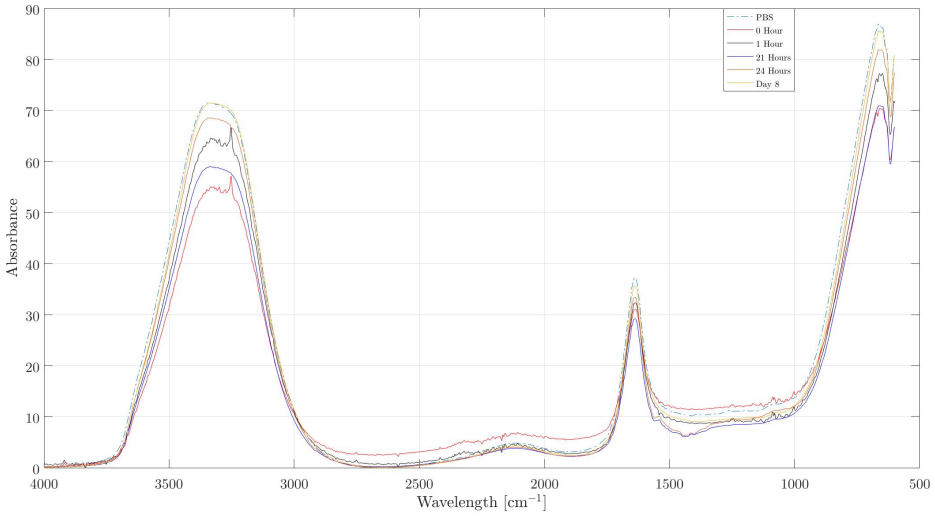

Figure 4.41 FTIR spectra of Group B obtained in reflection mode [Part 1]. No significant difference can be noticed between the spectra of the sample and PBS. The noise present for 0 and 1 Hour, noticeably the smaller peak in the midst of the 3000-3500 cm^{-1} peak was also there in the plain PBS spectra recorded on the same day and never reappeared over the course of the experiment.

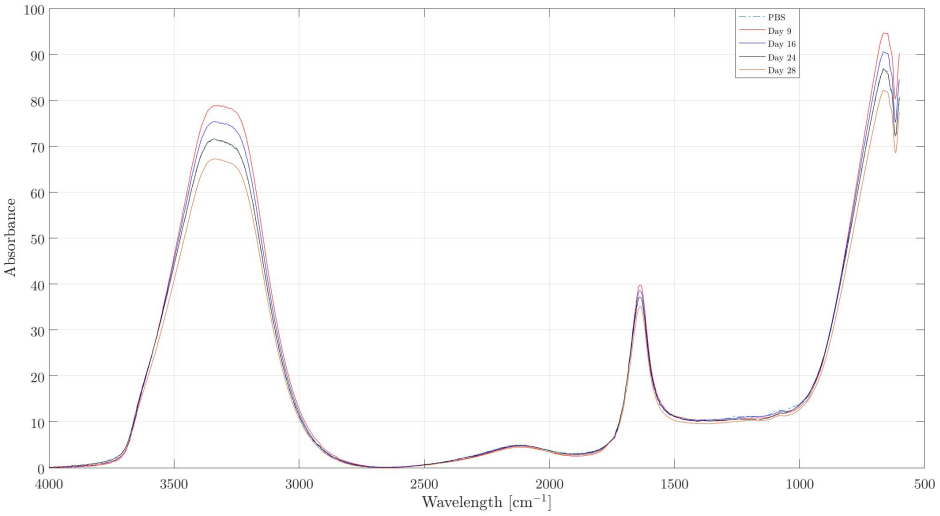

Figure 4.42 FTIR spectra of Group B obtained in reflection mode [Part 2]. No significant difference can be noticed between the spectra of the sample and PBS.

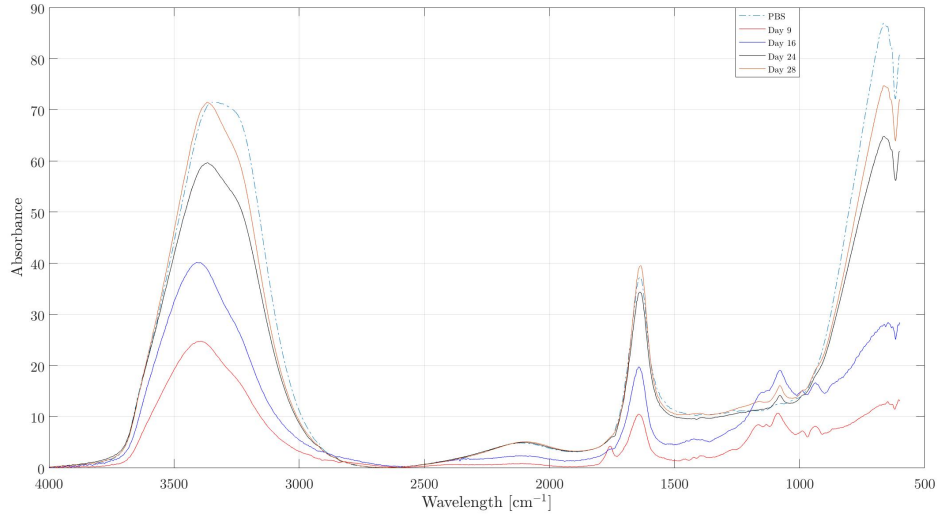

Figure 4.43 FTIR spectra of Group B obtained in reflection mode after a 10μL droplet of the sample was dried on the FTIR crystal. In the dried state new peaks appear in the 1000-1300 cm^{-1} region.

4.3.2 pH

The pH was used as an indicator of PLGA degradation, whose end products are of acidic nature. The pH of the samples stayed relatively close to the controls until the second week (day 15 and 16), when it began to continuously progress towards lower values, as the buffer effect of the PBS solution started to lose power against the increasing concentrations of glycolic and lactic acids. This was taken as a sign that PLGA had begun its degradation process. As can be observed in Figure 4.44, the process for the two groups followed the same trend for the first and second week, while from the third, the pH started lowering for Group B at a much faster rate, in compliance with the expected behaviour. It is important to point out that the particles were tested in a closed system, with acidic by-products accumulating in it through the weeks of testing. For this reason, it could be interesting, in a second iteration of the degradation tests, to simulate an open system, for example by removing a percentage of the solution periodically and exchanging it for fresh PBS, to better assess the impact of the degradation products on the pH of a tissue, and evaluate the possibility of triggering an inflammatory response.

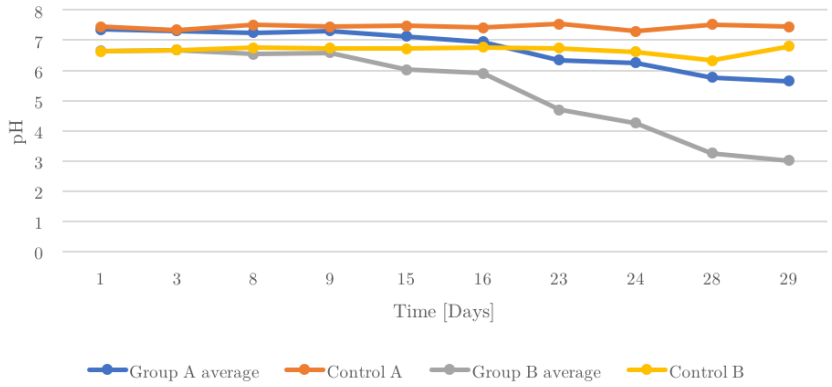

Figure 4.44 pH monitoring over the course of the experiment. Group A and Control A starting from a pH of 7.4; Group B and Control B starting from a pH of 6.6

4.3.3 Mass remaining

One sample from each group was taken out the incubator on day 2 of the testing and once a week for the duration of the experiment. The samples were desiccated and then weighted to assess mass remaining. From the design of this experiment, the total weight of the particles and their by-products was expected to stay constant throughout the weeks as the system was closed. What was then discovered during the analysis of the results, was that every

sample seemed to have been doubled in weight. In an effort to explain this fact, the protocol for these tests was taken under review. A possible reasoning was found in the precipitation of salts present in PBS, that had not been washed out from the solution before desiccation as it is custom. To confirm this hypothesis, an estimate of the salts' weight in the samples was made. In fact, the calculations showed that the order of magnitude of precipitated salts from PBS present in the vials was compatible with the weight increase. Since the estimate considered a uniform distribution of the salts in the PBS solution, the actual reliability of these tests is put into question, as it's not possible to actually distinguish between remaining mass from the particles and mass from the precipitated salts.

Moreover, upon reflection on this specific test and the information that it would have provided, a test performed by Gel permeation chromatography (GPC) would have supplied much more interesting data regarding the degradation process [19]. In fact, analysing the differences in molecular weight distribution of the PLGA samples over the course of the experiment, would have provided tangible information regarding the onset and the progress of the polymer's degradation. What would have been expected in this case, was to see PLGA maintain its molecular weight distribution during the first weeks, in which the polymer absorbs water; during the following weeks the GPC would have begun to show more and more particulates in the lower weight range, with a progressive decrease of heavier components [45].

4.3.4 Scanning Electron Microscopy (SEM)

SEM imaging taken at the end of the experiment offers some more insights on the degradation of PLGA. The expected behaviour was a swelling of the polymer in the first weeks, as it absorbed water into its matrix, followed by the actual dismantling of the particles into smaller fragments. Images available from day 3 of the tests (Figure 4.45), showed that aggregates had formed over the course of these days. An explanation of this phenomenon could have been obtained through an electrophoretic DLS test to measure the zeta potential. This parameter, in fact, can be used as a mean to assess the behaviour of particles in solution. Shnoudeh et al., report that particles with zeta potential values between -25 mV and +25 mV may be most likely subjected to phenomena of coagulation or flocculation [46], such as the present case. This is explained by the fact that particles lacking strong surface charges will be less likely to be reciprocally repulsed and, considering the dimensional scales involved, will at the same time experience strong van der Waals forces, bringing them together.

Whilst the presence of aggregates, together with approaching the resolution limits of the SEM used, made it harder to obtain clear images and analyse the changes in the single particles, an effort will still be made later to deduct their morphological progress. For what

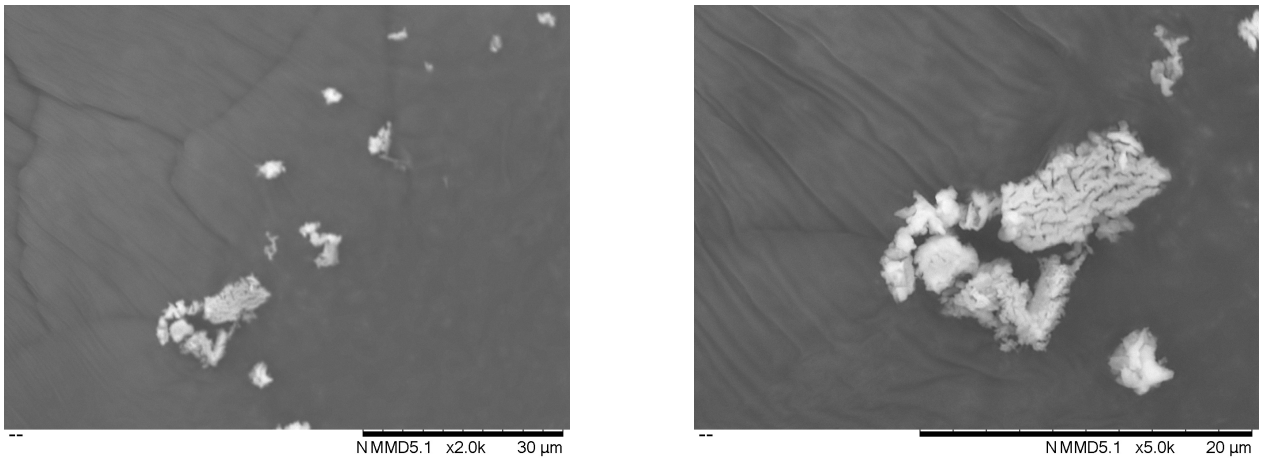

(a) (b)

Figure 4.45 Particle aggregation on SEM images from day 3 of testing: (a) aggregates wider view; (b) close up of aggregates; Scale bar: (a) 30 μm; (b) 20 μm.

concerns SEM limitations, Field Emission Scanning Electron Microscopy (FESEM) could be used to be able to have better resolution at the high magnification levels needed to better observe the particles' morphology [1]. The main difference between SEM and FESEM lies in the way electrons are generated. While SEM does so by employing thermionic emitters, FESEM utilizes a field emission gun, which provides more focused electron beams, improving the resolution [47]. In terms of the application, the aggregates have several consequences. The PLGA degradation will most likely be delayed, as it might have been the case in this experiment, due to the ratio of collective exposed surface area over total volume being reduced in comparison to single particles, with the inner layers being shielded, if not completely at least in a majority. This factor will strongly impact the time frame of the drug's release which will also be delayed proportionally to each cluster's dimension. The other issue is that the particle size strongly influences their biodistribution, meaning the paths the compounds take inside the body and the tissues they end up reaching (see Chapter 2) and agglomerates in the range of few tens of micrometers will most definitely have different distribution and clearance pathways than the expected. A further consideration has to be made in regards of the presence of clusters of particles of different dimension. In fact, smaller aggregates will have a much quicker degradation process in comparison to larger ones. For example, in Figures 4.46e and 4.48, two images acquired from the same sample show particles at two different merging stages, with the first having much more clear edges defining the single particles. This allows to hypothesise that the drug detected with FTIR spectroscopy may have come from either one of these smaller clusters or from the superficial layers of the bigger

ones.

The general behaviour of the two groups seems to be very similar with close-by particles progressively merging together. Until day 16 included, the edges of the different particles can still be recognized, although it is clear that as time goes by this distinction becomes more and more only a superficial feature (Figures from a) through f) 4.46). The edges of the single particles are not clearly identifiable in the images relative to day 23 and 28 (Figures 4.47 g) through j)), signaling a further progression of the merging process. In fact, in some areas, the original shapes can be recognized whereas in some others, the particles are completely merged in a matrix.

Once again, while the particles continued their merging process through day 28, the presence of clusters has noticeably slowed down the degradation process due to the lowered ratio of surface area exposed over volume. This is evident as particles seem to be still in the swelling stages and no porosity can be detected in the matrix for either of the two sample groups. The presence of porosity in this polymeric matrix would, in fact, signify the beginning of the fragmentation of the PLGA particles. While the lack of evident pores could be due to the low resolution of the images, it is not believed to be the case in this specific occurrence. In an effort to make a final comparison between the groups, clusters of similar dimension (Figures 4.46i and j), can be taken into account. In fact, removing the variable of different aggregate sizes, the particles in Group B (Figure 4.46j) seem to have reached a higher level of merging with one another, compared to the ones in Group A (Figure 4.46i), which would be compliant with the starker reduction in pH observed in Group B.

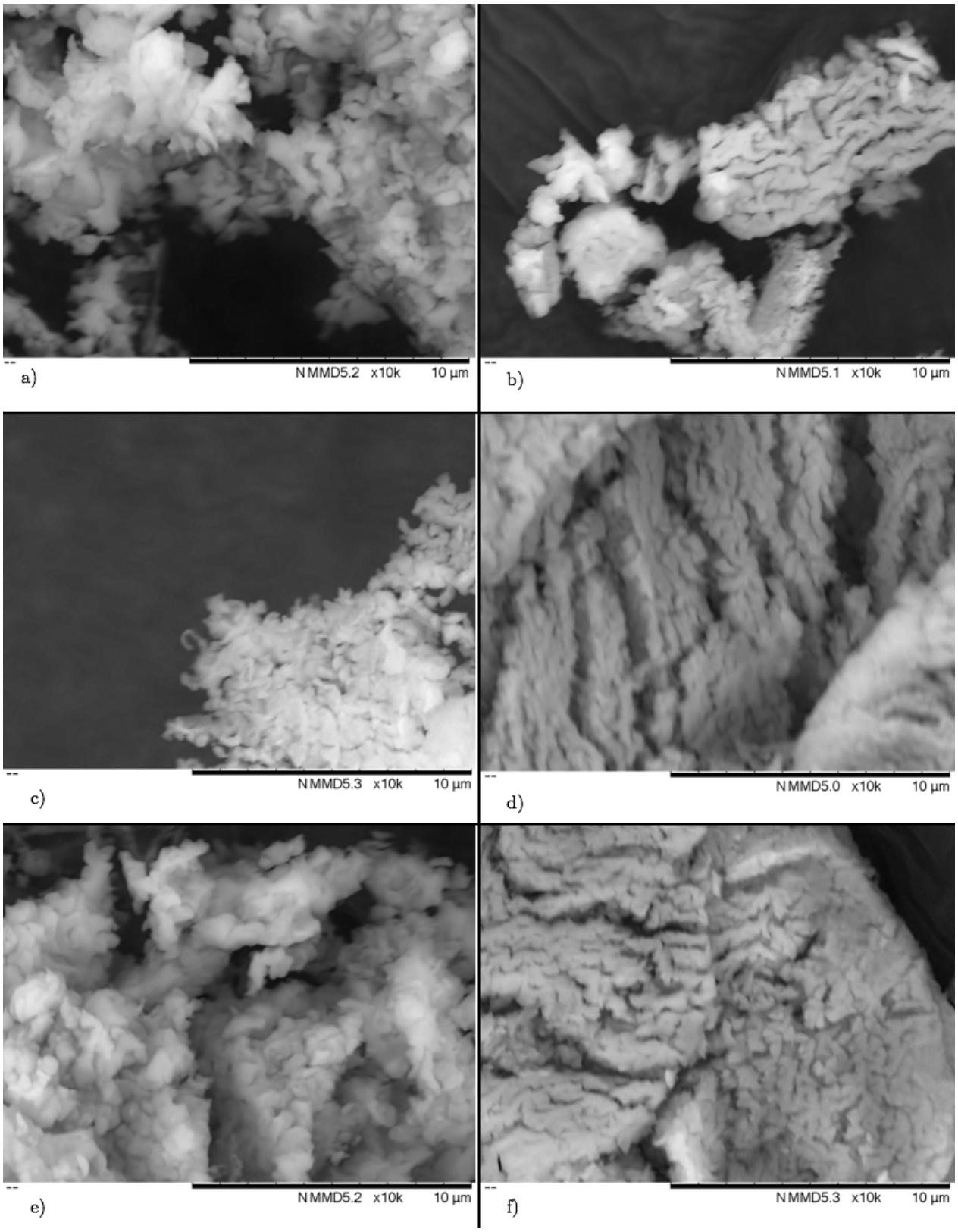

Figure 4.46 SEM images from the degradation tests (Part 1). On the left, are samples from Group A (pH 7.4), on the right are samples from Group B (pH 6.6). The time-points represented are as follows: a) and b) are from day 3; c) and d) are from day 9; e) and f) are from day 16.

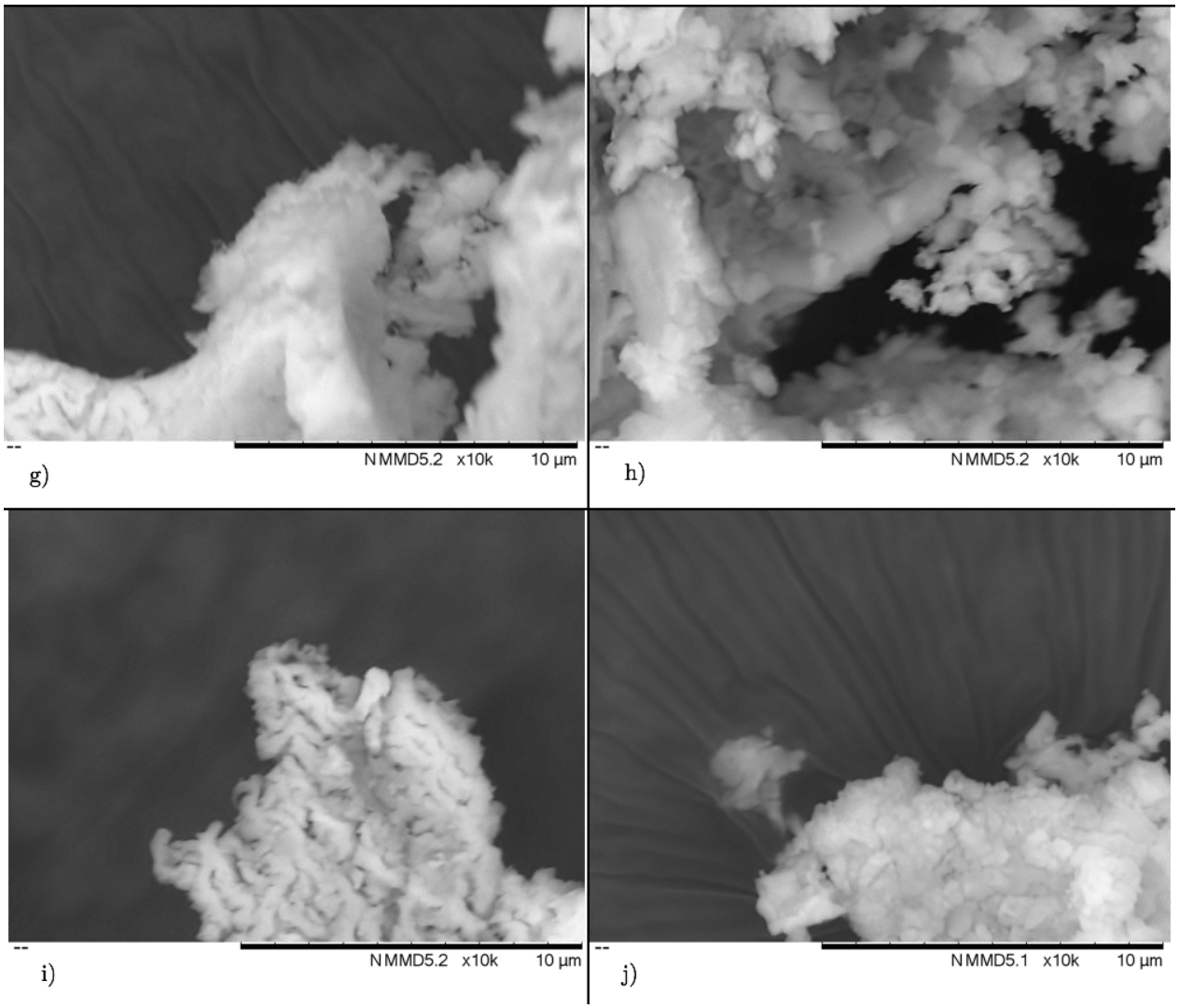

Figure 4.47 SEM images from the degradation tests (Part 2). On the left, are samples from Group A (pH 7.4), on the right are samples from Group B (pH 6.6). The time-points represented are as follows: g) and h) are from day 23; f) and j) are from day 28.

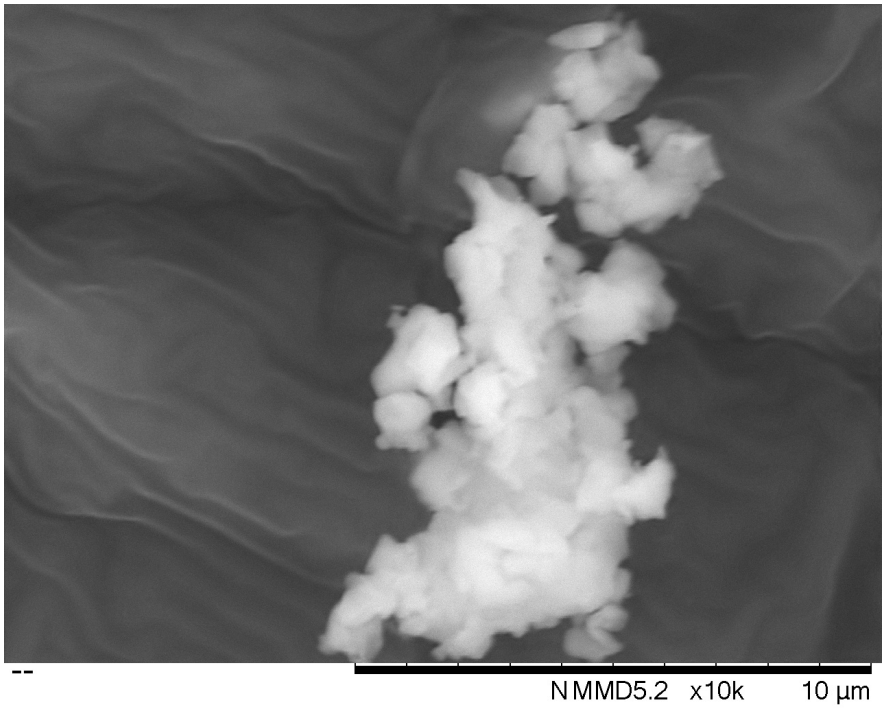

Figure 4.48 SEM image from the degradation tests. Group A (pH 7.4), from day 16. A smaller cluster seems to be further away in the degradation process than larger ones in the same sample (Figure 4.46e)

4.4 Image analysis

A brief commentary is needed regarding the image analysis. Two main issues and areas of improvement have been identified. The first, relates to the way the particles' diameters are computed. In fact, the software provides the user with the area occupied by each single particle. This value is then used to calculate the diameter under the hypothesis that the particles in the image are perfect circles, thus not accounting for the different eccentricities that may in reality be present and introducing possible errors.

The second area of improvement can be found in the software itself, specifically in its ability to identify different particles located in close contact or proximity. Often these will be considered by the software as one big cluster, as the thresholding process, necessary to run the particle analysis, inevitably removes the discontinuities that make us able to distinguish between two close ones. This effect becomes especially noticeable for groups of multiple close particles, as well as for images that may present differences in the background or speckles of noise across its area. The last two features may even be falsely recognized as particles themselves as they may present similar grey levels to actual ones, and therefore have been brought along through the analysis after thresholding. These types of errors may require the user to manually remove the false particles or divide clusters of real ones, rendering the process of image analysis lengthier and more taxing. Moreover, when this procedure is automatized, the user has less control over this issue which may bring about inaccurate results. A path worthy of investigation might be associating the thresholding process with recognition of the edges in the grayscale image, imposing eccentricity and dimensional limits on the contours recognized in order to more precisely convert the grayscale image to binary.

CHAPTER 5 CONCLUSION AND RECOMMENDATIONS

This project set out to design, fabricate and characterize a drug delivery structure using the electrospinning or electrospraying technique. The first objective was related to identifying a pharmaceutical agent that would benefit more of such approach in the field of cancer treatment, while also trying to look for a drug that was not yet commonly encapsulated using the aforementioned techniques.

Once this chemotherapeutic agent, doxorubicin, was decided upon, the focus switched to fulfilling the second objective, in which the most appropriate time frame and conditions for its delivery had to be defined, in order to gather the required properties of the material that would be used for this entrapment. The final idea was to have particles, under the micrometric scale, with a shell made of a material capable of bulk degradation, that would slowly lose mass and create paths for the drug to diffuse out of, in a gradual manner, over the course of three to four weeks. The chosen material was a 50/50 poly(lactic-co-glycolic acid) (PLGA) copolymer as previous applications, using the electrospraying technique with a different encapsulated agent, demonstrated the feasibility of its compliance with the set dimensional and temporal requirements. Ibuprofen was selected as a test drug to be used instead of DOX during the preliminary steps of the work.

The third objective, the optimization of the production process, took up the majority of this project. In fact, as well as identifying the most appropriate parameters, a period of familiarization with the electrospraying technique was required to fully understand the subtle interplay of the available variables, and which ones were to be adjusted to reach the final goal. Moreover, as the measures against Covid-19 had forced the experiments to a halt, the optimized parameters were tested by a change in the environmental conditions, in particular a rise in the humidity, once the access to the laboratories was restored. After a phase of tests geared towards reestablishing the ideal conditions for the optimized parameters, it was decided to utilize a different set-up, equipped with a system able to reduce humidity in the process' environment. To employ this new configuration, a number of instruments from different set-ups had to be specifically combined. A new parameter optimization phase was then quickly realized, partially thanks to the progress from the previous one, partially owing to a better understanding of the process and the variables' interplay.

Finally, the characterization of drug delivery, i.e. the last objective, could take place. A protocol for a degradation test was designed and put in place, once again within the limits of the safety measures set up for Covid-19. The polymer's degradation was observed

in two conditions: one at a pH of 7.4, one at pH 6.6, to better mimic the slightly acidic cancerous environment. This process was monitored for 4 weeks, taking note of the pH, the weight loss, recording the FTIR spectra, and setting samples aside for SEM observations. These experiments were able to hypothesise a time frame for the drug release, as well as confirm the ongoing degradation process of PLGA. Moreover, the SEM evidenced the presence of agglomerates, whose origin could have been explained by measuring the particles' zeta potential. Unfortunately, the forced pause in the work affected the last phase of the project, the *in vitro* cell tests, that had been originally planned but was not possible to safely realize. This contributed to the impossibility to completely fulfill the final objective, as well as the verification of the initial hypothesis of the possibility to lower treatment dosages by employing controlled delivery.

Despite the promises the technique of coaxial electrospraying offers, this project highlighted some of its issues in comparison to more classical methods used for core-shell particle production. In fact, while these often offer validated, reliable procedures that allow for a quick implementation of fabrication protocols, the same does not apply to coaxial electrospraying. In fact, one of its most praised features, its versatility, can sometimes be pointed out as the cause of lengthy optimization times. This is particularly true when the desired particle size falls under 400 nm, range which classical techniques have long proven to be able to reach, whereas coaxial electrospraying often has to sacrifice particle morphology to attempt to do so. However, the possibility of producing microscale core-shell particles in a one-step procedure, can still be considered as an attractive feature of this technique compared to others, and future works utilizing this method may be more appropriately applied in this higher target-scale, perhaps with a focus on how to improve production yield. In a similar manner, coaxial electrospinning may still be an extremely interesting and encouraging process for what concerns the fabrication of filaments and mats, that could be employed as drug-delivering scaffolds in applications of tissue regeneration and wound healing. One last recommendation relates to the susceptibility this technique has for changes in the surrounding environment. In fact, one should try to isolate the electrospraying system as much as feasible from outer conditions, in order to reduce the variability that may be brought on by possible modifications.

For what concerns future improvements and limitations specific to the present project, many opportunities for amelioration can be found in its last phases. In fact, the second optimization was carried out under a pressing time limit, therefore it was interrupted as soon as acceptable results were obtained, without further investigations on possibilities for improvements. Due to the combined effects of the chosen technique's poor yield and restricted access to the laboratories, the degradation study had to be limited both in the array of

samples and in the product's concentrations in each of them. This issue contributed to the impossibility of tracking the drug release in a quantitative manner. Another factor being the limits of the available FTIR spectrometer concerning transmission spectrometry of liquid samples. Finally, it was not possible to test the structure for its *in vitro* efficacy in the presence of a cancer cells culture, which was the ultimate aim of this project and would therefore be its natural progression, provided that the agglomeration seen thanks to SEM imaging is studied further. In this framework, useful information may be gathered by a direct comparison to liposomial formulations already in the market, highlighting advantages or disadvantages of the formulation presented in this work. Another focal point for the future development of this project should be the final administration to the patients, once the particle size achievable with the used technique has been determined. According to this size, as well as the particle's stability, different administration routes may be preferred after careful evaluation of their advantages and disadvantages. The information gathered during the present work seem to suggest that this type of formulation may be more appropriately delivered through an intratumoral local administration, which would widen the acceptable size range of the particles and limit the challenge of controlling the biodistribution of the particles in a more systemic administration route.

Several limitations were directly related to restrictions put in place in order to limit the spread of Covid-19, others were more indirect, such as the constant reality of needing to take a different approach or use a different instrument than what was originally planned. Some examples of such impact on this project were mentioned earlier, others were the reduced time points taken during the degradation tests and the impossibility of safely encapsulating and testing DOX whilst complying with the restrictions and avoiding the disruption of the work of other laboratory users. In this case, the hope is that if someone in future is planning to continue this work, they would be in the position of doing so in more normal conditions, in which these improvements and recommendations could be easily implemented.

REFERENCES

[1] N. Rescignano, L. Tarpani, A. Romani, I. Bicchi, S. Mattioli, C. Emiliani, L. Torre, J. Kenny, S. Martino, L. Latterini, and I. Armentano, "In-vitro degradation of plga nanoparticles in aqueous medium and in stem cell cultures by monitoring the cargo fluorescence spectrum," *Polymer Degradation and Stability*, vol. 134, pp. 296 – 304, 2016. [Online]. Available: http://www.sciencedirect.com/science/article/pii/S0141391016303342

[2] N. Bhardwaj and S. C. Kundu. The electrospinning apparatus. [Online]. Available: https://commons.wikimedia.org/wiki/File:Electrospinning_apparatus.jpg

[3] D. Peer, J. Karp, S. Hong, O. C. Farokhzad, R. Margalit, and R. Langer, "Nanocarriers as an emerging platform for cancer therapy," *Nature Nanotech*, no. 2, pp. 751—760, December 2007. [Online]. Available: https://www.nature.com/articles/nnano.2007.387

[4] C. U. Yurteri, R. P. Hartman, and J. C. Marijnissen, "Producing pharmaceutical particles via electrospraying with an emphasis on nano and nano structured particles - a review," *KONA Powder and Particle Journal*, vol. 28, pp. 91–115, 2010.

[5] J. Yujia, Z. Yihua, Y. Xiaoling, S. Jianhua, and L. Chunzhong, "Ultrasound-triggered smart drug release from multifunctional coreshell capsules one-step fabricated by coaxial electrospray method," *Langmuir*, vol. 27, no. 3, pp. 1175–1180, 2011, pMID: 21182239. [Online]. Available: https://doi.org/10.1021/la1042734

[6] Y. Dengke, Y. Ye, C. Hanxu, W. Fei, P. Daiyin, and H. Liqing, "Gambogic acid-loaded electrosprayed particles for site-specific treatment of hepatocellular carcinoma," *Molecular Pharmaceutics*, vol. 11, no. 11, pp. 4107–4117, 2014, pMID: 25290462. [Online]. Available: https://doi.org/10.1021/mp500214a

[7] Y. Wu, J. A. MacKay, J. R. McDaniel, A. Chilkoti, and R. L. Clark, "Fabrication of elastin-like polypeptide nanoparticles for drug delivery by electrospraying," *Biomacromolecules*, vol. 10, no. 1, pp. 19–24, 2009, pMID: 19072041. [Online]. Available: https://doi.org/10.1021/bm801033f

[8] Sigma-Aldrich. Sigma-aldrich. [Online]. Available: https://www.sigmaaldrich.com/

[9] F. Bray, J. Ferlay, I. Soerjomataram, R. L. Siegel, L. A. Torre, and A. Jemal, "Global cancer statistics 2018: Globocan estimates of incidence and mortality worldwide for

36 cancers in 185 countries," *CA: A Cancer Journal for Clinicians*, vol. 68, no. 6, pp. 394–424, 11 2018. [Online]. Available: https://doi.org/10.3322/caac.21492

[10] Mayo-Clinic-Staff. Chemotherapy for breast cancer. [Online]. Available: https://www.mayoclinic.org/tests-procedures/chemotherapy-for-breast-cancer/about/pac-20384931

[11] S. Talebian, J. Foroughi, S. J. Wade, K. L. Vine, A. Dolatshahi-Pirouz, M. Mehrali, J. Conde, and G. G. Wallace, "Biopolymers for antitumor implantable drug delivery systems: Recent advances and future outlook," *Advanced Materials*, vol. 30, no. 31, p. 1706665, 2018. [Online]. Available: https://onlinelibrary.wiley.com/doi/abs/10.1002/adma.201706665

[12] A. Haider, S. Haider, and I.-K. Kang, "A comprehensive review summarizing the effect of electrospinning parameters and potential applications of nanofibers in biomedical and biotechnology," *Arabian Journal of Chemistry*, vol. 11, no. 8, pp. 1165 – 1188, 2018. [Online]. Available: http://www.sciencedirect.com/science/article/pii/S1878535215003275

[13] K. M. Laginha, S. Verwoert, G. J. Charrois, and T. M. Allen, "Determination of doxorubicin levels in whole tumor and tumor nuclei in murine breast cancer tumors," *Clinical Cancer Research*, vol. 11, no. 19, pp. 6944–6949, 2005. [Online]. Available: https://clincancerres.aacrjournals.org/content/11/19/6944

[14] T. Grenader, A. Goldberg, and A. Gabizon, "Monitoring long-term treatment with pegylated liposomal doxorubicin: how important is intensive cardiac follow-up?" *Anti-Cancer Drugs*, vol. 21, no. 9, pp. 868—871, October 2010. [Online]. Available: https://journals.lww.com/anti-cancerdrugs/Abstract/2010/10000/Monitoring_long_term_treatment_with_pegylated.9.aspx

[15] U. Prabhakar, D. C. Blakey, H. Maeda, R. K. Jain, E. M. Sevick-Muraca, W. Zamboni, O. C. Farokhzad, S. T. Barry, A. Gabizon, and P. Grodzinski, "Challenges and key considerations of the enhanced permeability and retention effect (epr) for nanomedicine drug delivery in oncology," *Cancer Research*, 2013. [Online]. Available: https://cancerres.aacrjournals.org/content/early/2013/02/16/0008-5472.CAN-12-4561

[16] G. Yang, X. Li, Y. He, J. Ma, G. Ni, and S. Zhou, "From nano to micro to macro: Electrospun hierarchically structured polymeric fibers for biomedical applications," *Progress in Polymer Science*, vol. 81, pp. 80 – 113, 2018. [Online]. Available: http://www.sciencedirect.com/science/article/pii/S0079670017300138

[17] Y. Fu, X. Li, Z. Ren, C. Mao, and G. Han, "Multifunctional electrospun nanofibers for enhancing localized cancer treatment," *Small*, vol. 14, no. 33, p. 1801183, 2018. [Online]. Available: https://onlinelibrary.wiley.com/doi/abs/10.1002/smll.201801183

[18] M. A. Phillips, M. L. Gran, and N. A. Peppas, "Targeted nanodelivery of drugs and diagnostics," *Nano today*, vol. 5, no. 2, pp. 143—159, April 2010. [Online]. Available: http://europepmc.org/articles/PMC2882307

[19] E. M. Elmowafy, M. Tiboni, and M. E. Soliman, "Biocompatibility, biodegradation and biomedical applications of poly(lactic acid)/poly(lactic-co-glycolic acid) micro and nanoparticles," *J. Pharm. Investig.*, no. 49, pp. 347—380, July 2019. [Online]. Available: https://doi.org/10.1007/s40005-019-00439-x

[20] J. P. Jain, D. Chitkara, and N. Kumar, "Polyanhydrides as localized drug delivery carrier: an update," *Expert Opinion on Drug Delivery*, vol. 5, no. 8, pp. 889–907, 2008, pMID: 18712998. [Online]. Available: https://doi.org/10.1517/17425247.5.8.889

[21] H. K. Makadia and S. J. Siegel, "Poly lactic-co-glycolic acid (plga) as biodegradable controlled drug delivery carrier," *Polymers*, vol. 3, no. 3, pp. 1377—1397, 2011. [Online]. Available: https://doi.org/10.3390/polym3031377

[22] J. Heller, J. Barr, S. Y. Ng, K. S. Abdellauoi, and R. Gurny, "Poly(ortho esters): synthesis, characterization, properties and uses," *Advanced drug delivery reviews*, vol. 54, no. 7, p. 1015—1039, October 2002. [Online]. Available: https://doi.org/10.1016/s0169-409x(02)00055-8

[23] A. Tiwari, Y. K. Mishra, H. Kobayashi, and A. P. F. Turner, *Intelligent Nanomaterials*, ser. Advanced Material Series. Wiley, 2016. [Online]. Available: https://books.google.ca/books?id=xgI_DQAAQBAJ

[24] N. Bock, T. R. Dargaville, and M. A. Woodruff, "Electrospraying of polymers with therapeutic molecules: State of the art," *Progress in Polymer Science*, vol. 37, no. 11, pp. 1510 – 1551, 2012, topical Issue on Polymeric Biomaterials. [Online]. Available: http://www.sciencedirect.com/science/article/pii/S0079670012000366

[25] N. D. Nhat, C. Clasen, and G. Van den Mooter, "Pharmaceutical applications of electrospraying," *Journal of Pharmaceutical Sciences*, vol. 105, no. 9, pp. 2601–2620, 2019/09/10 2016. [Online]. Available: https://doi.org/10.1016/j.xphs.2016.04.024

[26] X. Huang, J. Gao, N. Zheng, W. Li, H. Xue, and R. K. Y. Li, "Influence of humidity and polymer additives on the morphology of hierarchically porous microspheres prepared

from non-solvent assisted electrospraying," *Colloids and Surfaces A: Physicochemical and Engineering Aspects*, vol. 517, pp. 17 – 24, 2017. [Online]. Available: http://www.sciencedirect.com/science/article/pii/S0927775717300031

[27] U. Bilati, E. Allémann, and E. Doelker, "Development of a nanoprecipitation method intended for the entrapment of hydrophilic drugs into nanoparticles," *European Journal of Pharmaceutical Sciences*, vol. 24, no. 1, pp. 67 – 75, 2005. [Online]. Available: http://www.sciencedirect.com/science/article/pii/S0928098704002507

[28] D. Moinard-Chécot, Y. Chevalier, S. Briançon, L. Beney, and H. Fessi, "Mechanism of nanocapsules formation by the emulsion–diffusion process," *Journal of Colloid and Interface Science*, vol. 317, no. 2, pp. 458 – 468, 2008. [Online]. Available: http://www.sciencedirect.com/science/article/pii/S0021979707014348

[29] C. E. Mora-Huertas, H. Fessi, and A. Elaissari, "Polymer-based nanocapsules for drug delivery," *International Journal of Pharmaceutics*, vol. 385, no. 1, pp. 113 – 142, 2010. [Online]. Available: http://www.sciencedirect.com/science/article/pii/S0378517309007273

[30] N. Leister and H. P. Karbstein, "Evaluating the stability of double emulsions—a review of the measurement techniques for the systematic investigation of instability mechanisms," *Colloids and Interfaces*, vol. 4, no. 1, 2020. [Online]. Available: https://www.mdpi.com/2504-5377/4/1/8

[31] J. A. Tapia-Hernández, P. I. Torres-Chávez, B. Ramírez-Wong, A. Rascón-Chu, M. Plascencia-Jatomea, C. G. Barreras-Urbina, N. A. Rangel-Vázquez, and F. Rodríguez-Félix, "Micro- and nanoparticles by electrospray: Advances and applications in foods," *Journal of Agricultural and Food Chemistry*, vol. 63, no. 19, pp. 4699–4707, 2015, pMID: 25938374. [Online]. Available: https://doi.org/10.1021/acs.jafc.5b01403

[32] H. Cheng, X. Yang, X. Che, M. Yang, and G. Zhai, "Biomedical application and controlled drug release of electrospun fibrous materials," *Materials Science and Engineering: C*, vol. 90, pp. 750 – 763, 2018. [Online]. Available: http://www.sciencedirect.com/science/article/pii/S0928493117322701

[33] J. Xie, L. K. Lim, Y. Phua, J. Hua, and C.-H. Wang, "Electrohydrodynamic atomization for biodegradable polymeric particle production," *Journal of Colloid and Interface Science*, vol. 302, no. 1, pp. 103 – 112, 2006. [Online]. Available: http://www.sciencedirect.com/science/article/pii/S0021979706005546

[34] L. Ding, T. Lee, and C.-H. Wang, "Fabrication of monodispersed taxol-loaded particles using electrohydrodynamic atomization," *Journal of Controlled Release*, vol. 102, no. 2, pp. 395 – 413, 2005. [Online]. Available: http://www.sciencedirect.com/science/article/pii/S0168365904004924

[35] H. Nie, Y. Fu, and C.-H. Wang, "Paclitaxel and suramin-loaded core/shell microspheres in the treatment of brain tumors," *Biomaterials*, vol. 31, no. 33, pp. 8732 – 8740, 2010. [Online]. Available: http://www.sciencedirect.com/science/article/pii/S014296121000952X

[36] C. Yang, W. Bochu, W. Yazhou, and L. Deshuai, "Polymer-controlled core–shell nanoparticles: a novel strategy for sequential drug release," *RSC Adv.*, vol. 4, pp. 30 430–30 439, 2014. [Online]. Available: http://dx.doi.org/10.1039/C4RA03610G

[37] K. Songsurang, N. Praphairaksit, K. Siraleartmukul, and N. Muangsin, "Electrospray fabrication of doxorubicin-chitosan-tripolyphosphate nanoparticles for delivery of doxorubicin," *Arch. Pharm. Res.*, no. 34, p. 583, 2011. [Online]. Available: https://doi.org/10.1007/s12272-011-0408-5

[38] H. Park, P.-H. Kim, T. Hwang, O.-J. Kwon, T.-J. Park, S.-W. Choi, C.-O. Yun, and J. H. Kim, "Fabrication of cross-linked alginate beads using electrospraying for adenovirus delivery," *International Journal of Pharmaceutics*, vol. 427, no. 2, pp. 417 – 425, 2012. [Online]. Available: http://www.sciencedirect.com/science/article/pii/S0378517312001044

[39] J. Schindelin, I. Arganda-Carreras, and E. Frise, "Fiji: an open-source platform for biological-image analysis," *Nature methods*, vol. 9, no. 7, pp. 676—682, July 2012. [Online]. Available: https://www.nature.com/articles/nmeth.2019#rightslink

[40] G. Minotti, P. Menna, E. Salvatorelli, G. Cairo, and L. Gianni, "Anthracyclines: Molecular advances and pharmacologic developments in antitumor activity and cardiotoxicity," *Pharmacological Reviews*, vol. 56, no. 2, pp. 185–229, 2004. [Online]. Available: https://pharmrev.aspetjournals.org/content/56/2/185

[41] N. Bhattarai, H. R. Ramay, S. H. Chou, and M. Zhang, "Chitosan and lactic acid-grafted chitosan nanoparticles as carriers for prolonged drug delivery," *International journal of nanomedicine*, vol. 1, no. 2, p. 181—187, 2006. [Online]. Available: https://doi.org/10.2147/nano.2006.1.2.181

[42] G. Singh, K. Tanurajvir, K. Ravinder, and A. Kaur, "Recent biomedical applications and patents on biodegradable polymer-plga," *International Journal of Pharmacology and Pharmaceutical Sciences*, vol. 1, pp. 30–42, 01 2014.

[43] M. L. Vueba, M. E. Pina, and L. A. E. Batista de Carvalho, "Conformational stability of ibuprofen: Assessed by dft calculations and optical vibrational spectroscopy," *Journal of Pharmaceutical Sciences*, vol. 97, no. 2, pp. 845–859, 2008. [Online]. Available: https://onlinelibrary.wiley.com/doi/abs/10.1002/jps.21007

[44] Shimadzu-Corporation. Measurement methods for liquid samples. [Online]. Available: https://www.shimadzu.com/an/service-support/technical-support/analysis-basics/ftirtalk/talk9.html

[45] D. T. Birnbaum and L. Brannon-Peppas, "Molecular weight distribution changes during degradation and release of plga nanoparticles containing epirubicin hcl," *Journal of biomaterials science*, vol. 1, no. 14, pp. 87—102, 2003. [Online]. Available: https://doi.org/10.1163/15685620360511155

[46] A. J. Shnoudeh, I. Hamad, R. W. Abdo, L. Qadumii, A. Y. Jaber, H. S. Surchi, and S. Z. Alkelany, "Chapter 15 - synthesis, characterization, and applications of metal nanoparticles," in *Biomaterials and Bionanotechnology*, ser. Advances in Pharmaceutical Product Development and Research, R. K. Tekade, Ed. Academic Press, 2019, pp. 527 – 612. [Online]. Available: http://www.sciencedirect.com/science/article/pii/B9780128144275000159

[47] U. P. de València. Field emission scanning electron microscopy. [Online]. Available: http://www.upv.es/entidades/SME/info/859071normali.html

APPENDIX A ELECTROSPRAYING PARAMETERS

Some representative combinations of parameters are presented in the following tables.
The needles used were 26G (0.45 mm outer diameter; 0.23 inner diameter) for the inner one and a 19G (1.06 mm outer diameter; 0.70 mm inner diameter) for the outer one.
Flow rates (F.R.) combinations:

- Combination A: 0.1 mL/h for the inner solution, 0.3 mL/h for the outer;
- Combination B: 0.2 mL/h for the inner solution, 0.5 mL/h for the outer;
- Combination C: 0.1 mL/h for the inner solution, 0.2 mL/h for the outer.

The solute concentration combinations:

- Combination A: 5 wt% for both solutions;
- Combination B: 5 wt% for the inner solution, 7 wt% for the outer.

Table A.1 Same solvent combination of 50/50 THF/MeCN; drum collector.

Test	**TTC [cm]**	**wt%**	**A.V. [kV]**	**F.R. [mL/h]**
10 A	10	2	15.00	0.7
10 B	10	2	10.00	0.7
10 C	10	2	7.00	0.7
10 D	10	2	7.00	0.5
10 E	10	2	10.00	0.5
10 F	10	2	15.00	0.5
11 A	10	3	7.00	0.7
11 B	10	3	10.00	0.7
11 C	10	3	15.00	0.7
11 D	10	3	20.00	0.7
11 E	10	3	20.00	0.5
11 F	10	3	15.00	0.5
11 G	10	3	10.00	0.5
11 H	10	3	7.00	0.5

Table A.2 Same solvent combination of 50/50 THF/MeCN; combination A for the solutes; drum collector.

Test	**TTC [cm]**	**A.V. [kV]**	**F.R. [mL/h]**
12 A	10	15.00	0.7
12 B	10	10.00	0.7
12 C	10	20.00	0.7
12 D	10	20.00	0.5
12 E	10	15.00	0.5
12 F	10	10.00	0.5
12 G	10	7.00	0.5
12 H	10	7.00	0.7
13 D	10	7.00	0.2
13 F	10	10.00	0.2
13 E	10	15.00	0.2

Table A.3 Same solvent combination of 30/70 THF/MeCN; combination A for the solutes; drum collector.

Test	**TTC [cm]**	**A.V. [kV]**	**F.R. [mL/h]**
14 A	10	7.00	0.5
14 B	10	10.00	0.5
14 C	10	15.00	0.5
14 D	10	20.00	0.5
14 E	10	7.00	0.2
14 F	10	10.00	0.2
14 G	10	15.00	0.2

Table A.4 Same solvent combination of 50/50 THF/MeCN; combination A for the solutes; drum collector.

Test	**TTC [cm]**	**A.V. [kV]**	**F.R. [mL/h]**
15 A	2.5	7.00	0.5
15 B	2.5	10.00	0.5
15 C	2.5	15.00	0.5
15 D	2.5	7.00	0.2
15 E	2.5	10.00	0.2
15 F	2.5	15.00	0.2
15 G	2.5	7.00	0.3
15 H	2.5	10.00	0.3
15 I	2.5	15.00	0.3
16 D	4.5	15.00	0.5
16 E	4.5	10.00	0.5
16 F	4.5	7.00	0.5
16 A	4.5	7.00	0.2
16 B	4.5	10.00	0.2
16 C	4.5	15.00	0.2
16 G	4.5	15.00	0.3
16 H	4.5	10.00	0.3
16 I	4.5	7.00	0.3
17 A	4.5	7.00	0.5
17 B	4.5	10.00	0.5
17 C	4.5	15.00	0.5

Table A.5 Same solvent combination of 40/60 THF/MeCN; combination A for the solutes; drum collector.

Test	**TTC [cm]**	**A.V. [kV]**	**F.R. [mL/h]**
18 A	4.5	7.00	0.5
18 B	4.5	10.00	0.5
18 C	4.5	15.00	0.5
18 D	4.5	15.00	0.2
18 E	4.5	10.00	0.2
18 F	4.5	7.00	0.2
18 G	10	7.00	0.2
18 H	10	10.00	0.2
18 I	10	15.00	0.2
19 A	10	7.00	0.5
19 B	10	10.00	0.5
19 C	10	15.00	0.5
19 D	2.5	7.00	0.2
19 E	2.5	10.00	0.2
19 F	2.5	15.00	0.2
19 G	2.5	15.00	0.5
19 H	2.5	10.00	0.5
19 I	2.5	7.00	0.5
19 L	2.5	15.00	0.7
19 M	2.5	10.00	0.7
19 N	2.5	7.00	0.7
20 A	10	7.00	0.5
20 B	10	10.00	0.5
20 C	10	15.00	0.5
20 D	10	15.00	0.2
20 E	10	10.00	0.2
20 F	10	7.00	0.2
20 H	6	7.00	0.2
20 G	6	10.00	0.2
20 I	6	15.00	0.2
20 L	6	15.00	0.5
20 M	6	10.00	0.5
20 N	6	7.00	0.5

Table A.6 Inner solvent was 40/60 THF/MeCN; Outer solvent was 10/30/60 DMF/THF/MeCN; combination A for the solutes; drum collector.

Test	**TTC [cm]**	**A.V. [kV]**	**F.R. [mL/h]**
21 A	10	7.00	0.5
21 B	10	10.00	0.5
21 C	10	15.00	0.5
21 D	10	8.60	0.5
21 E	10	7.00	0.2
21 F	10	8.60	0.2
21 G	10	10.00	0.2
21 H	10	15.00	0.2
21 I	6	7.00	0.2
21 L	6	10.00	0.2
21 M	6	15.00	0.2
21 N	6	15.00	0.5
21 O	6	10.00	0.5
21 P	6	7.00	0.5
23 A	10	7.00	B
23 B	10	10.00	B
23 C	10	15.00	B
23 D	6	7.00	B
23 F	6	10.00	B
23 E	6	15.00	B
23 G	4.5	7.00	B
23 H	4.5	10.00	B
23 I	4.5	15.00	B
24 D	15	15.00	B
24 E	15	13.00	B
24 F	15	10.00	B
25 A	15	7.00	B
25 D	20	15.00	0.2
25 E	20	15.00	0.5
25 F	20	10.00	0.5
25 G	20	10.00	0.2
25 H	20	7.00	0.2
25 I	20	15.00	B

Table A.7 Inner solvent was 40/60 THF/MeCN; Outer solvent was 15/35/50 DMF/THF/MeCN; both with 2.5 wt% of drug and polymer; flat plate collector.

Test	**TTC [cm]**	**A.V. [kV]**	**F.R. [mL/h]**
29 A	20	15.00	B
29 B	20	10.00	B
29 C	20	20.00	B
29 D	26	20.00	B
29 E	26	15.00	B
29 F	26	10.00	B

Table A.8 Inner solvent was 40/60 THF/MeCN; Outer solvent was 15/35/50 DMF/THF/MeCN; with 5 wt% of drug and 2.5 wt% of polymer; flat plate collector.

Test	**TTC [cm]**	**A.V. [kV]**	**F.R. [mL/h]**
30 A	20	15.00	B
30 B	26	15.00	B
30 C	26	20.00	B
30 D	26	10.00	B
30 E	20	10.00	B
30 F	20	20.00	B
30 G	15	15.00	B
30 H	15	10.00	B
30 I	15	20.00	B
30 L	12	20.00	B
30 M	12	15.00	B
30 N	12	10.00	B

Table A.9 Combination A for the solutes; Core solvent 40/60 THF/MeCN; flat plate collector.

Test	**TTC [cm]**	**A.V. [kV]**	**F.R. [mL/h]**	**Shell solvent**
31 A	20	10.00	B	DMF/THF/MeCN 15/35/50
31 B	20	15.00	B	DMF/THF/MeCN 15/35/50
31 C	20	20.00	B	DMF/THF/MeCN 15/35/50
31 D	20	7.00	B	DMF/THF/MeCN 15/35/50
31 I	20	13.00	B	DMF/THF/MeCN 15/35/50
31 L	20	14.00	B	DMF/THF/MeCN 15/35/50
32 A	20	10.00	B	DMF/MeCN 50/50
32 B	20	15.00	B	DMF/MeCN 50/50
32 C	20	20.00	B	DMF/MeCN 50/50
32 D	20	13.00	B	DMF/MeCN 50/50
32 E	20	14.00	B	DMF/MeCN 50/50

Table A.10 Inner solvent was 40/60 THF/MeCN; Outer solvent was 60/40 DMF/ MeCN; combination A for the solutes; ethanol bath collector.

Test	**TTC [cm]**	**Negative A.V. [kV]**	**Positive A.V. [kV]**	**F.R. [mL/h]**
35	20	-3	10	B
36 A	20	-4	12	B
36 B	20	-3	10.5	B
37 E	20	-3	7.5	C
37 F	20	-3	8.5	B
40 A	21	-3	11	B

Table A.11 Inner solvent was 40/60 THF/MeCN; Outer solvent was 60/40 DMF/ MeCN; combination A for the solutes; flat plate collector; the substrate was covered with a silicone-based spray.

Test	**TTC [cm]**	**Negative A.V. [kV]**	**Positive A.V. [kV]**	**F.R. [mL/h]**
41 A	21	-3	12	B
41 B	21	-3	24	B
41 C	30	-3	24	B
41 D	30	-3	12	B

Table A.12 Inner solvent was 40/60 THF/MeCN; Outer solvent was 60/40 DMF/ MeCN; combination A for the solutes; flat plate collector.

Test	TTC [cm]	Negative A.V. [kV]	Positive A.V. [kV]	F.R. [mL/h]
33 A	20	-	10	B
33 B	20	-	13	B
33 C	20	-	14	B
33 D	20	-	15	B
33 E	20	-	20	B
33 F	26	-	10	B
33 G	26	-	13	B
33 H	26	-	14	B
33 I	26	-	15	B
37 A	20	-3	10	B
37 B	26	-3	10	B
37 C	26	-3	10	C
37 D	20	-2	8	C
38 B	21	-3	12	B
38 C	21	-3	12	A
39 D	21	-	15	C
42 B	21	-	15	B
42 D	21	-	15	C
42 E	21	-3	9	B

Table A.13 Big box set-up parameters. Inner solvent was 40/60 THF/MeCN; Outer solvent was 60/40 DMF/MeCN; flat plate collector.

Test	TTC [cm]	wt%	A.V. [kV]	F.R. [mL/h]
44 A	21	A	15.00	A
44 B	21	A	15.00	B
44 C	12	A	15.00	B
44 F	21	A	18.00	B
49 G	21	A	13.00	A
50 A	34	A	15.00	A
50 C	34	A	15.00	B
52 A	30	B	15.00	B
52 B	30	B	15.00	A
52 C	15	B	15.00	A